

Hg supply piping simulation (No MHD)

Stony Brook University

Yan Zhan

Prof. Foluso Ladeinde

July 2nd, 2010

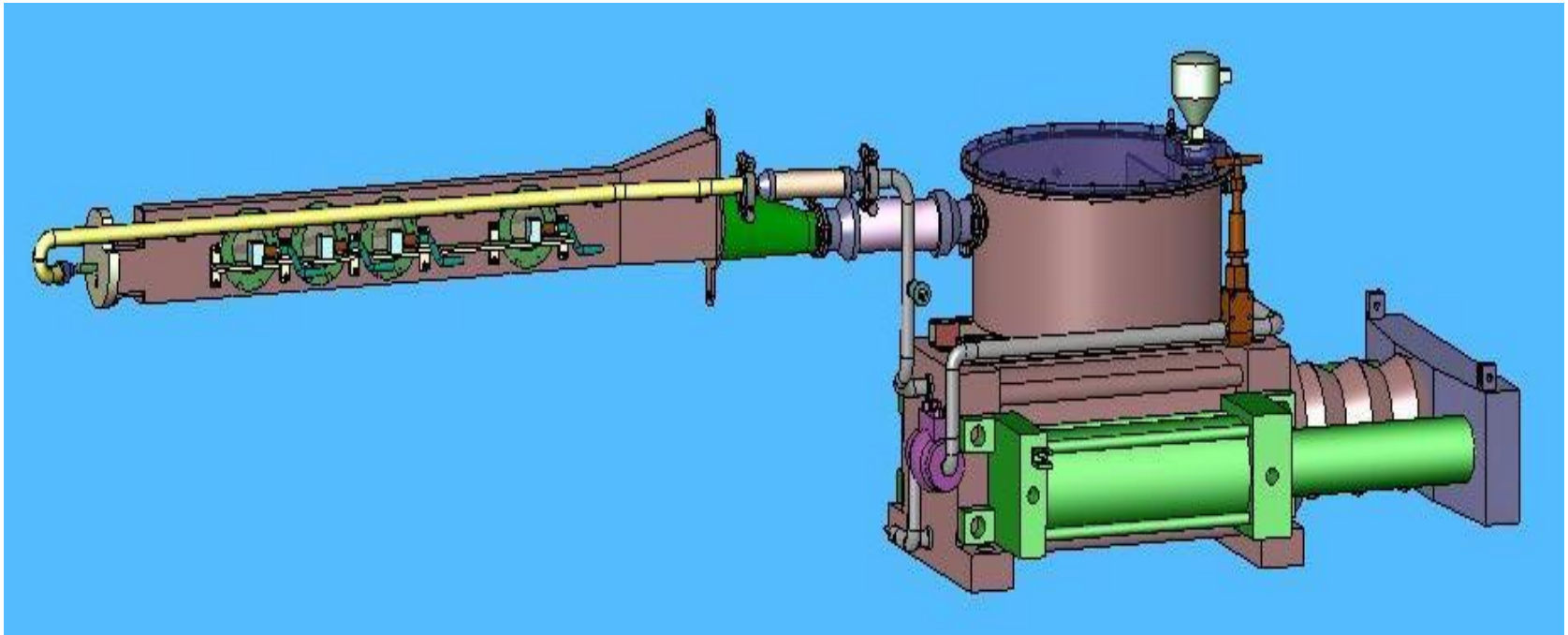
Outline

- Hg supply piping in Muon Collider
- Turbulence models for bend pipe flow
- Problems need studying
- Arrangements in the near future

Outline

- Hg supply piping in Muon Collider
 - Hg supply piping
 - Simplified simulation model
 - Curved pipe flow regime
 - Inlet pressure
 - Inlet velocity profile
- Turbulence models for bend pipe flow
- Problems need studying
- Arrangements in the near future

Hg supply piping in Muon Collider— Hg supply piping (1)



Hg supply flow path:

1-inch Sch 40 pipe (OD=1.315-inch, Wall thickness=0.133-inch)

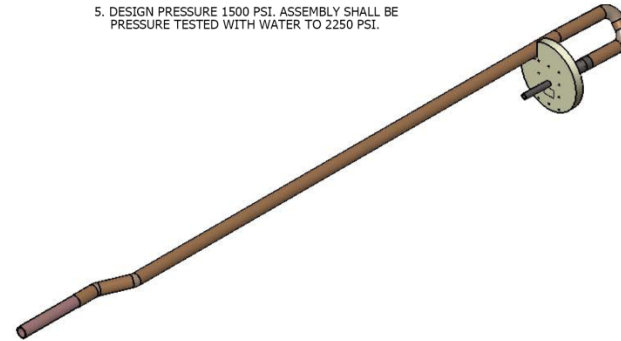
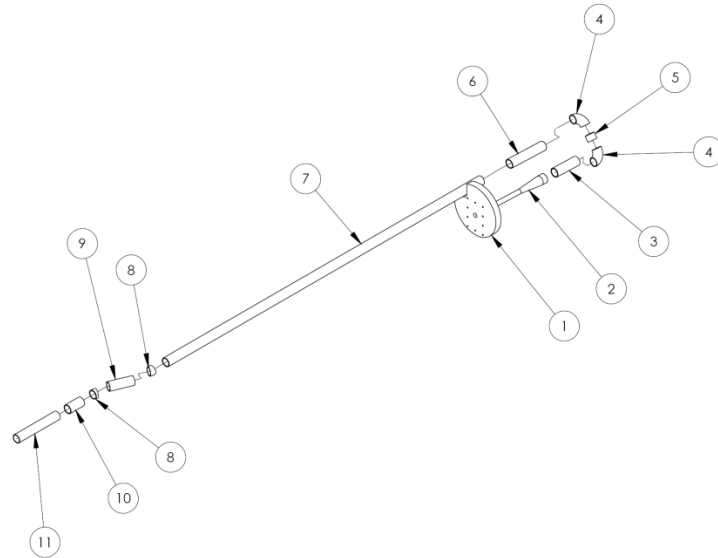
1-inch flex metal hose w/sanitary fittings

1-inch, 0.065-wall rigid tubing

12mm-dia, 1mm-wall rigid tubing

Hg supply piping in Muon Collider— Hg supply piping(1)

THIS DRAWING PRODUCED ON SOLIDWORKS



- NOTES
1. MATERIAL CERTIFICATIONS REQUIRED.
 2. WELDING AND INSPECTION SHALL BE PERFORMED IN ACCORDANCE WITH ASME SECTION IX OR OTHER APPROVED STANDARD. NO CODE STAMP REQUIRED.
 3. 100% RADIOGRAPHY INSPECTION REQUIRED.
 4. ASSEMBLY SHALL BE ANODIZED PER AEROSPACE MATERIAL SPECIFICATION 2487 "ANODIC TREATMENT OF TITANIUM AND TITANIUM ALLOYS".
 5. DESIGN PRESSURE 1500 PSI. ASSEMBLY SHALL BE PRESSURE TESTED WITH WATER TO 2250 PSI.

ITEM	NAME	MATERIAL	DESCRIPTION	DWG	test/QTY.
11	HG SUPPLY INLET TUBE	TI GRADE 2, ASTM B-861	RIGID SEAMLESS TUBE, 1.000 X .065 WALL X 3.500	N/A	1
10	HG SUPPLY TI PIPING	TI GRADE 2, ASTM B-861	RIGID SEAMLESS PIPE, 3/4" SCH10, 2.000 L	N/A	1
9	HG SUPPLY TI PIPING	TI GRADE 2, ASTM B-861	RIGID SEAMLESS PIPE, 3/4" SCH10, 2.819 L	N/A	1
8	HG SUPPLY TI ELBOW	TI GRADE 2, ASTM B-861	RIGID SEAMLESS ELBOW, 3/4" SCH10	N/A	2
7	HG SUPPLY TI PIPING	TI GRADE 2, ASTM B-861	RIGID SEAMLESS PIPE, 3/4" SCH10, 46.700 L	203-HJT-0629	1
6	HG SUPPLY TI PIPING	TI GRADE 2, ASTM B-861	RIGID SEAMLESS PIPE, 3/4" SCH10, 5.000 L	203-HJT-0628	1
5	HG SUPPLY TI PIPING	TI GRADE 2, ASTM B-861	RIGID SEAMLESS PIPE, 3/4" SCH10, .700 L	N/A	1
4	HG SUPPLY TI ELBOW	TI GRADE 2, ASTM B-861	RIGID SEAMLESS ELBOW, 3/4" SCH10	N/A	2
3	HG SUPPLY TI PIPING	TI GRADE 2, ASTM B-861	RIGID SEAMLESS PIPE, 3/4" SCH10, 3.250 L	N/A	1
2	HG SUPPLY REDUCER NOZZLE	TI-6AL-4V, ASTM B-265	FLOW REDUCER AND NOZZLE	203-HJT-0627	1
1	HG NOZZLE FLANGE STRAIGHT	TI-6AL-4V, ASTM B-265	NOZZLE FLANGE	203-HJT-0626	1

THIRD-ANGLE PROJECTION

UNLESS OTHERWISE NOTED

1. ALL DIMENSIONS ARE IN INCHES
2. INTERPRET DIMENSIONS AND TOLERANCES PER ASME Y14.5M
3. MACHINED FINISH 125 MICROS INCHES RMS
4. CONCENTRICITY .010 TIR
5. MACHINED ANGLES ±1/2°
6. BREAK SHARP CORNERS AND REMOVE ALL BURRS
7. WHOLE NUMBERS AND FRACTIONS:

+	±.110
0	±.030
1	±.010
2	±.005
8. X° DECIMALS
9. XX DECIMALS
10. XXXX DECIMALS

DRAWING APPROVALS

DES	DATE
V GRAVES	12/08/2006
DRW	12/08/2006
CHK	12/12/2006
ENG	12/08/2006

OAK RIDGE NATIONAL LABORATORY
operated for the U.S. Department of Energy under contract DE-AC05-00OR22725 Oak Ridge, TN

REMOTE SYSTEMS GROUP
NUCLEAR SCIENCE & TECHNOLOGY DIVISION

**MERIT EXPERIMENT
PRIMARY TUBE ASSEMBLY
HG STRAIGHT NOZZLE ASSY**

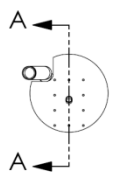
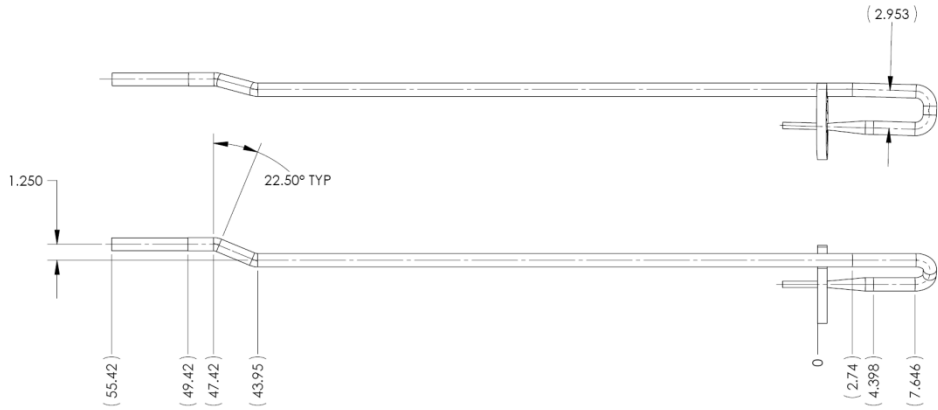
CAD FILE	PREV ASSY	SCALE	SHEET
HG STRAIGHT NOZZLE ASSY	203-HJT-0610	1:6	1 of 2
SIZE	DWG NO.	REV	
C	203-HJT-0625	0	

0	ORIGINAL ISSUE	12/14/2006	VBG	VBG
REV	DESCRIPTION	DATE	BY	APPROVED

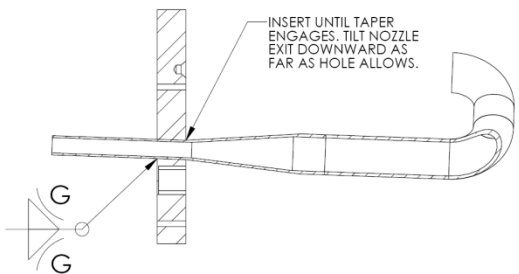
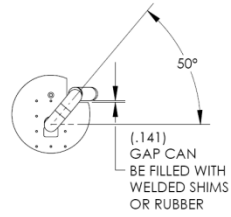
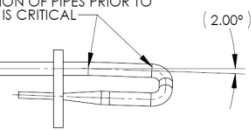
DWG NO. 203-HJT-0625

Hg supply piping in Muon Collider— Hg supply piping(2)

THIS DRAWING PRODUCED ON SOLIDWORKS



ORIENTATION OF PIPES PRIOR TO WELDING IS CRITICAL



SECTION A-A
SCALE 1 : 2

- NOTES
1. MATERIAL CERTIFICATIONS REQUIRED.
 2. WELDING AND INSPECTION SHALL BE PERFORMED IN ACCORDANCE WITH ASME SECTION IX OR OTHER APPROVED STANDARD. NO CODE STAMP REQUIRED.
 3. 100% RADIOGRAPHY INSPECTION REQUIRED.
 4. ASSEMBLY SHALL BE ANODIZED PER AEROSPACE MATERIAL SPECIFICATION 2487 "ANODIC TREATMENT OF TITANIUM AND TITANIUM ALLOYS".
 5. DESIGN PRESSURE 1500 PSI. ASSEMBLY SHALL BE PRESSURE TESTED WITH WATER TO 2250 PSI.

<p>THIRD-ANGLE PROJECTION</p> <p>UNLESS OTHERWISE NOTED</p> <ol style="list-style-type: none"> 1. ALL DIMENSIONS ARE IN INCHES 2. INTERPRET DIMENSIONS AND TOLERANCES PER ASME Y14.5M 3. MACHINED FINISH 125 MICRO-INCHES RMS 4. CONCENTRICITY ± 0.10 TIR 5. MASHINED ANGLES $\pm 11/2^{\circ}$ 6. FORMED ANGLES $\pm 1^{\circ}$ 7. BREAK SHARP CORNERS AND REMOVE ALL BURRS 8. HOLE NUMBERS AND FRACTIONS $\pm 1/16$ 9. .X DECIMALS ± 0.00 10. .XX DECIMALS ± 0.01 10. XXXX DECIMALS ± 0.005 	<p>This drawing was prepared by ORNL solely for use in work performed under Department of Energy contract number DE-AC05-00OR22725 and applicable Work for Others Agreements and Cooperative Research and Development Agreements. This drawing is property of ORNL and must be returned upon REQUEST.</p>															
	<table border="1"> <tr> <td>DES</td> <td>V GRAVES</td> <td>12/08/2006</td> </tr> <tr> <td>DRW</td> <td>V GRAVES</td> <td>12/08/2006</td> </tr> <tr> <td>CHK</td> <td>W SANDS</td> <td>12/12/2006</td> </tr> <tr> <td>ENG</td> <td>V GRAVES</td> <td>12/08/2006</td> </tr> <tr> <td>QA</td> <td></td> <td></td> </tr> </table>	DES	V GRAVES	12/08/2006	DRW	V GRAVES	12/08/2006	CHK	W SANDS	12/12/2006	ENG	V GRAVES	12/08/2006	QA		
DES	V GRAVES	12/08/2006														
DRW	V GRAVES	12/08/2006														
CHK	W SANDS	12/12/2006														
ENG	V GRAVES	12/08/2006														
QA																

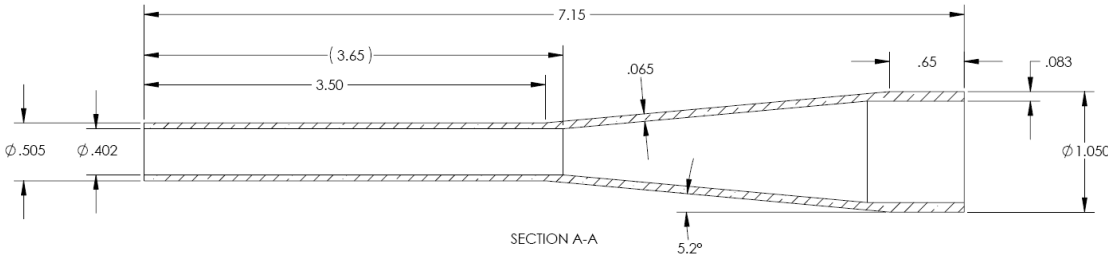
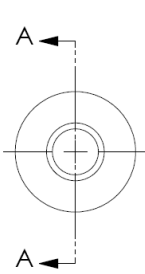
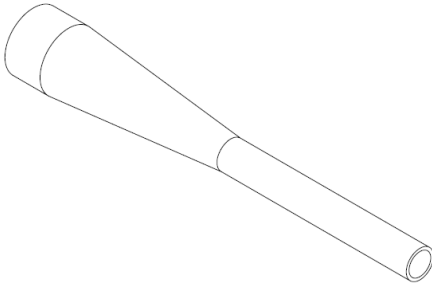
<p>OAK RIDGE NATIONAL LABORATORY operated for the U.S. Department of Energy under contract DE-AC05-00OR22725 Oak Ridge, TN</p>		<p>REMOTE SYSTEMS GROUP NUCLEAR SCIENCE & TECHNOLOGY DIVISION</p>	
<p>MERIT EXPERIMENT PRIMARY TUBE ASSEMBLY HG STRAIGHT NOZZLE ASSY</p>			
<p>CAD FILE HG STRAIGHT NOZZLE ASSY</p>	<p>PREV ASSY 203-HJT-0610</p>	<p>SCALE 1:6</p>	<p>SHEET 2 of 2</p>
<p>SIZE C</p>	<p>DWG NO. 203-HJT-0625</p>	<p>REV 0</p>	

DWG NO. 203-HJT-0625

Hg supply piping in Muon Collider— Hg supply piping(3)

S THIS DRAWING PRODUCED ON SOLIDWORKS

NOTES
1. MATERIAL CERTIFICATIONS REQUIRED.



MATERIAL: TI-6AL-4V, ASTM B-265

THIRD-ANGLE PROJECTION		This drawing was prepared by ORNL solely for use in work performed under Department of Energy contract number DE-AC05-00OR22725 and applicable Work for Others Agreements and Cooperative Research and Development Agreements. This drawing is property of ORNL and must be returned upon request.	
UNLESS OTHERWISE NOTED			
1.	ALL DIMENSIONS ARE IN INCHES	DES	V GRAVES 12/07/2006
2.	INTERPRET DIMENSIONS AND TOLERANCES PER ASME Y14.4M	DRW	V GRAVES 12/08/2006
3.	MACHINED FINISH 1/16 MIRRORS INCHES RMS	CHK	W SANDS 12/12/2006
4.	CONCENTRICITY .010 TIR	ENG	V GRAVES 12/07/2006
5.	MACHINED ANGLES ±1/2°		
6.	FORMED ANGLES ±1°		
7.	BREAK SHARP CORNERS AND REMOVE ALL BURRS		
8.	WHOLE NUMBERS AND FRACTIONS ±1/16	QA	
9.	X DECIMALS ±.030		
10.	XX DECIMALS ±.010		
11.	XXX DECIMALS ±.008		
DRAWING APPROVALS		DATE	

OAK RIDGE NATIONAL LABORATORY
 operated for the U.S. Department of Energy under contract DE-AC05-00OR22725 Oak Ridge, TN
 REMOTE SYSTEMS GROUP
 NUCLEAR SCIENCE & TECHNOLOGY DIVISION

MERIT EXPERIMENT HG SUPPLY SYSTEM ASSY FLOW REDUCER	
CAD FILE	PREV ASSY
HG SUPPLY REDUCER NOZZLE	203-HJT-0625
SCALE	3:2
SHEET	1 of 1
SIZE	DWG NO.
C	203-HJT-0627
REV	0

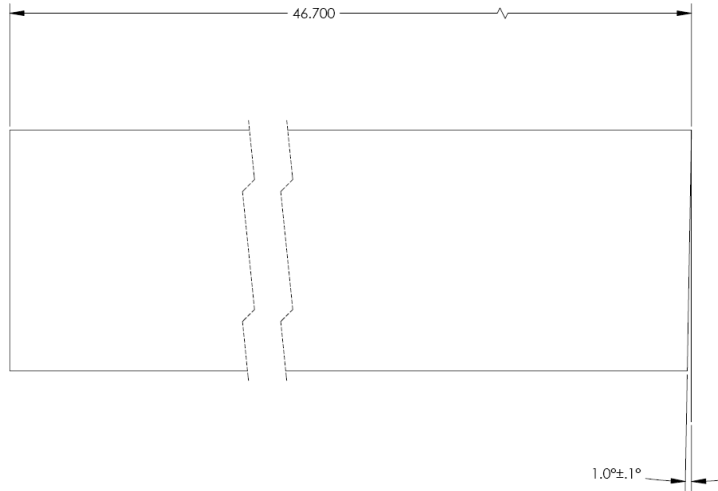
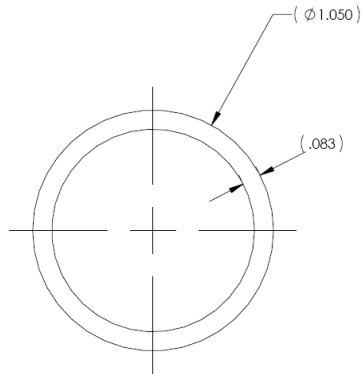
0	ORIGINAL ISSUE	12/14/2006	VBG	VBG
REV	DESCRIPTION	DATE	BY	APPROVED

DWG NO. 203-HJT-0627

Hg supply piping in Muon Collider— Hg supply piping(4)

S THIS DRAWING PRODUCED ON SOLIDWORKS

NOTES
1. MATERIAL CERTIFICATIONS REQUIRED.



MATERIAL: TI GRADE 2, ASTM B-861

<p>THIRD-ANGLE PROJECTION</p>	This drawing was prepared by ORNL solely for use in work performed under Department of Energy contract number DE-AC05-00OR22725 and applicable Work for Others Agreements and Cooperative Research and Development Agreements. This drawing is property of ORNL and must be returned upon request.																									
	<p>UNLESS OTHERWISE NOTED</p> <ol style="list-style-type: none"> 1. ALL DIMENSIONS ARE IN INCHES 2. INTERPRET DIMENSIONS AND TOLERANCES PER ASME Y14.6M 3. MACHINED FINISH 125 MICRO-INCHES RMS 4. CONCENTRICITY .010 T14 5. MACHINED ANGLES ±1.0° 6. FORMED ANGLES ±1.0° 7. BREAK SHARP CORNERS AND REMOVE ALL BURRS 8. WHOLE NUMBERS AND FRACTIONS ±1/16 9. .X DECIMALS ±.005 10. XX DECIMALS ±.010 11. XXX DECIMALS ±.005 	<table border="1"> <tr> <td>DES</td> <td>V GRAVES</td> <td>12/08/2006</td> </tr> <tr> <td>DRW</td> <td>V GRAVES</td> <td>12/08/2006</td> </tr> <tr> <td>CHK</td> <td>W SANDS</td> <td>12/12/2006</td> </tr> <tr> <td>ENG</td> <td></td> <td></td> </tr> <tr> <td>QA</td> <td></td> <td></td> </tr> <tr> <td></td> <td></td> <td></td> </tr> </table>	DES	V GRAVES	12/08/2006	DRW	V GRAVES	12/08/2006	CHK	W SANDS	12/12/2006	ENG			QA						<table border="1"> <tr> <td>SIZE</td> <td>DWG NO.</td> <td>203-HJT-0629</td> </tr> <tr> <td>C</td> <td></td> <td></td> </tr> </table>	SIZE	DWG NO.	203-HJT-0629	C	
DES	V GRAVES	12/08/2006																								
DRW	V GRAVES	12/08/2006																								
CHK	W SANDS	12/12/2006																								
ENG																										
QA																										
SIZE	DWG NO.	203-HJT-0629																								
C																										

OAK RIDGE NATIONAL LABORATORY
 operated for the U.S. Department of Energy under contract DE-AC05-00OR22725 Oak Ridge, TN

REMOTE SYSTEMS GROUP
 NUCLEAR SCIENCE & TECHNOLOGY DIVISION

MERIT EXPERIMENT
HG SUPPLY SYSTEM ASSEMBLY
SUPPLY PIPING

CAD FILE	PREV ASSY	SCALE	SHEET
HG SUPPLY TI PIPING	203-HJT-0625	3:1	1 of 1
DRAWING APPROVALS	DATE		REV 0

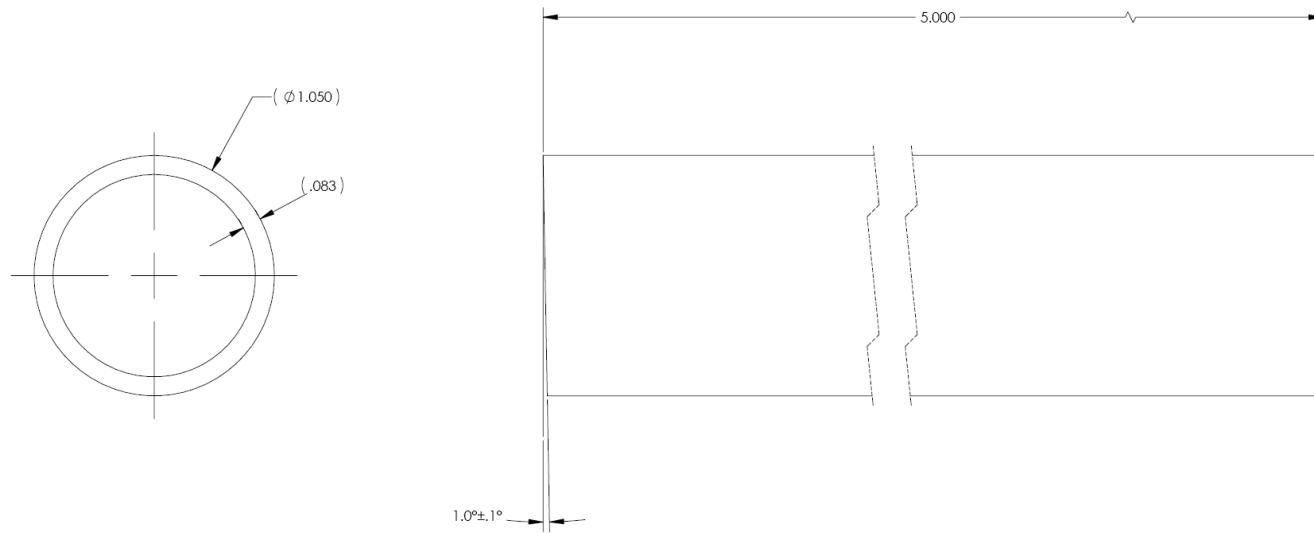
0	ORIGINAL ISSUE	12/14/2006	VBG	VBG
REV	DESCRIPTION	DATE	BY	APPROVED

DWG NO. 203-HJT-0629

Hg supply piping in Muon Collider— Hg supply piping(5)

S THIS DRAWING PRODUCED ON SOLIDWORKS

NOTES
1. MATERIAL CERTIFICATIONS REQUIRED.



MATERIAL: TI GRADE 2, ASTM B-861

THIRD-ANGLE PROJECTION

This drawing was prepared by ORNL solely for use in work performed under Department of Energy contract number DE-AC05-00OR22725 and applicable Work for Others Agreements and Cooperative Research and Development Agreements. This drawing is property of ORNL and must be returned upon request.

UNLESS OTHERWISE NOTED

1. ALL DIMENSIONS ARE IN INCHES
2. INTERPRET DIMENSIONS AND TOLERANCES PER ASME Y14.5M
3. MACHINED FINISH 125 MICRO-INCHES RMS
4. CONCENTRICITY $.010$ TIR
5. MACHINED ANGLES $\pm 1/2^\circ$
6. FORMED ANGLES $\pm 1^\circ$
7. BREAK SHARP CORNERS AND REMOVE ALL BURRS
8. WHOLE NUMBERS AND FRACTIONS $\pm .1/16$
9. X DECIMALS $\pm .030$
10. XX DECIMALS $\pm .010$
11. XXX DECIMALS $\pm .005$

DES	V GRAVES	12/08/2006
DRW	V GRAVES	12/08/2006
CHK	W SANDS	12/12/2006
ENG		
QA		

DRAWING APPROVALS

ORNL OAK RIDGE NATIONAL LABORATORY
operated for the U.S. Department of Energy under contract DE-AC05-00OR22725 Oak Ridge, TN

NSTB NUCLEAR SCIENCE & TECHNOLOGY DIVISION

REMOTE SYSTEMS GROUP

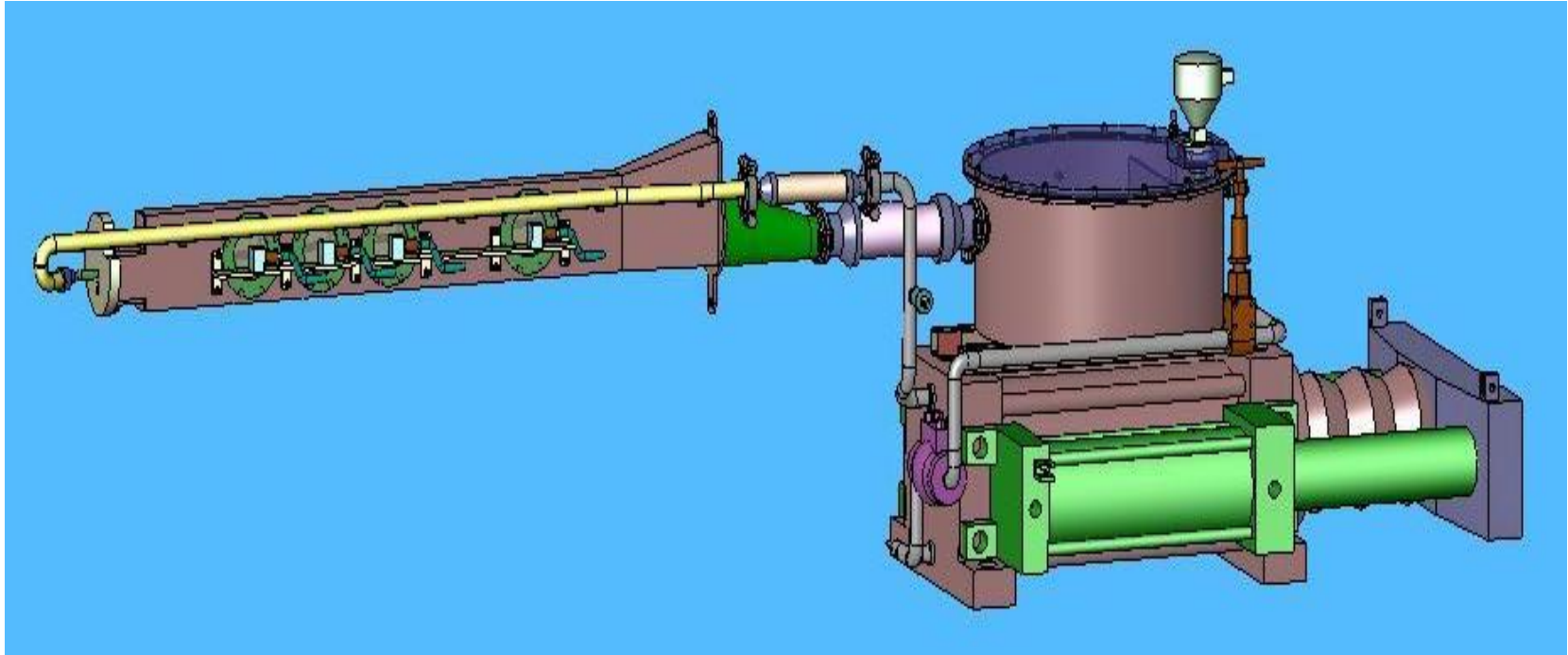
**MERIT EXPERIMENT
HG SUPPLY SYSTEM ASSEMBLY
SUPPLY PIPING**

0	ORIGINAL ISSUE	12/14/2006	VBG	VBG
REV	DESCRIPTION	DATE	BY	APPROVED

CAD FILE	HG SUPPLY TI PIPING	PREV ASSY	203-HJT-0625	SCALE	3:1	SHEET	1 of 1
SIZE	C	DWG NO.	203-HJT-0628			REV	0

DWG NO. 203-HJT-0628

Hg supply piping in Muon Collider— Simplified simulation model (1)

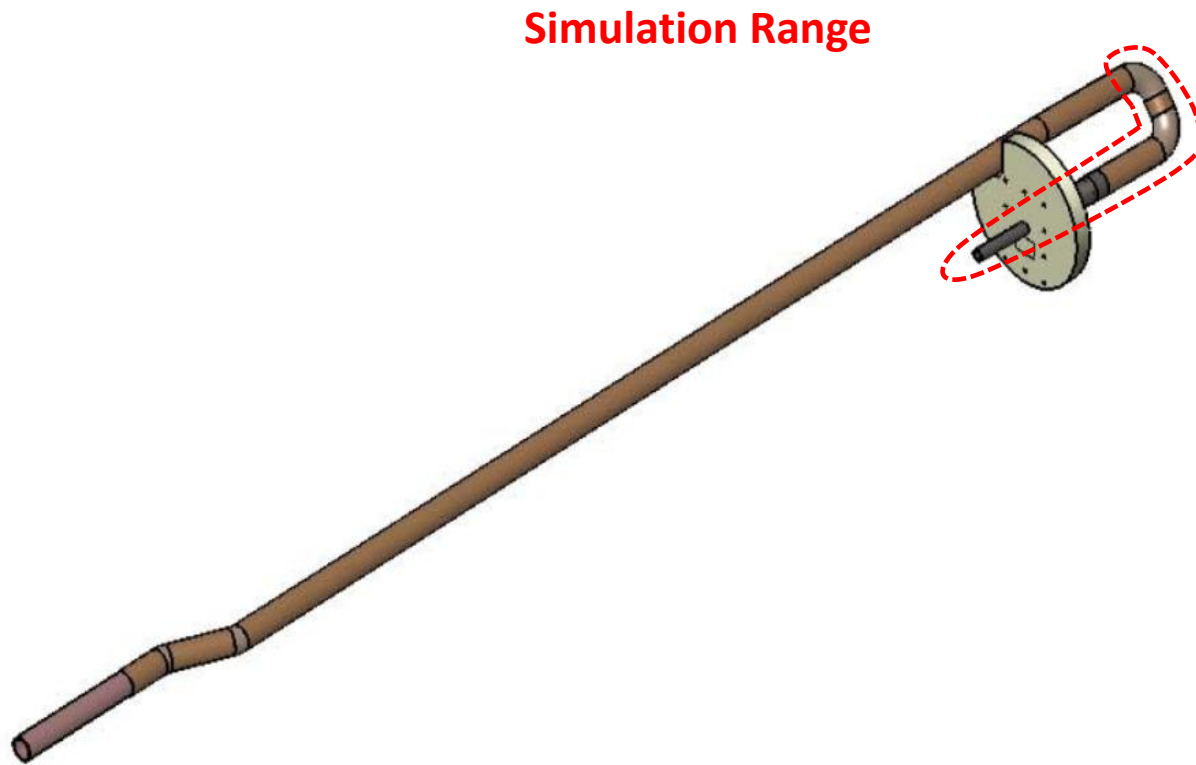


Is it necessary to simulate the whole pipe system?

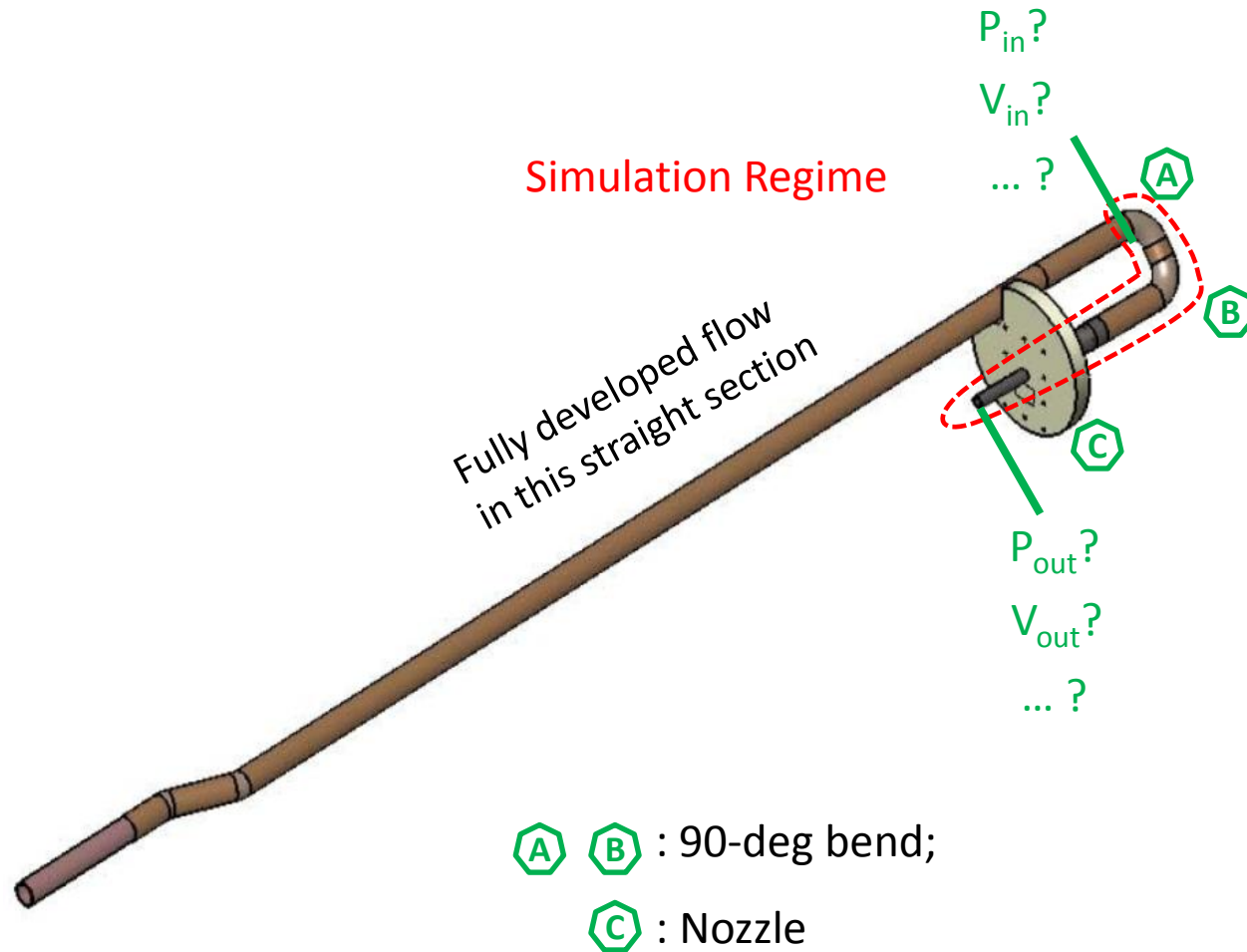
Probably Not

Hg supply piping in Muon Collider— Simplified simulation model (2)

Interests: Influence of nozzle & nozzle upstream on jet exit



Hg supply piping in Muon Collider— Simplified simulation model (3)



Hg supply piping in Muon Collider— Curved pipe flow regime (1)

Table 1 Parameters table

Variable Values	
Pipe ID	0.884 inch
Nozzle exit ID	0.402 inch
Driving pressure	30 bar
Frequency for Hg supply	12 s
Maximum Cycles	100
Jet Velocity	20 m/s
Jet Diameter	1 cm
Jet Flow rate	1.6 L/sec
Environment	1 atm air /vacuum
Air Density Outside Jet	0.0013kg/L

Table 2 Hg properties table

Mercury Properties (25 °C)	
Density	13.546 kg/L
Sound Speed	1451 m/s
Bulk Modulus	2.67×10^{10} Pa
Dynamic Viscosity	1.127 m ² /s
Thermal Conductivity	8.69 W/m·K
Electrical Conductivity	10 ⁶ Siemens/m
Specific Heat	0.139 J/kg·K
Prandtl Number	0.025
Surface Tension	465 dyne/cm
Permeability	4*PI*1E-7

Hg supply piping in Muon Collider— Curved pipe flow regime (2)

$$u_{pipe} = \frac{\text{flow rate}}{A} = \frac{1.6 \times 10^{-3}}{\pi/4 \times (0.884 \times 2.54 \times 10^{-2})^2} \approx 4.04 \text{ m/s}$$

$$\text{Re}_{pipe} = \frac{\rho u_{pipe} d_{pipe}}{\mu} = \frac{13.546 \times 10^3 \times 0.884 \times 2.54 \times 10^{-2} \times 4.04}{1.526 \times 10^{-3}} = 8.05 \times 10^5$$

$$c_{Hg} = \sqrt{\frac{K}{\rho}} = \sqrt{\frac{2.67 \times 10^{10}}{13.546 \times 10^3}} \approx 1400 \text{ m/s}$$


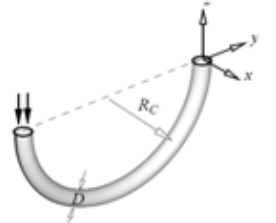
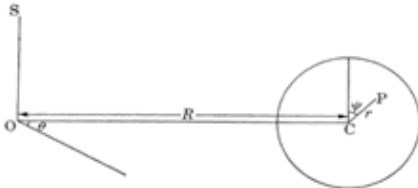
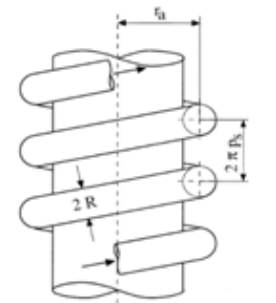
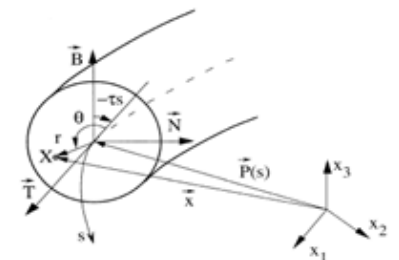
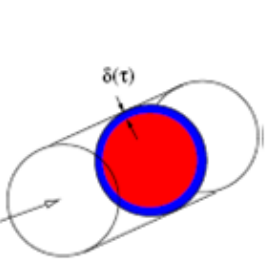
$$\text{Ma}_{pipe} = \frac{u_{pipe}}{c_{Hg}} = \frac{4.04}{1400} = 0.003 \ll 0.3$$

$$\delta_4 = \frac{R_c}{r_{pipe}} = \frac{1.1265}{0.442} \approx 2.86$$

$$\text{De}_4 = (2\delta_4)^{-0.5} \text{Re}_{pipe} = (2 \times 2.86)^{-0.5} \times 8.05 \times 10^5 \approx 3.566 \times 10^5$$

The Hg flow inside the pipe is **incompressible** flow

Hg supply piping in Muon Collider— Curved pipe flow regime (3)

Flow type	Coordinate	Similarity Parameters	Transition to Turbulence
Straight pipe flow 	Cylindrical (r, z)	Reynolds Number $Re_D = \frac{\rho U D}{\mu} = \frac{\rho U^2}{\mu U / D}$	$Re_{Dcrit} = 2000$
Planar curved pipe flow 	Toroidal (r, ψ, θ) 	Reynolds Number Dean Number $De = 4 \sqrt{\frac{D}{R_c}} Re_D = 4 \sqrt{\frac{\rho \bar{R}_c \frac{U^2}{R_c^2} \times \rho U^2}{\frac{\mu U}{D}}}$ Where $\bar{R}_c = R_c / D$	$Re_{Dcrit} = 5000$ ($R/a=31.9$) $De_{Dcrit} = 5000$
Helically coiled pipe flow 	Orthogonal helical (s, r, θ) 	Reynolds Number Dean Number Germano Number $Gn = (D/2)\tau Re_D$ Where τ is torsion $\gamma = \frac{Gn}{De^{3/2}}$ is important in determining the flow response to torsion.	
Unsteady flow 		Reduced Velocity Womersley Number $U_{red} = \frac{UT}{D}$ $Wo = \frac{D}{2} \sqrt{\frac{2\pi}{vT}} \propto \frac{D}{\sqrt{vT}}$ Where T is the fundamental period of the oscillatory flow $U_{red} = \frac{\pi Re_D}{2 Wo^2}$	

The Hg flow inside the pipe is **turbulent** flow

Hg supply piping in Muon Collider— Inlet pressure(1)

Pipe flow with fully developed velocity

Laminar velocity profiles

$$u_z(r) = \frac{R^2}{4\mu} \left(-\frac{dP}{dx}\right) \left[1 - \left(\frac{r}{R}\right)^2\right]$$

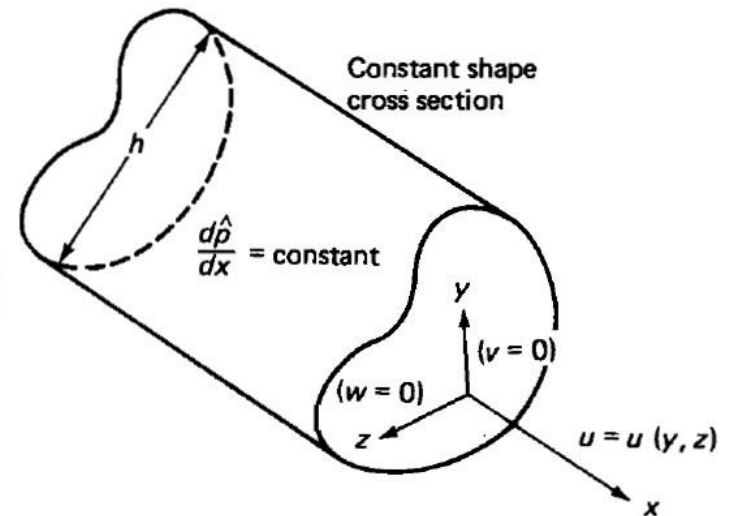
Turbulent velocity profiles

$$u_m = \frac{1}{\pi R^2} \int_0^R \bar{u} 2\pi r dr = v^* \left(\frac{1}{\kappa} \ln \frac{av^*}{\nu} + B - \frac{3}{2\kappa} \right)$$

wall-friction velocity $v^* = \left(\frac{\tau_w}{\rho}\right)^{1/2}$

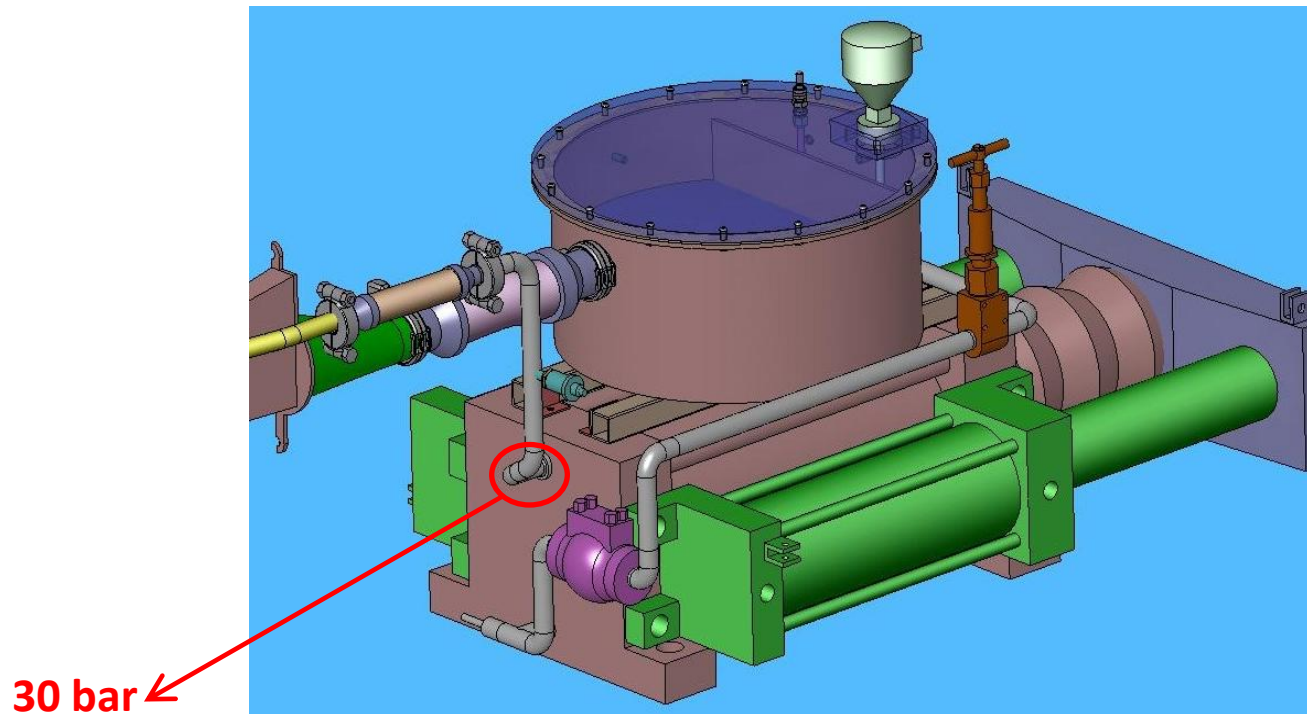
Where $\tau_w = -\frac{1}{2} \frac{dP}{dx} R$

Constants $\kappa \approx 0.41, B = 5.0$



The velocity profile depends on the pressure.

Hg supply piping in Muon Collider— Inlet pressure(2)



30 bar ←

Pressure loss = Wall friction + Elevation changes + Bend loss

$$= \sum \Delta P_1 + \sum \Delta P_2 + \sum \Delta P_3$$

$$= \lambda_s \frac{L}{D} \frac{\rho V^2}{2} + \Delta P_B(\lambda_c) + \rho g \Delta h$$

The friction coefficient in straight pipe, λ_s , depends on Re and δ ;

The friction coefficient in curved pipe, λ_c , depends on Re and $\frac{r}{R}$;

Hg supply piping in Muon Collider— Inlet pressure(3)

(1) Pressure loss due to the wall friction in straight pipe

Re		λ_s
$Re < 22\left(\frac{d}{\delta}\right)^{8/7}$	$3000 < Re < 10^5$	$\lambda_s = 0.3164/Re^{0.25}$
	$10^5 < Re < 10^8$	$\lambda_s = 0.308/(0.842 - \lg Re)^2$
$22\left(\frac{d}{\delta}\right)^{8/7} < Re < 597\left(\frac{d}{\delta}\right)^{9/8}$		$\lambda_s = [1.14 - 2\lg\left(\frac{d}{\delta} + \frac{21.25}{Re^{0.9}}\right)]^{-2}$
$Re > 597\left(\frac{d}{\delta}\right)^{9/8}$		$\lambda_s = 0.11\left(\frac{d}{\delta}\right)^{0.25}$

Note: δ = relative roughness of tube or duct wall (mm), δ/d = the roughness ratio

Roughness table: http://www.engineeringtoolbox.com/major-loss-ducts-tubes-d_459.html

(2) Pressure loss due to the elevation

$$\Delta P_{elevation} = \rho g \Delta h$$

Hg supply piping in Muon Collider— Inlet pressure(4)

(3) Pressure loss due to the bends

Prediction of turbulent pressure drop in curved pipes

$$\phi_c = \phi_s + 0.005 \left(\frac{d}{D} \right)^{0.5}$$

$$\phi_c \left(\frac{D}{d} \right)^{0.5} = 0.003625 + 0.038 \left[\text{Re} \left(\frac{d}{D} \right)^2 \right]^{-0.25}$$

$$\phi_c = \phi_s \left[\text{Re} \left(\frac{d}{D} \right)^2 \right]^{0.05}$$

$$\phi_c = \phi_s \exp \left[2\pi \frac{d}{D} \right]$$

$$\phi_c = 0.0395 \left(\frac{d}{D} \right)^{0.5} \left[\text{Re} \left(\frac{d}{D} \right)^2 \right]^{-0.2}$$

$$\phi_c = \phi_s \left[1 + 0.0823 \left(1 + \frac{d}{D} \right) \left(\frac{d}{D} \right)^{0.53} \text{Re}^{0.25} \right]$$

$$\phi_c \left(\frac{D}{d} \right)^{0.5} = 0.0395 \left[\text{Re} \left(\frac{d}{D} \right)^2 \right]^{-0.2} \left[1 + 0.112 \left[\text{Re} \left(\frac{d}{D} \right)^2 \right]^{-0.2} \right]$$

$$\phi_c \left(\frac{D}{d} \right)^{0.5} = 0.024 \left[\text{Re} \left(\frac{d}{D} \right)^2 \right]^{-0.167} \left[1 + 0.068 \left[\text{Re} \left(\frac{d}{D} \right)^2 \right]^{-0.167} \right]$$

$$\phi_c = 0.042 \left[\text{Re} \left(\frac{D}{d} \right)^{0.5} \right]^{-0.2}$$

$$\phi_c = \phi_s \left[1.83 \left(\frac{d}{D} \right)^{0.1} \right]$$

$$\phi_c \left(\frac{D}{d} \right)^{0.5} = 0.00206 + 0.0394 \left[\text{Re} \left(\frac{d}{D} \right)^2 \right]^{-0.227}$$

$$\phi_c = 0.001875 + 0.3165 \left(\frac{d}{D} \right)^{0.275} \text{Re}^{-0.4}$$

$$\phi_c = \phi_s + 0.00375 \left(\frac{d}{D} \right)^{0.5}$$

$$\phi_c = \phi_s + 8.7891 \left(\frac{d}{D} \right)^{0.3621} \text{Re}^{-0.3137} \left(\frac{L}{d} \right)^{0.4885}$$

Hg supply piping in Muon Collider— Inlet velocity profile (1)

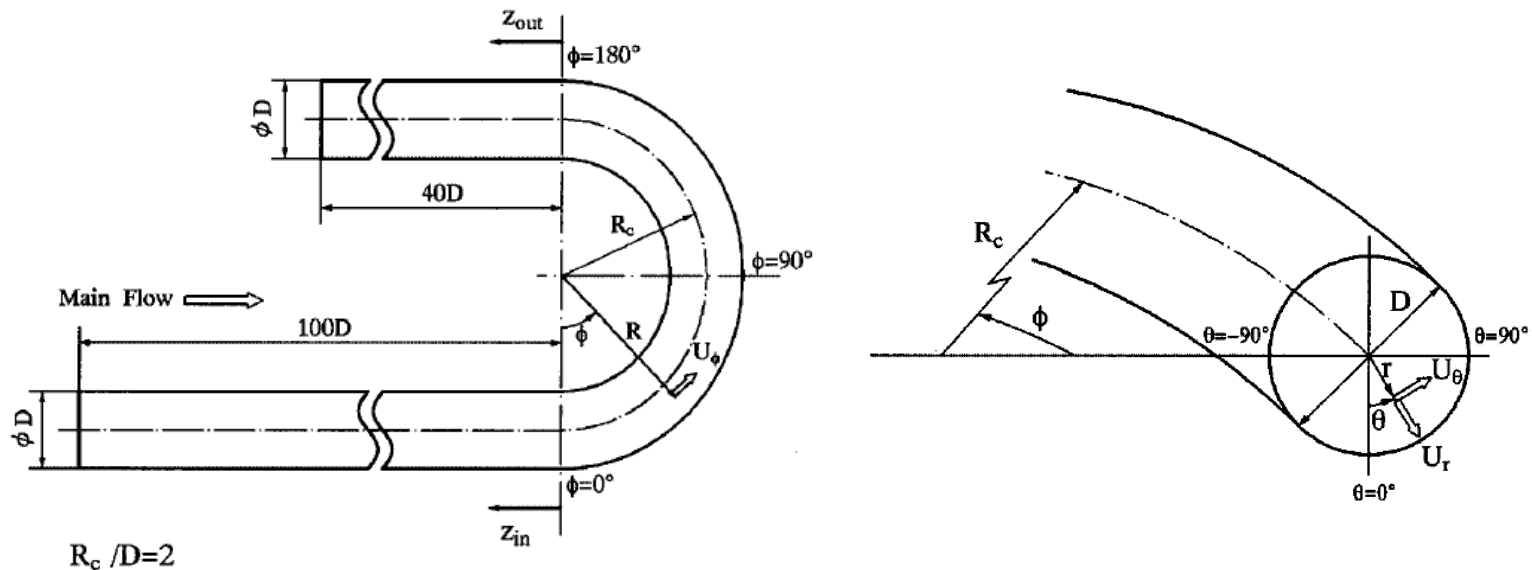
Laminar pipe flow (straight VS. bend)

Circular pipes		Straight pipe		Bend pipe	
No. of dimension		2 Dimension		3 Dimension	
Turbulent transition parameter		Re=2000		De=5000	
Entry length ($l_c < l_s$)	Laminar	$l_s = 0.06 \times Re \times D$ ($\sim \mathcal{O}(aRe)$ and $\sim \mathcal{O}(a)$)		$l_c = e_1 (De/\delta)^{1/2} a$ ($\sim \mathcal{O}(aR)^{1/2}$)	
	Turbulent	$l_s = 4.4 \times Re^{1/6} \times D$		50D upstream and 70D downstream of the bend to ensure fully developed flows;	
Velocity profile		<p>Axial velocity only with peak at the pipe center:</p> <p>Velocity Profiles</p> <p>Smooth Pipe $N_R = 10^5$, $f = 0.012$</p> <p>Turbulent Flow $N_R < 2,000$</p> <p>Laminar Flow $N_R < 2,000$</p> <p>Rough Pipe $N_R = 10^5$, $f = 0.04$</p> <p>f = friction factor N_R = Reynolds Number</p> <p>Increasing Velocity \rightarrow</p> <p>Pipe</p> <p>Laminar Flow</p> <p>Turbulent Flow</p>		<p>Axial velocity peak near the bend outside;</p> <p>Secondary flow exhibit at the pipe cross-section</p> <p>Center of Curvature</p> <p>Radius of Curvature</p>	
<p>a is the pipe radius; R is the bend radius, Curvature $\delta = a/R$; Dean number $De = 2\delta^{1/2} Re$; e_1 is the coefficient of entry length*</p> <p>* L.S. Yao and S.A. Berger, Entry flow in a curved pipe, J. Fluid Mech., Vol. 67, 177-196, 1975</p>					

Hg supply piping in Muon Collider— Inlet velocity profile (2)

Turbulent flow (fully developed downstream)

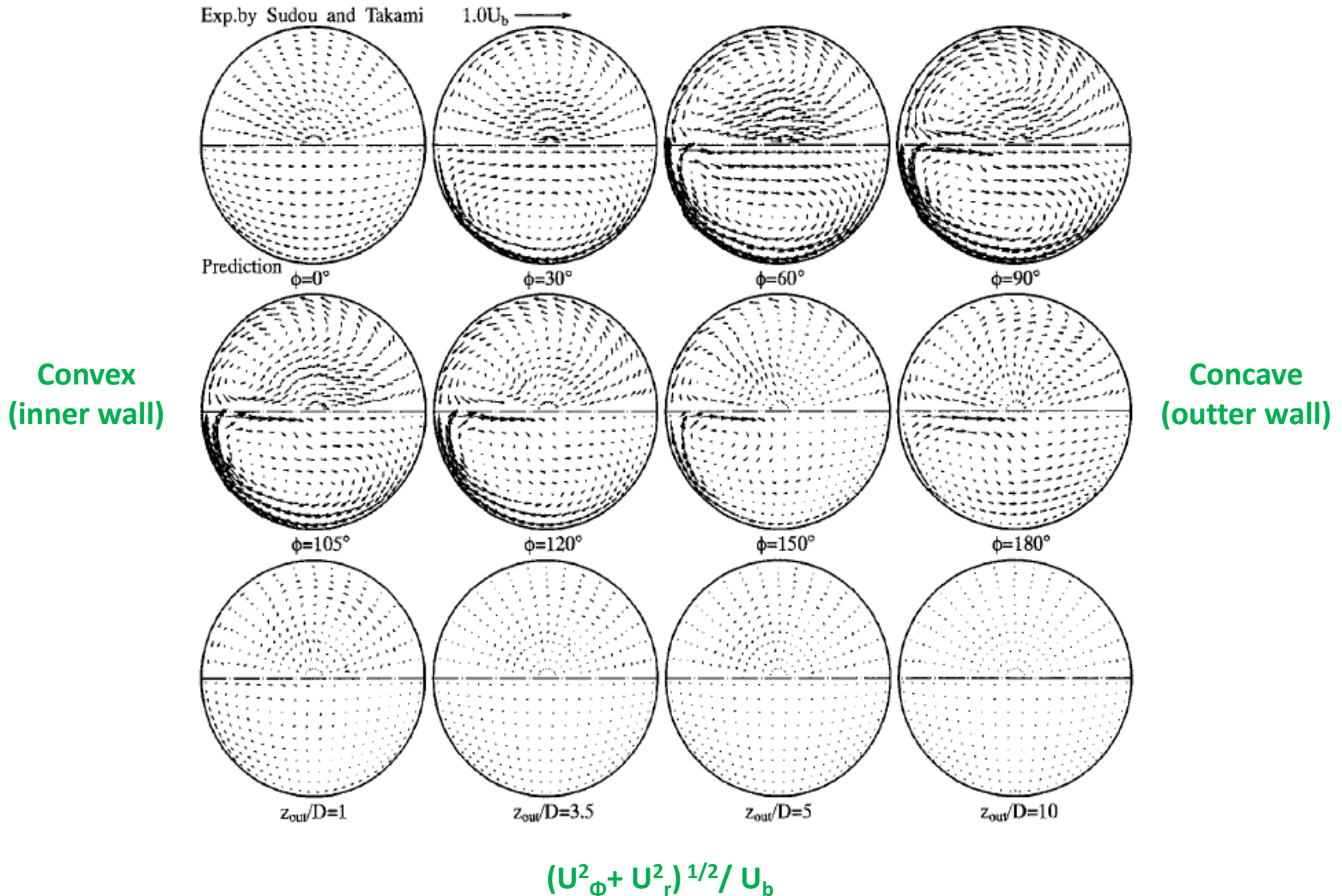
- ❑ Cross-stream velocity (secondary flow)
- ❑ Stream-wise velocity



180° bend tube ($Re= 6 \times 10^4$, $R_c=4R$, $De= 2.12 \times 10^4$)

Hg supply piping in Muon Collider— Inlet velocity profile (3)

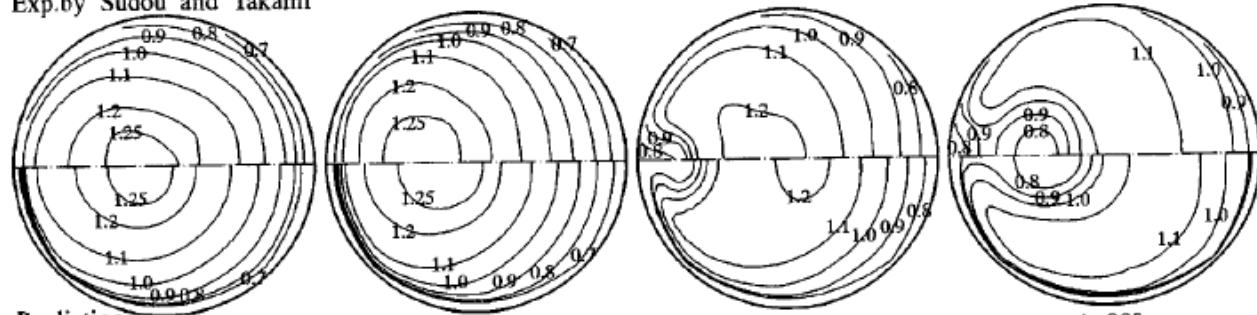
Cross-stream velocity (secondary flow)



Hg supply piping in Muon Collider— Inlet velocity profile (4)

Stream-wise mean velocity

Exp. by Sudou and Takami



Prediction

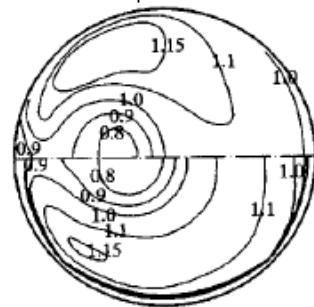
$\phi=0^\circ$

$\phi=30^\circ$

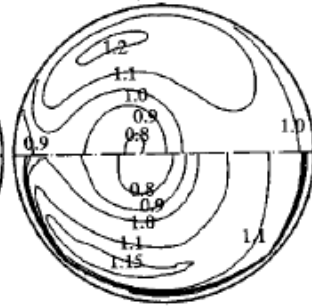
$\phi=60^\circ$

$\phi=90^\circ$

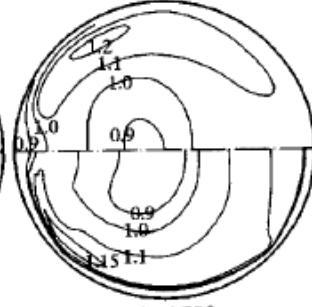
Convex
(Inner)



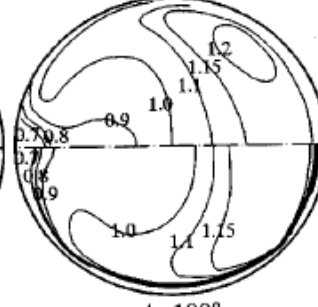
$\phi=105^\circ$



$\phi=120^\circ$

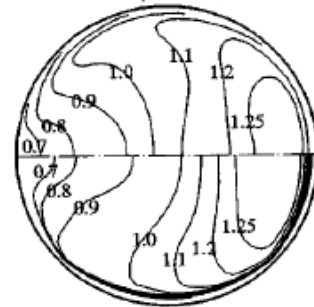


$\phi=150^\circ$

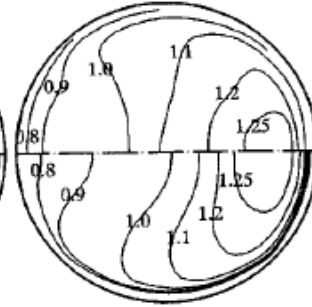


$\phi=180^\circ$

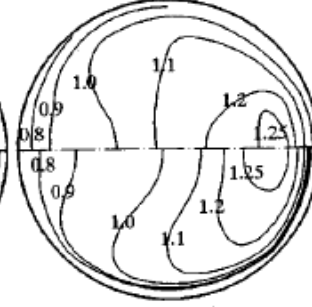
Concave
(Outer)



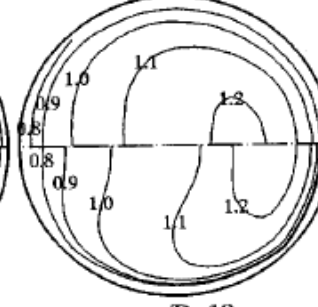
$z_{out}/D=1$



$z_{out}/D=3.5$



$z_{out}/D=5$

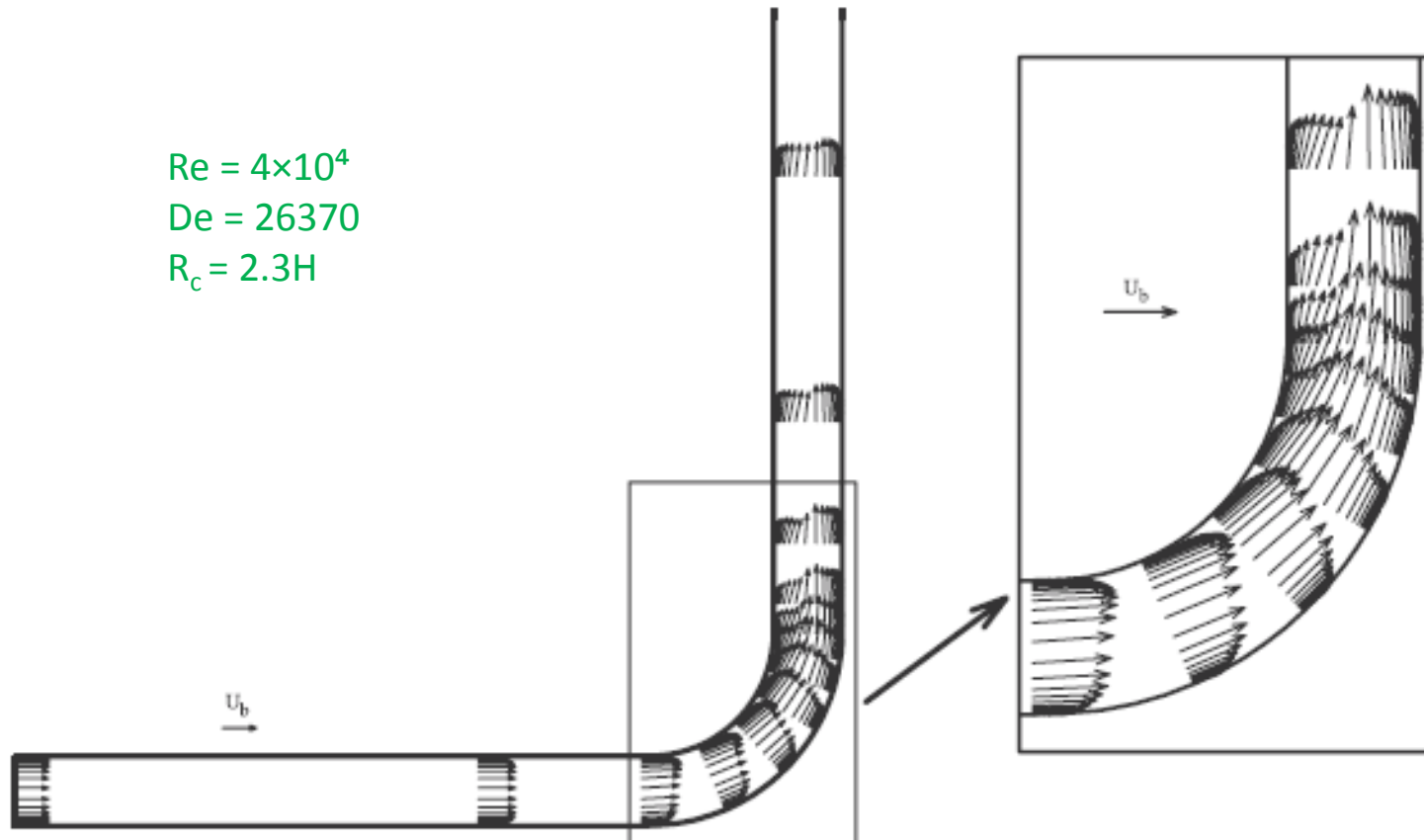


$z_{out}/D=10$

U_ϕ/U_b

Hg supply piping in Muon Collider— Inlet velocity profile (5)

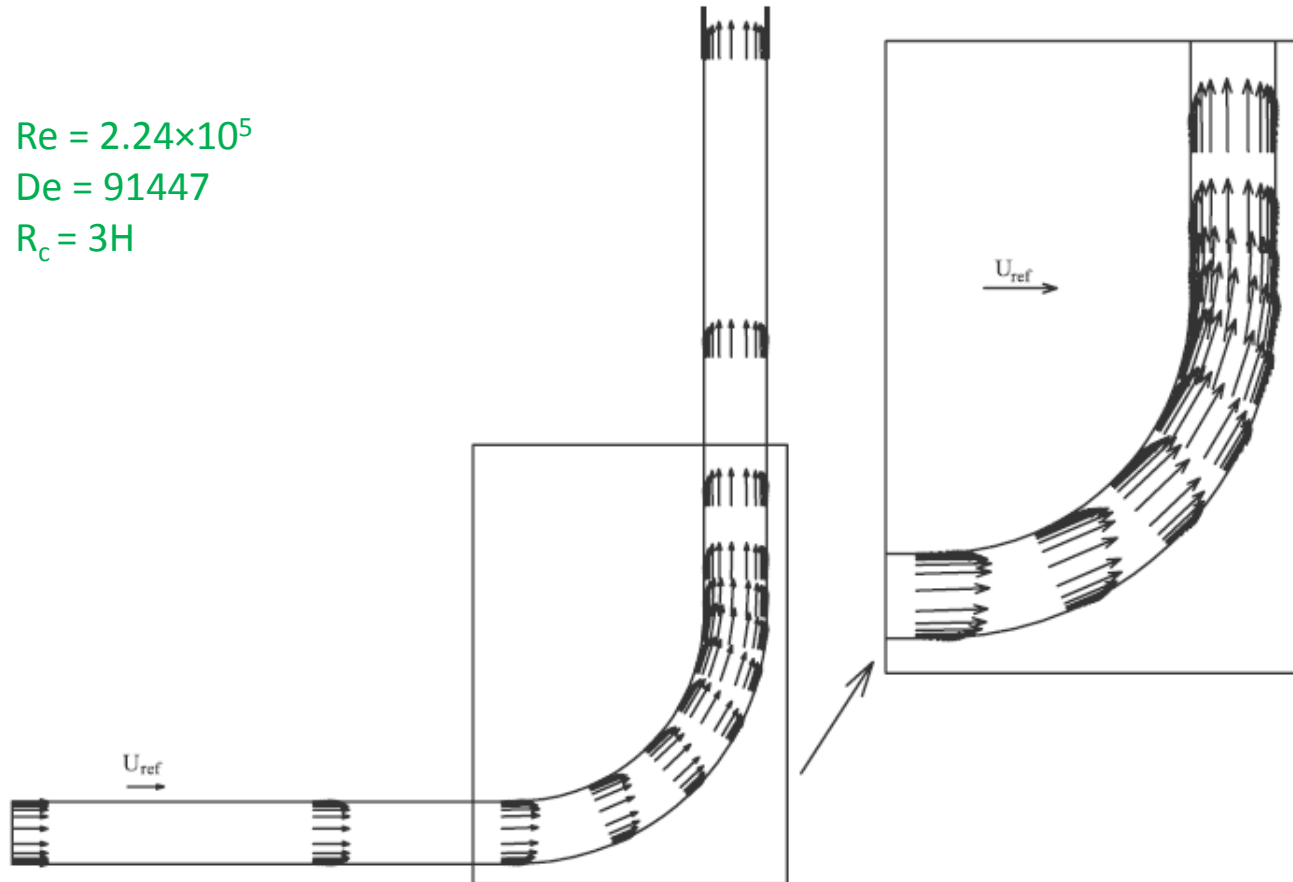
Stream-wise velocity in middle plane of the square 90° bend



Hg supply piping in Muon Collider— Inlet velocity profile (6)

Stream-wise velocity in middle plane of the rectangular 90° bend

$Re = 2.24 \times 10^5$
 $De = 91447$
 $R_c = 3H$



Hg supply piping in Muon Collider— Inlet velocity profile (7)

Conclusions:

For fully developed turbulent downstream (bend pipe)

❑ Cross-stream velocity

The strength of secondary flow **rapidly decreases** in the downstream

Straight tube section ($Z \approx 3.5D$)

❑ Stream-wise velocity

Contour lines approach gradually the **concentric circular** contour, forming the **high value** of contours **near the outer wall side** of the circular tube

Hg supply piping in Muon Collider— Inlet velocity profile (8)

Inlet velocity profile for Hg supply piping ($L_{\text{upstream}} \approx 53.5D$)

❑ Cross-stream velocity

No secondary flow

❑ Stream-wise velocity

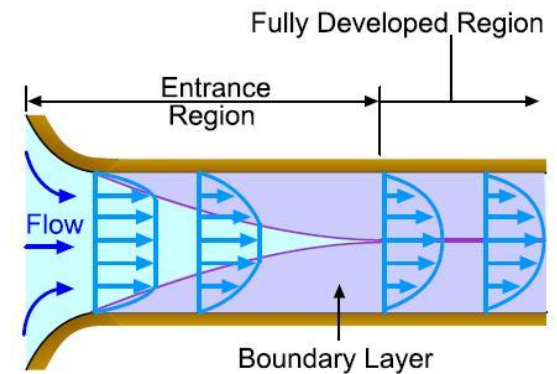
Simple guess

Concentric circular contour lines with high value at the center

$$(L_e)_{\text{straight}} > (L_e)_{\text{curved}}$$

$$(L_e)_{\text{curved} + \text{turbulent}} < (L_e)_{\text{straight} + \text{turbulent}}$$

$$\text{Where } (L_e)_{\text{straight} + \text{turbulent}} = 4.4\text{Re}^{1/6} D \approx 42.4D$$



Outline

- Hg supply piping in Muon Collider
- **Turbulence models for bend pipe flow**
 - Turbulence model requirement
 - Turbulence models
 - Past work on curved ducts
 - Curvature-corrected k- ϵ models
- Problems need studying
- Arrangements in the near future

Turbulence models for bend pipe flow

—Turbulence model requirement

Bradshaw (1973)

Strong or even moderate curvature can significantly impact the turbulence structure, which will influence the mean flow development.

Muck et al., (1985); Hoffman et al. (1985)

Convex curvature is **stabilizing** and **suppresses** turbulence levels, while **concave** curvature is **destabilizing** and tends to **augment** turbulence.

Correct response to curvature effects

Turbulence models for bend pipe flow

—Turbulence models (1)

□ **RANS-based turbulence models**

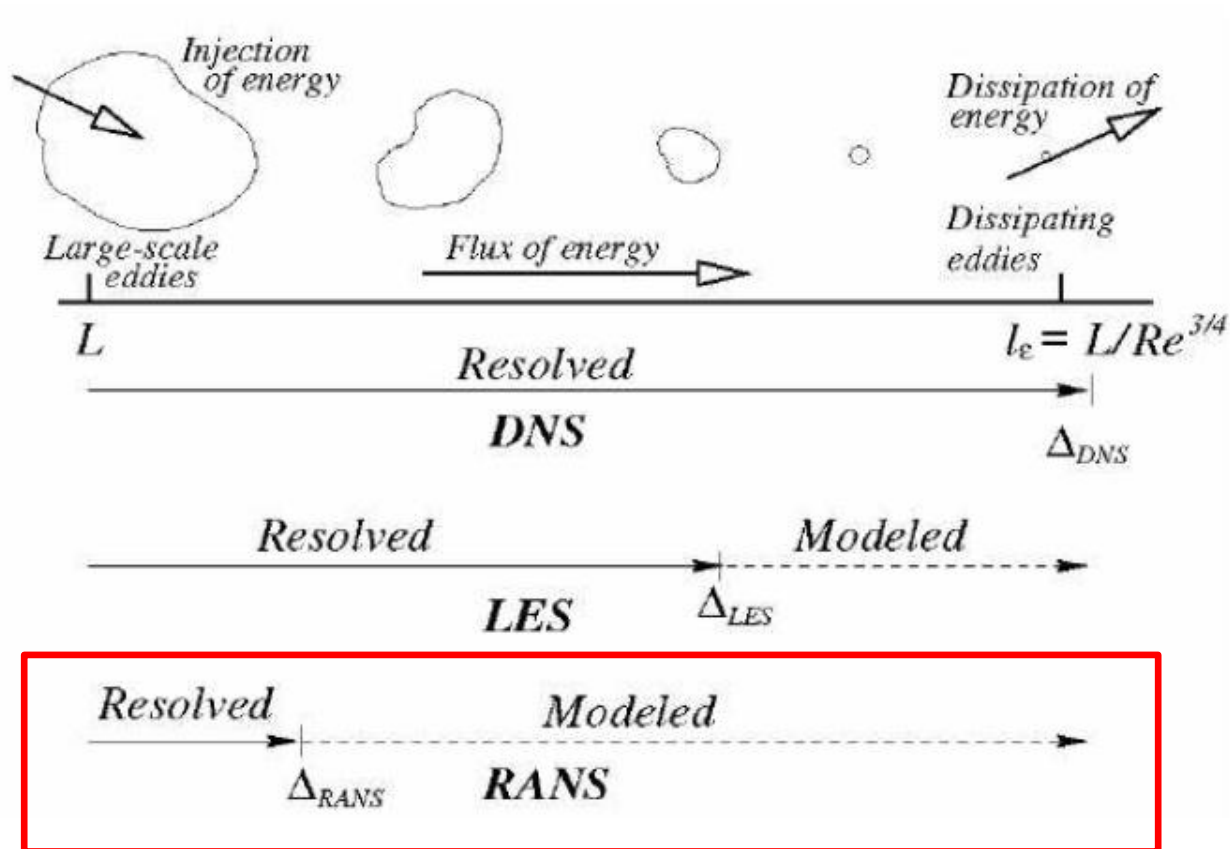
- Linear eddy viscosity models (LEVM)
 - Algebraic stress models
 - One equation models
 - Two equation models
- Nonlinear eddy viscosity models (NLEVM)
- Reynolds stress model(RSM)

□ **Computation of fluctuation quantities**

- Large eddy simulation (LES)
- Direct numerical simulation (DNS)

Turbulence models for bend pipe flow

—Turbulence models (2)



Turbulence models for bend pipe flow

—Turbulence models (3)

Comparison among RANS-based turbulence models

Model	Cons	Pros
RSM	Numerically instability and stiffness; Non-ideal in engineering applications.	Explicitly and well predicting flow with streamline curvature
NLEVM	Still computationally costly; Higher order terms in algebraic expression	Comparable with RSM in capturing curvature effects but lower cost
LEVM	Modification needed in simulating flows with curvature effects, adverse pressure gradient, separation, rotation, etc.	Reasonable compromise between expense and physical realism in engineering practice

Curvature-corrected k- ϵ model for engineering bend pipe flow problem

Turbulence models for bend pipe flow

—Past work on curved ducts (1)

k-ε model: [Standard k-ε model](#); Realisable k-ε model; RNG k-ε model.

Continuity equation

$$\frac{\partial \rho}{\partial t} + \frac{\partial}{\partial x_j}(\rho u_j) = 0$$

Momentum equation

$$\rho \left(\frac{\partial u_i}{\partial t} + u_j \frac{\partial u_i}{\partial x_j} \right) = -\frac{\partial P}{\partial x_i} + \frac{\partial}{\partial x_i} \left[\mu \left(\frac{\partial u_i}{\partial x_j} + \frac{\partial u_j}{\partial x_i} - \frac{2}{3} \delta_{ij} \frac{\partial u_k}{\partial x_k} \right) \right] + \frac{\partial}{\partial x_i} (-\overline{\rho u_j u_i})$$

Turbulent kinetic energy transportation equation

$$\underbrace{\frac{\partial(\rho k)}{\partial t}}_{\text{uns steady}} + \underbrace{\frac{\partial(\rho u_j k)}{\partial x_j}}_{\text{convection}} = \underbrace{\frac{\partial}{\partial x_j} \left[\left(\mu + \frac{\mu_t}{\sigma_k} \right) \frac{\partial k}{\partial x_j} \right]}_{\text{diffusion}} + \underbrace{G_k + G_b}_{\text{source}} - \underbrace{\rho \epsilon}_{\text{dissipation}} - \underbrace{Y_M + SS_k}_{\text{compression}}$$

Turbulent kinetic energy dissipation rate transportation equation

$$\underbrace{\frac{\partial(\epsilon \rho)}{\partial t}}_{\text{uns steady}} + \underbrace{\frac{\partial(\epsilon \rho u_j)}{\partial x_j}}_{\text{convection}} = \underbrace{\frac{\partial}{\partial x_j} \left[\left(\mu + \frac{\mu_t}{\sigma_\epsilon} \right) \frac{\partial \epsilon}{\partial x_j} \right]}_{\text{diffusion}} + \underbrace{C_{1\epsilon} \frac{\epsilon}{k} (G_k + C_{3\epsilon} G_b)}_{\text{source}} - \underbrace{C_{2\epsilon} \rho \frac{\epsilon^2}{K}}_{\text{dissipation}}$$

Eddy viscosity

$$\mu_t = C_\mu \rho \frac{k^2}{\epsilon}$$

Reynolds stress model

$$-\overline{\rho u_i u_j} = 2\mu_t S_{ij} - \frac{2}{3} \delta_{ij} \left(\mu_t \frac{\partial U_i}{\partial x_i} + \overline{\rho k} \right) \quad (\text{Boussinesq approximation})$$

Constants

$$C_\mu = 0.09, \sigma_k = 1.0, \sigma_\epsilon = 1.3, C_{1\epsilon} = 1.44, C_{2\epsilon} = 1.92$$

Where $\mu = \mu_t + \mu_l$, u_i is the mean velocity vector, u_i' is the fluctuation velocity vector

Turbulence models for bend pipe flow

—Past work on curved ducts (2)

Curvature correction into k- ϵ models

1. Ad-hoc parameterization modification

Grooray, A.M. et al.(1985), Park, S.W. et al.(1989)

2. High-Re turbulence models + Wall-function approximation/Damping functions

Patankar, et al. (1975), Kreskovsky et al. (1981), Chang, et al.(1983),

Azzola, et al. (1986), Iacovides, et al. (1987), Choi, et al.(1989),

William, et al.(2009)

3. Low-Re turbulence models

Raisee , et al.(2006)

Ability to resolve the near-wall motion

(Secondary motion is strongest within the near-wall regions)

Turbulence models for bend pipe flow

—Curvature-corrected k- ϵ models (1)

Linear low-Re turbulence model (Raisee , et al.2006)

Continuity $\frac{\partial u_j}{\partial x_j} = 0$

Momentum $\frac{\partial(u_j u_i)}{\partial x_j} = -\frac{1}{\rho} \frac{\partial P}{\partial x_i} + \frac{\partial}{\partial x_i} (v \frac{\partial u_i}{\partial x_j} - \overline{u_j u_i})$

Reynolds Stress $\overline{u_i u_j} = -v_t (\frac{\partial u_i}{\partial x_j} + \frac{\partial u_j}{\partial x_i}) + \frac{2}{3} k \delta_{ij}$

Turbulent viscosity $v_t = c_{\mu} f_{\mu} \frac{k^2}{\epsilon}$

Transportation equation of the turbulent kinetic energy

$$\frac{\partial(u_j k)}{\partial x_j} = \frac{\partial}{\partial x_j} [(v + \frac{v_t}{\sigma_k}) \frac{\partial k}{\partial x_j}] + P_k - \epsilon - 2v (\frac{\partial \sqrt{k}}{\partial x_j})^2$$

Transportation equation for the homogeneous dissipation rate

$$\frac{\partial(u_j \epsilon)}{\partial x_j} = \frac{\partial}{\partial x_j} [(v + \frac{v_t}{\sigma_k}) \frac{\partial \epsilon}{\partial x_j}] + f_1 C_{1\epsilon} \frac{\epsilon}{k} P_k - f_2 C_{2\epsilon} \frac{\epsilon^2}{k} + E + S_{\epsilon}$$

Where $E = 2v v_t (\frac{\partial^2 u_i}{\partial x_i \partial x_j})^2, S_{\epsilon} = NYP = \max[C_{\omega} F(F+1) \frac{\epsilon^2}{k}, 0]$

Where $F = [(\frac{\partial l}{\partial x_j} \frac{\partial l}{\partial x_j})^{1/2} - \frac{\partial l_{\epsilon}}{\partial y}] / C_1$

with $l = \frac{k^{3/2}}{\epsilon}, \frac{\partial l_{\epsilon}}{\partial y} = C_1 [1 - \exp(-B_{\epsilon} R_t) + B_{\epsilon} C_1 R_t \exp(-B_{\epsilon} R_t)]$

Here $C_1 = 2.55, B_{\epsilon} = 0.1069, C_{\omega} = 0.83$

Turbulence models for bend pipe flow

—Curvature-corrected k-ε models (2)

Linear low-Re turbulence model (Rai et al. 2006)

The homogeneous dissipation rate relates with the real dissipation rate through:

$$\bar{\epsilon} = \epsilon - 2\nu \left(\frac{\partial \sqrt{k}}{\partial x_j} \right)^2$$

The damping functions f_μ , f_1 and f_2 are given by

$$f_\mu = \exp[-3.4/(1 + 0.02\bar{R}_t^2)], f_1 = 1, f_2 = 1 - 0.3 \exp(-\bar{R}_t^2)$$

Where $\bar{R}_t = \frac{k^2}{\nu \bar{\epsilon}}$ is the local turbulent Reynolds number

Constants: $C_\mu = 0.09, \sigma_k = 1.0, \sigma_\epsilon = 1.3, \sigma_\Gamma = 0.9 \sim 1, C_{1\epsilon} = 1.43, C_{2\epsilon} = 1.92$

Turbulence models for bend pipe flow

—Curvature-corrected k-ε models (3)

Two-layer linear k-ε model (William D. York, et al.2009)

Turbulent kinetic energy transport equation

$$\frac{\partial(\bar{\rho}k)}{\partial t} + \frac{\partial}{\partial x_j}(\bar{\rho}U_jk) = \frac{\partial}{\partial x_j}[(\mu + \frac{\mu_T}{Pr_k})\frac{\partial k}{\partial x_j}] + [2\mu_T(S_{\psi\psi} - \frac{1}{3}\delta_{\psi\psi}\frac{\partial U_1}{\partial x_1}) - \frac{2}{3}\bar{\rho}k\delta_{\psi\psi}]\frac{\partial U_i}{\partial x_j} - \bar{\rho}\epsilon$$

Turbulent dissipation rate transport equation

$$\frac{\partial(\bar{\rho}\epsilon)}{\partial t} + \frac{\partial}{\partial x_j}(\bar{\rho}U_j\epsilon) = \frac{\partial}{\partial x_j}[(\mu + \frac{\mu_T}{Pr_\epsilon})\frac{\partial \epsilon}{\partial x_j}] + C_{\epsilon 1}\frac{\epsilon}{k}[2\mu_T(S_{\psi\psi} - \frac{1}{3}\delta_{\psi\psi}\frac{\partial U_1}{\partial x_1}) - \frac{2}{3}\bar{\rho}k\delta_{\psi\psi}]\frac{\partial U_i}{\partial x_j} - C_{\epsilon 2}\bar{\rho}\frac{\epsilon^2}{k}$$

Turbulent stress (Boussinesq's Assumption)

$$-\overline{\rho u_i u_j} = 2\mu_T S_{\psi\psi} - \frac{2}{3}\delta_{\psi\psi}(\mu_T\frac{\partial U_1}{\partial x_1} + \bar{\rho}k)$$

Turbulent viscosity

$$\mu_T = C_\mu \bar{\rho} \frac{k^2}{\epsilon}$$

Turbulent viscosity coefficient

$$C_\mu = \frac{K_1 + K_2 C_\mu (\frac{Sk}{\epsilon})^2 + K_3 C_\mu (\frac{Sk}{\epsilon}) + K_4 C_\mu^2 (\frac{Sk}{\epsilon})^3}{K_5 + K_6 C_\mu (\frac{Sk}{\epsilon})^2 + K_7 C_\mu^2 (\frac{Sk}{\epsilon})^4 + K_8 (\frac{Wk}{\epsilon})^2}$$

Where

$$S = \sqrt{2S_{\psi\psi}S_{\psi\psi}}, W = \sqrt{2W_{\psi\psi}W_{\psi\psi}}$$

Modified flow rotation term

$$W = \left| S \cdot \left(1 - \frac{C_4 - 4}{C_4 - 2}\right) + \Omega \cdot \frac{C_4 - 4}{C_4 - 2} \right| = \left| \frac{9}{4}\Omega - \frac{5}{4}S \right|$$

Where the relative fluid rotation rate magnitude computed in an inertial frame is:

$$\Omega = \sqrt{2\Omega_{\psi\psi}\Omega_{\psi\psi}}$$

Model turbulent length scale

$$L_T = \min\left(\frac{C_{LY} k^{3/2}}{\epsilon}\right)$$

Turbulence models for bend pipe flow

—Curvature-corrected k-ε models (4)

Two-layer linear k-ε model (William D. York, et al.2009)

Near-wall turbulent dissipation rate (when $\frac{C_{DY}}{\varepsilon}$ is minimum)

$$\varepsilon = \frac{k^{3/2}}{l_\varepsilon}$$

Where $l_\varepsilon = C_{DY}[1 - \exp(-\frac{Re_y}{A_\varepsilon})]$

Near-wall turbulent viscosity (when $\frac{C_{DY}}{\varepsilon}$ is minimum)

$$\mu_T = C_{\mu\bar{p}}\sqrt{k}C_{DY}[1 - \exp(-\frac{Re_y}{A_\varepsilon})],$$

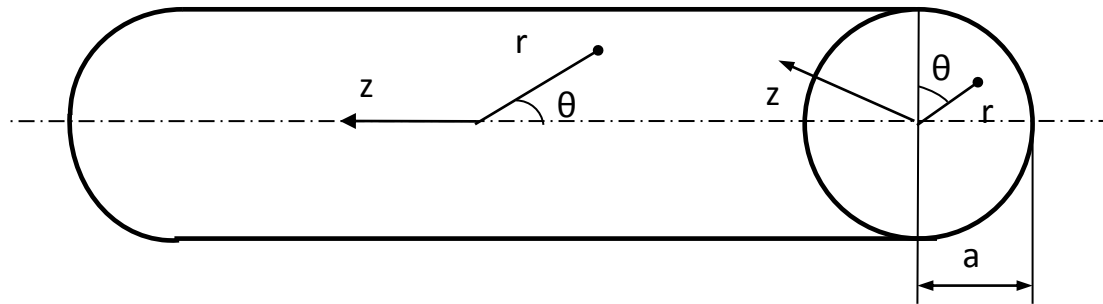
Where $Re_y = \frac{\sqrt{k}y}{\nu}$

Model constants

$$Pr_k = 1.0, Pr_\varepsilon = 1.19, C_{\varepsilon 1} = 1.44, C_{\varepsilon 2} = 1.92, K_1 = 0.66, K_2 = 3.9, K_3 = 1.0, K_4 = 5.3, K_5 = 2.9, \\ K_6 = 17.0, K_7 = 10.0, K_8 = 3.84, C_4 = 0.4, C_I = 2.495, A_\varepsilon = 4.99, A_\mu = 25.0$$

Turbulence models for bend pipe flow

—Curvature-corrected k- ϵ models (5)



Cylindrical Coordinate System

r : distance from the center of the cross-section of the pipe;

θ : angle between the radius vector and the normal to the plane of symmetry;

z : stream-wise direction.

Bend:

Inlet at $z=0$; outlet at $z= R_c \cdot \text{bend angle}$

Where R_c is curvature radius

Outline

- Hg supply piping in Muon Collider
- Turbulence models for bend pipe flow
- **Problems need studying**
- Arrangements in the near future

Hg supply piping in Muon Collider

— Problems need studying (1)

Influence of nozzle upstream on jet exit

- Bend curvature
- Bend angle

Influence of nozzle shapes on jet exit

- Nozzle length
- Nozzle taper

Turbulence level of the jet exit



Hg supply piping in Muon Collider

— Problems need studying (2)

Parameters' Range

The size of the curved bend is limited by the solenoid bore ($d=15\text{cm}$)

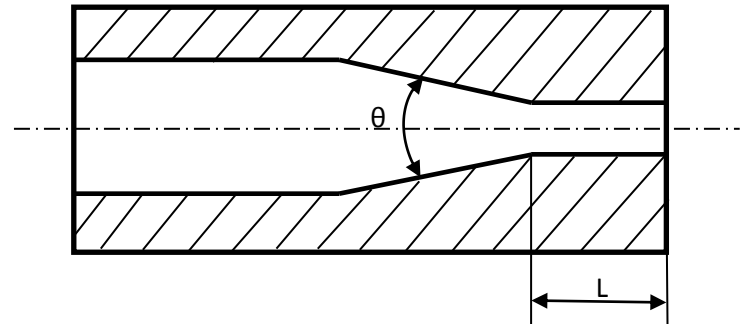
$ID_{\text{pipe}} = 0.884 \text{ inch} \approx 2.25\text{cm}$

Bend curvature (δ): $\delta < 15/2.25 \approx 6.6$ (U-bend)

Bend angle (α): $0 \leq \alpha < \infty$

Nozzle taper* (θ): $6^\circ \leq \theta \leq 20^\circ$

Nozzle length* (L): $2 * ID_{\text{pipe}} \leq L \leq 4 * ID_{\text{pipe}}$



Hg supply piping in Muon Collider

— Problems need studying (3)

Turbulence level (turbulence intensity)

$$TI = \frac{u'}{U}$$

$$u' = \sqrt{\frac{1}{3}(u_x'^2 + u_y'^2 + u_z'^2)} = \sqrt{\frac{2}{3}k}$$

$$U = \sqrt{U_x^2 + U_y^2 + U_z^2}$$

Where u' is root-mean-square of the turbulence velocity fluctuations;
 U is the mean velocity (Reynolds averaged)

Outline

- Hg supply piping in Muon Collider
- Turbulence models for bend pipe flow
- Problems need studying
- Arrangements in the near future

Work in near future

1. Grid generation for curved pipe with Gridgen
2. Implement the curvature-corrected k - ϵ models in CFD tool
3. Test the corrected model
4. MHD equations for curved pipe flow (if possible)

Nomenclature

AR	Aspect ratio $AR = H/D$
D	Hydraulic diameter (m)
De	Dean number $De = Re(D/2R_c)^{1/2}$
I	Turbulence intensity (%)
k	Turbulence kinetic energy (m^2/s^2)
P	Pressure (N/m^2)
R_c	Radius of curvature of U-bend (m)
Re	Reynolds number, $\rho U_0 H/\mu$
U	Mean streamwise velocity component (m/s)
U_0	Average inlet velocity (m/s)
$\overline{u_i u_j}$	Reynolds stress tensor
V	Mean transverse velocity component (m/s)
x	Streamwise direction
y	Spanwise direction
z	Direction normal to the duct symmetry plane

Greek Letters

δ_{ij}	Kronecker delta
ϵ	Dissipation rate (m^2/s^2)
μ	Laminar viscosity of fluid ($Pa \cdot s$)
μ_t	Turbulent viscosity of fluid ($Pa \cdot s$)
ρ	Density of fluid (kg/m)

Abbreviation

EASM	Explicit Algebraic Stress Model
TCL SMC	Two Component Limit Second Moment Closure Model
LES	Large Eddy Simulations
NLEVM	Nonlinear Eddy Viscosity Turbulence Model
RSM	Reynolds Stress Model
RNG	Renormalization-group $k - \epsilon$ model
RKE	Realizable $k - \epsilon$ model
SKE	Standard $k - \epsilon$ model
EARSM	Explicit Algebraic Reynolds Stress Model

Literature review of turbulent flow in curved ducts

Existing experimental studies of the turbulent flow in curved ducts

Authors	Year	R_c/D	Re	De	Cross-section (angle)
Rowe ^[1]	1970	12	2.36×10^5	4.8×10^4	Circular (U)
Chang et al. ^[2]	1983	3.357	5.67×10^4	2.1×10^4	Square (U)
Azzola et al. ^[3]	1986	3.375	$5.74 \times 10^4 - 1.1 \times 10^5$	2.2×10^4	Circular (U)
Sandborn, Shin ^[4]	1989	1	$7 \times 10^4 - 5 \times 10^5$	$4.95 \times 10^4 - 3.535 \times 10^5$	Rectangular, $AS = 10$ (U)
Taylor ^[23]	1982	2.3	4×10^4	1.86×10^4	Square (90°)
Answer et al. ^[5]	1989	6.5	5×10^4	13868	Circular (U)
Enayet et al. ^[21]	1982	2.8	4.3×10^4	1.82×10^4	Circular (90°)
Monson, Seegmiller ^[6]	1992	1	$10^5, 10^6$	$7.07 \times 10^4, 7.07 \times 10^5$	Rectangular, $AS = 10$ (U)
Cheah et al. ^[7]	1996	0.65	10^5	8.77×10^4	Square (U)
Sudo et al. ^[20]	1998	4.0	6×10^4	2.12×10^4	Circular(90°)
Sudo et al. ^[8]	2000	2.0	6×10^4	3×10^4	Circular (U)
Lee et al. ^[9]	2007	3.357	5.74×10^4	2.2×10^4	Circular (U)

Where R_c the radius of the pipe centerline,

D the pipe diameter (for rectangular duct, D the duct width and H the duct height),

Dean number is defined as $De = Re(D/2R_c)^{0.5}$

Re is the Reynolds number $Re = \rho U_0 H / \mu$.

In the curved part of the U-bend, the cylindrical coordinate (r, θ, z) corresponds to spanwise, streamwise, and normal directions, with $\theta = 0^\circ$ at the beginning of the curve.

Author: Rowe

Year: 1970

Title: Measurements and Computations of Flow in Pipe Bends

Journal: Journal of Fluid Mechanics, Vol. 43, Part 4, pp. 771-783.

Problem: Experimental data for turbulent flow of 180° bend pipe in the early stage. ($Re = 2.36 \times 10^5$; $R_c/D = 12$)

Results: The secondary flows cause a complete interchange of the slow moving wall fluid and the faster central core, in an S-bend. Also, he reported that the reversed flow of the secondary flow was generated locally near the bend angle 90° for the turbulent flow of 180° bend tube under the condition of Reynolds number 2.36×10^5 .

Author: M. M. Enayet, M. M. Gibson, A. M. K. P. Taylor and M. Yianneskis

Year: 1982

Title: Laser-doppler measurements of laminar and turbulent flow in a pipe bend

Journal: International Journal of Heat and Fluid Flow, Vol.3, issue4, 213–219.

Problem: Laser-Doppler measurements are reported for laminar and turbulent flow through a 90° bend of circular cross-section.

(laminar: $Re = 500, 1093$; turbulent: $Re = 4.3 \times 10^4$; $R_c/D = 2.8$)

Results: The results show the development of strong pressure-driven secondary flows in the form of a pair of counter-rotating vortices in the streamwise direction. The strength and character of the secondary flows were found to depend on the thickness and nature of the inlet boundary layers, inlet conditions which could not be varied independently of Reynolds number.

Author: Chang et al.

Year: 1983

Title: Measurements and Computations of Flow in Pipe Bends

Journal: PhysicoChemical Hydrodynamics, Vol. 4, No. 3, pp. 243-269.

Problem: 180° U-bend flow with a long upstream section which was used to develop an essentially fully-developed flow at the inlet in which the boundary layers completely filled the duct. ($Re = 5.67 \times 10^4$; $R_c/D = 3.357$)

Results: From the bend entry to the 90° plane the destabilizing effects of the curvature at the concave wall were shown by the increase in the measured Reynolds stresses in this region. Between 90° and 180° striking variations in the Reynolds stresses were measured in the radial direction.

Author: Azzola et al

Year: 1986

Title: Measurements and Computations of Flow in Pipe Bends

Journal: ASME Journal of Fluids Engineering, Vol. 108, pp. 214-221.

Problem: 180° bend flow with circular cross section. ($Re = 5.74 \times 10^4 - 1.1 \times 10^5$; $R_c/D = 3.357$)

Results: The flow produced in this configuration was quite different from the flow in a square U-bend. In a circular cross-section U-bend the anisotropies between the normal stresses (generated at the corners of a square

cross-section duct) which modified the secondary motion were not present. However, the strong cross-stream pressure gradients remained. The experiments showed that between $45^\circ - 135^\circ$ the cross-stream secondary flow was reversed and redirected back towards the inner wall (in the inner half of the flow). Hence, there were four secondary flow vortices; two each side of the symmetry plane.

Author: Sandborn and Shin

Year: 1989

Title: Water Flow Measurements in a 180 Degree Turn-Around Duct

Journal: Report Prepared under Contract No. NAS8-36354.

Problem: Investigated 10-by-100 centimeter, 180° -turn water tunnel, with a 10cm centerline radius of curvature thus $R_c/D = 1$. Measurements for a range of Reynolds numbers from 70,000 to 500,000 were reported.

Results: The large aspect ratio, $AS = 10$, of the duct produced a quasi-twodimensional flow, fig. 1. At the turn entrance, the flow along the outer concave surface experienced an adverse pressure gradient, which produced a near separation condition for the lowest Reynolds number flow. However, at the higher Reynolds numbers no separation was observed. A separation bubble occurred on the inner convex surface at approximately 150° around the turn. The separation bubble persisted for some distance downstream of the turn exit.

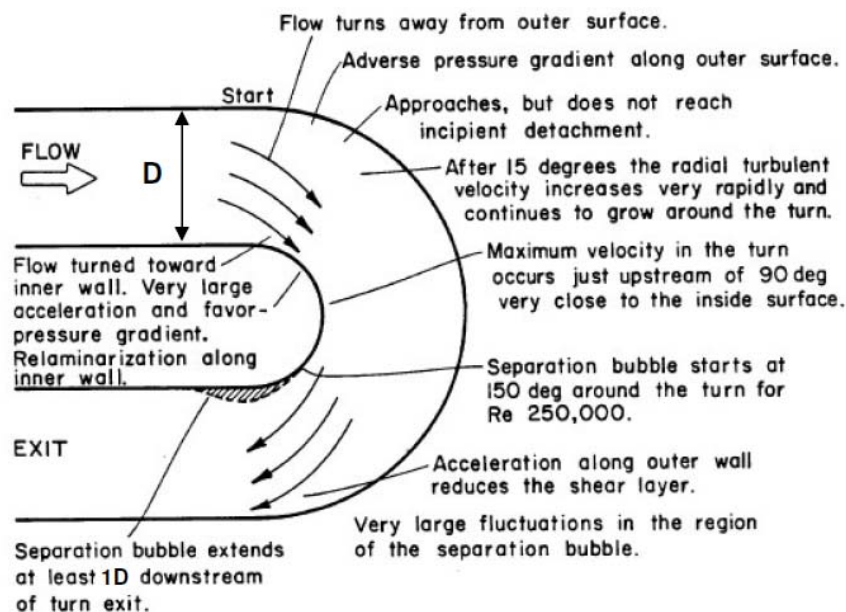


Fig.1 Global characteristics observed in the U-bend, Sandborn and Shin

Author: Anwer et al.

Year: 1989

Title: Perturbation by and Recovery from Bend Curvature of a Fully Developed Turbulent Pipe Flow

Journal: Journal of Physics of Fluids A, Vol. 1, No. 8, pp. 1387-1397.

Problem: Measured the mean flow and turbulence through a U-bend of circular cross section and downstream tangent.

$(Re = 5 \times 10^4; R_c/D = 6.5)$

Results: Contrary to Rowe's^[1] finding; they found that the flow failed to achieve a fully developed state within the U-bend. They concluded that the complete recovery would take more than 18 diameters downstream tangent

of the bend exit.

Author: Monson and Seegmiller

Year: 1992

Title: An Experimental Investigation of Subsonic Flow in a Two-Dimensional U-Duct

Journal: NASA Technical Memorandum 103931.

Problem: Nominally two-dimensional experiment on flow through U-duct. ($Re = 10^5, 10^6; R_c/D = 1$)

Results: The significant observations about the flow were: 1) large turbulence enhancement occurred near the outer (concave) wall; 2) almost total damping of turbulence occurred near the inner (convex) wall; 3) separation, the extent of which increases with increasing Reynolds number, occurred on the inner wall at the bend exit; and 4) high levels of turbulence and unsteadiness occurred in all regions of the flow downstream of the bend.

Author: Sudo et al.

Year: 1998

Title: Experimental Investigation on Turbulent Flow through a Circular-Sectioned 90° Bend

Journal: Experiments in Fluids, Vol. 25, pp. 42-49.

Problem: The steady, turbulent flow in a circular-sectioned 90° bend with smooth walls. The bend had long, straight upstream and downstream pipes

($Re = 6 \times 10^4, 10^6; R_c/D = 4.0$)

Results: The longitudinal, circumferential and radial components of mean and fluctuating velocities, and the Reynolds stresses in the pipe cross section at several longitudinal stations were obtained. The velocity fields of the primary and secondary flows, and the Reynolds stress distributions in the cross section were illustrated. (1) In the inlet region of the bend, the primary flow accelerates near the inner wall and a secondary flow moving from the outer to the inner wall of the bend occurs in the bend cross section; (2) At station $\phi = 30^\circ$ in the bend, the secondary flow develops into a pair of vortices, as seen in fully developed curved pipe flows, but the primary flow remains deflected toward the inner wall. The Reynolds stress $\overline{w'u'}$ tends to decrease in the inner part of the cross section and $\overline{v'w'}$ increases in the outer part; (3) Between $\phi = 75^\circ$ and 90° , the velocity contours of primary flow are greatly distorted and a depression in the contour plot is formed in the inner part of the bend cross section. The turbulence intensity and the Reynolds stresses increase around the depression of contours, coinciding with the large velocity gradient there; (4) Just behind the bend exit, the primary flow velocity in the central region of the pipe decreases and the correlations of fluctuating velocities exhibit a complicated distribution according to the variation of primary flow velocity profiles; (5) At successive downstream stations, the distribution of primary flow velocity gradually becomes smooth. The secondary flow weakens and vortices break down. The influence of the bend on the flow, however, remains even at $z/d = 10$.

Author: Sudo et al.

Year: 2000

Title: Experimental Investigation on Turbulent Flow through a Circular-Sectioned 180° Bend

Journal: Experiments in Fluids, Vol. 28, pp. 51-57.

Problem: Steady, developing turbulent flow in a circular sectioned 180° bend. ($Re = 6 \times 10^4; R_c/D = 2.0$)

Results: They measured the longitudinal, radial and circumferential components of mean velocity, and

corresponding components of the Reynolds stress at various longitudinal stations. In the section between $\theta = 40^\circ$ and 60° , two vortices in the cross section were developed rapidly and accordingly the fluid with high velocity near the inner wall was transported towards the outer wall by the secondary flow. Meanwhile, the fluid near the upper and lower walls, the momentum of which was small in the longitudinal direction, was forced inwardly along the walls by the vivid secondary flow. In the section from the bend angle of 90° , the high-velocity regions occurred near the upper and lower walls as a result of strong secondary flow and the turbulence with high level emerged in the central region of the bend. Just behind the bend exit, an additional pair of vortices appeared in the outer part of the cross section owing to the transverse pressure difference. In the downstream tangent, the flow returned slowly to the proper flow in a straight pipe.

Author: Lee, G.H. et al.

Year: 2007

Title: Measurement of Developing Turbulent Flow in a U-Bend of Circular Cross-Section

Journal: Journal of Mechanical Science and Technology, Vol. 21, No. 2, pp. 348- 359.

Problem: Hot-wire measurements of the full mapping of the velocity and Reynolds stress components for developing turbulent flow in a strongly curved 180° pipe and its tangents. ($Re = 5.74 \times 10^4$; $R_c/D = 3.357$)

Results: The strength of secondary flow was reached up to the 35% of bulk mean velocity. The strong counter-rotating vortex pair induced by the transverse pressure gradient and centrifugal force imbalance was grown up to $\theta = 67.5^\circ$ into the bend. But the counter-rotating vortex pair was broken down into two cell pattern after $\theta = 67.5^\circ$ of the bend. Significant double maxima in the streamwise velocity profiles were appeared in the bend region due to the breakdown of counter-rotating vortex pair. In the bend, the mean longitudinal velocity component was changed little after $\theta = 90^\circ$, but secondary flow never achieved fully-developed state. Similar behavior was observed in the normal and circumferential stresses.

Existing numerical studies of the turbulent flow in curved ducts

The problem of numerical simulation of developing flow in U-bend has been the subject of considerable research for the past twenty years

Authors	Year	Turbulence Model	Near Wall Treatment	Cross-Section	Re	De
Patankar et al. ^[18]	1975	$k - \varepsilon$ model	Wall function	Circular	2.36×10^5	3.41×10^4
Kreskovsky et al. ^[22]	1981	Simple mean field closure model for Reynolds stresses	- - -	Square (90°)	4×10^4	26370
Chang et al. ^[2]	1983	Standard $k - \varepsilon$ model	$W\eta$	Square(U)	5.67×10^4	2.1×10^4
Azzola et al. ^[3]	1986	Standard $k - \varepsilon$ model	MLH Van Driest damping	Square (90°)	5.74×10^4	2.22×10^4
Iacovides et al. ^[24]	1987	Standard $k - \varepsilon$ model	MLH	Square (90°)	4×10^4	26370
Choi et al. ^[10]	1989	$k - \varepsilon$ model and ASM	MLH	Square (U)	5.8×10^4	2.23×10^4
Iacovides et al. ^[11]	1990	ASM	MLH Van Driest damping			
Rumsey et al. ^[12]	2000	EASM and one and two-equation eddy viscosity model	- - -			
Suga ^[13]	2003	TCL SMC and Shima Model	- - -	Square(mild) Square(strong)	5.67×10^4 10^5	2.1×10^4 8.77×10^4
Sugiyama et al. ^[14]	2005	ASM	Wall function		6×10^4	2.12×10^4
Raisee et al. ^[25]	2006	Cubic non-linear low-Re $k - \varepsilon$ model	- - - - - -	Square(90°) Rectangular	4×10^4 2.24×10^5	26370 91447
Münch, Métais ^[15]	2007	LES	- - -	Square(U)	6×10^4	2.27×10^4 1.66×10^4 1.31×10^4
Xu et al. ^[16]	2008	NLEVM, EASM and RSM	Wall function	2D U-duct	10^6	7.07×10^5
Djebedjian et al. ^[17]	2008	$k - \varepsilon$ model, RNG model, Realizable $k - \varepsilon$ model, $k - \omega$ model and RSM	- - - - - -	Square(mild) Square(strong)	5.67×10^4 10^5	2.1×10^4 8.77×10^4
William, et al. ^[19]	2009	Linear $k - \varepsilon$ model	Two-layer near-wall		10^6	5×10^5

Author: S.V.Patankar, D.B.Spalding

Year: 1975

Title: Prediction of turbulent flow in curved pipes

Journal: J. Fluid Mech., Vol. 67, 583-595,

Problem: Finite difference procedure to predict the development of turbulent flow in curved pipes. ($Re = 2.36 \times 10^5$; $R_c/D = 23.9$)

Model: $k - \epsilon$ turbulence model + wall function

Equations: The turbulence model used involves the solution of two differential equations, one for kinetic energy and the other for its dissipation rate. Wall functions were used to specify the near-wall velocity, shear stress, dissipation rate and dissipation term.

The equations are described in toroidal coordinate (r, ψ, θ) . The flow is treated as parabolic and the diffusion flux in the ψ direction together with terms of small order of magnitude are neglected:

The governing differential equations in the central region of the flow (fully turbulent flows)

$$\frac{\partial U_r}{\partial r} + \frac{U_r}{r} + \frac{U_r \sin \psi}{R + r \sin \psi} + \frac{1}{r} \frac{\partial U_\psi}{\partial \psi} + \frac{U_\psi \cos \psi}{R + r \sin \psi} = 0$$

$$\rho \left(U_r \frac{\partial U_r}{\partial r} + \frac{U_\theta}{r} \frac{\partial U_r}{\partial \theta} - \frac{U_\theta^2}{r} + \frac{1}{R} \frac{\partial U_r}{\partial \psi} - \frac{U_\psi^2 \cos \theta}{R} \right) = -\frac{\partial P}{\partial r} + \frac{\partial \tau_{rr}}{\partial r} + \frac{1}{r} \frac{\partial \tau_{r\theta}}{\partial \theta} - \frac{\tau_{\theta\theta}}{r} + \frac{\tau_{rr}}{r} - \frac{\tau_{\psi\psi}}{R} \cos \theta + \frac{\tau_{rr}}{R} \cos \theta - \frac{\tau_{r\theta}}{R} \sin \theta$$

$$\rho \left(U_r \frac{\partial U_\theta}{\partial r} + \frac{U_\theta}{r} \frac{\partial U_\theta}{\partial \theta} + \frac{U_r U_\theta}{r} + \frac{U_\psi}{R} \frac{\partial U_\theta}{\partial \psi} + \frac{U_\psi^2 \sin \theta}{R} \right) = -\frac{1}{r} \frac{\partial P}{\partial \theta} + \frac{\partial \tau_{r\theta}}{\partial r} + \frac{1}{r} \frac{\partial \tau_{\theta\theta}}{\partial \theta} + \frac{2\tau_{r\theta}}{r} + \frac{r}{R^2} \tau_{\theta\psi} \sin \theta + \frac{\tau_{r\theta}}{R} \cos \theta - \frac{\tau_{\theta\theta}}{R} \sin \theta$$

$$\rho \left[U_r \frac{\partial U_\psi}{\partial r} + \frac{U_\theta}{r} \frac{\partial U_\psi}{\partial \theta} + \frac{U_\psi}{R} \frac{\partial U_\psi}{\partial \psi} + \frac{U_\psi}{R} \left(\frac{U_r \cos \theta - U_\theta \sin \theta}{R} \right) \right] = -\frac{1}{R} \frac{\partial \bar{P}}{\partial \psi} + \frac{\partial \tau_{r\psi}}{\partial r} + \frac{\tau_{r\psi}}{R} \cos \theta + \frac{1}{r} \frac{\partial \tau_{\psi\theta}}{\partial \theta} - \frac{\tau_{\theta\psi}}{R} \sin \theta + \frac{\tau_{r\psi}}{r}$$

$$\rho \left(U_r \frac{\partial k}{\partial r} + \frac{U_\theta}{r} \frac{\partial k}{\partial \theta} + \frac{U_\psi}{R} \frac{\partial k}{\partial \psi} \right) = \frac{1}{r} \frac{\partial}{\partial r} \left(\frac{\mu_t}{\sigma_k} r \frac{\partial k}{\partial r} \right) + \frac{\mu_t}{R \sigma_k} \left(\frac{\partial k}{\partial r} \cos \theta - \frac{\partial k}{r \partial \theta} \sin \theta \right) + \frac{\partial}{r^2 \partial \theta} \left(\frac{\mu_t}{\sigma_k} r \frac{\partial k}{\partial \theta} \right) + G - \rho \epsilon$$

$$\rho \left(U_r \frac{\partial \epsilon}{\partial r} + \frac{U_\theta}{r} \frac{\partial \epsilon}{\partial \theta} + \frac{U_\psi}{R} \frac{\partial \epsilon}{\partial \psi} \right) = \frac{1}{r} \frac{\partial}{\partial r} \left(\frac{\mu_t}{\sigma_\epsilon} r \frac{\partial \epsilon}{\partial r} \right) + \frac{\mu_t}{R \sigma_\epsilon} \left(\frac{\partial \epsilon}{\partial r} \cos \theta - \frac{\partial \epsilon}{r \partial \theta} \sin \theta \right) + \frac{\partial}{r^2 \partial \theta} \left(\frac{\mu_t}{\sigma_\epsilon} r \frac{\partial \epsilon}{\partial \theta} \right) + C_1 \frac{\epsilon}{k} G -$$

Shear stress

$$\tau_{ij} = (\mu_l + \mu_t) D_{ij}$$

Where

μ_l is the molecular viscosity of the fluid (assumed constant throughout the pipe cross-section).

$$\mu_t = C_\mu \rho k^2 / \epsilon$$

$\{D_{ij}\}$ is the deformation tensor,

Expanding D_{ij} in the (r, ψ, θ) coordinate

$$\tau_{rr} = 2\mu \frac{\partial U_r}{\partial r},$$

$$\tau_{r\theta} = \mu \left(\frac{\partial U_r}{r \partial \theta} - \frac{U_\theta}{r} + \frac{\partial U_\theta}{\partial r} \right) = \tau_{\theta r},$$

$$\tau_{r\psi} = \mu \left(\frac{\partial U_r}{r \partial \psi} - \frac{U_\psi \cos \theta}{R} + \frac{\partial U_\psi}{\partial r} \right) = \tau_{\psi r},$$

$$\tau_{\theta\psi} = \mu \left(\frac{\partial U_\psi}{r \partial \theta} + \sin \theta \frac{U_\psi}{R} + \frac{\partial U_\theta}{R \partial \psi} \right) = \tau_{\psi \theta},$$

$$\tau_{\psi\psi} = 2\mu \left(\frac{\partial U_\psi}{R \partial \psi} + \frac{1}{R} (U_r \cos \theta - U_\theta \sin \theta) \right),$$

$$\tau_{\theta\theta} = 2\mu \left(\frac{\partial U_\theta}{r \partial \theta} + \frac{U_r}{r} \right),$$

$$G = \mu_t \left\{ 2 \left[\left(\frac{\partial U_r}{\partial r} \right)^2 + \left(\frac{\partial U_\theta}{r \partial \theta} \right)^2 + \left(\frac{U_r}{r} \right)^2 + \frac{2}{r^2} U_r \frac{\partial U_\theta}{\partial \theta} - \frac{U_\theta}{r} \left(\frac{\partial U_r}{r \partial \theta} + \frac{\partial U_\theta}{\partial r} \right) \right] + \left(\frac{\partial U_\theta^2}{\partial r} + \frac{\partial U_r}{r \partial \theta} \right) \right. \\ \left. + \left(\frac{\partial U_\psi^2}{\partial r} \right) + \left(\frac{\partial U_\psi}{r \partial \theta} \right)^2 + \frac{U_\theta^2}{r^2} + \frac{U_\psi^2}{R^2} + \frac{2}{R} U_\psi \left(\frac{\partial U_\psi}{r \partial \theta} \sin \theta - \frac{\partial U_\psi}{\partial r} \right) \right\}$$

With constants: $C_\mu = 0.09$, $C_1 = 1.47$, $C_2 = 1.92$, $\sigma_k = 1.0$, $\sigma_\epsilon = 1.3$

Wall regions (low Reynolds number of turbulence $\rho k^{1/2} l / \mu_l$, where $l = k^{3/2} / \epsilon$)

Point P is located sufficiently far from the wall for the local turbulent Reynolds number $(\rho k^{1/2} l / \mu_l)_P$ to be much greater than unity. It is then assumed that a logarithmic velocity profile prevails in the region between the wall and the node P, the expression for the velocity being

Near-wall shear stress

$$\tau_P = \frac{\rho \kappa C_\mu^{1/4} k_P^{1/2} U_P}{\ln(E y_P C_\mu^{1/4} k_P^{1/2} / \mu_l)}$$

Where the subscript P indicates values at grid node P,

y_P is the distance of P from the wall,

κ and E are the log-law constants.

Near-wall shear stress kinetic dissipation rate (the length scale varies linearly with the distance from the wall)

$$\epsilon_P = C_\mu^{3/4} k_P^{3/2} / \kappa y_P$$

Where k_P represents the turbulent kinetic energy near the wall and is calculated from the regular balance equation, the diffusion of energy being set equal to zero. The dissipation term in the kinetic-energy equation is assigned an average value over the control volume for the node near the wall,

$$\rho \bar{\epsilon} = \rho \int_0^{y_N} \epsilon dy = C_\mu^{3/4} k_P^{3/2} \int_0^{y_N} \frac{1}{\kappa y} dy$$

Results: The agreement of predicted total-velocity contours with Rowe's^[1] measurements for the developing flow in a 180° bend is fairly satisfactory: for both of the predictions and the experiments, the velocity field is distorted with the velocity maximum shifted to the outside of the bend; The secondary velocities increase up to a distance of 30° and then decrease, owing to the production of streamwise vorticity of opposite sign. The predictions also display such a reduction in the secondary flow.

Author: Kreskovsky, J.P., Briley, W.R., McDonald, H.

Year: 1981

Title: Prediction of laminar and turbulent primary and secondary flows in strongly curved ducts

Journal: NASA Report, No. CR.3388

Problem: Employed a simple closure model for the Reynolds stresses to predict the 90° bend flow of square cross-section.

($Re = 4 \times 10^4$; $R_c/D = 1.15$)

Model: Simple mean field closure model for Reynolds stresses

Equations:

Results: Good agreement was achieved compared with Taylor's experiment, though there was insufficient growth of the boundary layer on the convex inner surface toward the end of the bend where the flow on that surface encountered a substantial adverse pressure gradient.

Author: Iacovides H, Launder B.E., Loizou P.A.

Year: 1987

Title: Prediction of laminar and turbulent primary and secondary flows in strongly curved ducts

Journal: NASA Report, No. CR.3388

Problem: Using a two-layer EVM (effective viscosity model), to performed numerical computations for a 90° bend flow of square cross-section. ($Re = 4 \times 10^4$; $R_c/D = 1.15$)

Model: Standard $k - \epsilon$ model + MLH

Equations: Standard $k - \epsilon$ eddy-viscosity was employed for the main flow region, while the mixing-length hypothesis was used across the low-Re near-wall region

Results: The computational results showed that the curvature induces a pair of counter-rotating vortices within the duct cross-section.

Conclusions: The level of agreement was better than obtained by Kreskovsky et al.

Author: S.M. Chang, J.A.C. Humphrey, A. Modavi,

Year: 1983

Title: Turbulent Flow in a Strongly Curved U-bend and Downstream Tangent of Square Cross-Sections

Journal: PhysicoChemical Hydrodynamics, Vol. 4, No. 3, pp. 243-269.

Problem: Using a two-layer EVM (effective viscosity model), to performed numerical computations for a U-bend flow of square cross-section. ($Re = 5.67 \times 10^4$; $R_c/D = 3.645$)

Model: High-Reynolds-number linear $k - \epsilon$ model + wall function

Equations: Two-equation high-Reynolds-number linear $k - \epsilon$ model to calculate the flow, using wall functions to specify the near-wall velocity and turbulence conditions. To reduce the computational requirements, a semi-elliptic procedure was adopted which required only the pressure to be stored over the whole domain. Other variables (U, V, k, ϵ) were calculated on a plane by plane basis, with the code "sweeping" through the planes in the streamwise direction.

Results: As the numerical model employed was isotropic, the redistributive effects of the cross-stream normal stresses were not present and the minima in the streamwise velocity between 90° and 130° were not predicted. They also failed to calculate the vortex at the convex (inner) wall corner which was associated with local separation.

Author: Azzola, J., Humphrey, J.A.C., Iacovides, H., and Launder, B.E.

Year: 1986

Title: Turbulent Flow in a Strongly Curved U-bend and Downstream Tangent of Square Cross-Sections

Journal: PhysicoChemical Hydrodynamics, Vol. 4, No. 3, pp. 243-269.

Problem: Incorporated some important improvements to their numerical model, over that used previously by Chang et al. ($Re = ; R_c/D =$)

Model: High-Reynolds-number linear $k - \varepsilon$ model + zonal model (MLH with VanDriest damping term)

Equations: Semi-elliptic linear $k - \varepsilon$ model was retained, but the wall functions were dropped and a zonal model was applied, extending a fine grid right up to the wall. In the wall-region the Mixing Length Hypothesis (MLH) was employed with a Van Driest damping term.

Conclusions: On the whole, the semi-elliptic linear $k - \varepsilon$ model calculated the flow, including the secondary motions, reasonably well. As expected the levels of secondary flow induced in the U-bend were less than those present in a square sectioned U-bend.

Author: Choi, Y-D., Iacovides, H., and Launder, B.E.

Year: 1989

Title: Numerical Computation of Turbulent Flow in a Square Cross-Sectioned 180° Bend

Journal: ASME Journal of Fluids Engineering, Vol. 111, pp. 59-68.

Problem: Used the $k - \varepsilon$ model and Algebraic Stress Model (ASM) for the numerical calculations of the square sectioned U-bend

($Re = 5.8 \times 10^4; R_c/D = 3.357$)

Model: High-Reynolds-number linear $k - \varepsilon$ model + zonal model (MLH with VanDriest damping term)

Equations: Semi-elliptic linear $k - \varepsilon$ model was retained, but the wall functions were dropped and a zonal model was applied, extending a fine grid right up to the wall. In the wall-region the Mixing Length Hypothesis (MLH) was employed with a Van Driest damping term.

Results: At the 130° station in the bend the model with the ASM predicted a complex flow pattern with four vortices either side of the symmetry plane. (The linear $k - \varepsilon$ /MLH model predicted three vortices; the linear $k - \varepsilon$ /wall function model predicted two). Whilst the experimental measurements were too coarse to compare the measured and calculated secondary flow profiles in detail, it seemed highly likely that the four-vortex pattern was indeed accurate due to the improvements in predicting the streamwise velocity profiles.

Conclusions: Calculations using an Algebraic Stress Model (ASM) in place of the linear $k - \varepsilon$ model improved the predicted flow further.

Author: Iacovides, H., Launder, B.E., Loizou, P.A., and Zhao, H.H.

Year: 1990

Title: Turbulent Boundary-Layer Development around a Square-Sectioned UBend: Measurements and Computation

Journal: ASME Journal of Fluids Engineering, Vol. 112, pp. 409-415.

Problem: Carried out calculations on the square sectioned U-bend with thin boundary layers ($0.15D$) at the bend inlet.

Model: Semi-elliptic ASM + MLH with VanDriest damping term

Equations:

Results: The flow profile was calculated at least as well as by Choi et al.^[10], when they had calculated the flow with fully developed inlet conditions. However, the secondary flow plot at 135° showed five vortices either side of the symmetry plane, and so despite the lower amount of Reynolds stress anisotropy and secondary flow at

the inlet to the bend, the flow seemingly broken down into an even more complex secondary flow pattern. Choi et al.^[10] noted that this breakdown of the classic single secondary vortex occurred later in the calculations than in the measurements.

Author: Rumsey, C.L., Gatski, T.B.

Year: 2000

Title: Turbulence Model Prediction of Strongly Curved Flow in a U-Duct

Journal: AIAA Journal, Vol. 38, No. 8, pp. 1394-1402.

Problem: Studied the ability of three types of turbulence models to predict the effects of curvature on the flow in a U-duct ($Re = ; R_c/D =$)

Model: EASM, one- or two-equation eddy viscosity models

Equations:

Conclusions: The Explicit Algebraic Stress Model (EASM) performed better than one- or two-equation eddy viscosity models, provided that the variation of the production-to-dissipationrate ratio in the flow was accounted in the EASM formulation.

Author: Suga, K.

Year: 2003

Title: Predicting Turbulence and Heat Transfer in 3-D Curved Ducts by Near-Wall Second Moment Closures

Journal: AIAA Journal, Vol. 38, No. 8, pp. 1394-1402.

Problem: Predicted turbulence and heat transfer in two types of square sectioned U-bend duct flows using two versions of the wall-reflection free low-Reynolds-number second moment closures (mild: $Re = 5.67 \times 10^4, R_c/D = 3.357$; strong: $Re = 10^5, R_c/D = 0.65$)

Model: TCL SMC and Shima model

Equations: Component Limit Second Moment Closure (TCL SMC) turbulence model and the Shima model are used. For the turbulent heat transfer fields, the standard and the higher order generalized gradient diffusion hypothesis (GGDH) heat flux models were respectively coupled with the Shima and the TCL SMCs.

Conclusions: The prediction by the TCL SMC was generally reliable for the flow fields in the U-bend ducts with both curvature ratios. Its overall performance was better than the one by the Shima model.

Author: Sugiyama, H., and Hitomi, D.

Year: 2005

Title: Numerical Analysis of Developing Turbulent Flow in a 180° Bend Tube by an Algebraic Reynolds Stress Model

Journal: International Journal for Numerical Methods in Fluids, Vol. 47, pp. 1431-1449.

Problem: Numerical analysis for three dimensional developing turbulent flow in a U-bend with circular cross-section using an algebraic Reynolds stress model. ($Re = 6 \times 10^4; R_c/D = 4$)

Model: ASM + wall function

Equations:

Results: Calculated results were compared with available experimental data. The calculated results showed a comparatively good agreement with the experimental data of the time-averaged velocity and the secondary vectors in both the bent tube and straight outlet sections. For example, the location of the maximum streamwise velocity, which appeared near the top or bottom wall in the bent tube, was predicted correctly by their method.

Conclusions: The prediction by the TCL SMC was generally reliable for the flow fields in the U-bend ducts with both curvature ratios. Its overall performance was better than the one by the Shima model.

Author: Münch, C., and Métais, O.

Year: 2007

Title: Large Eddy Simulations in Curved Square Ducts: Variation of the Curvature Radius

Journal: Journal of Turbulence, Vol. 8, No. 28, pp. 1-18.

Problem: Investigated numerically the influence of the curvature radius R_c on the flow carrying out three Large Eddy Simulations (LES) for U-bends with $R_c/D_h = 3.5, 6.5$ and 10.5 . ($Re = 6 \times 10^4$)

Model: Large Eddy Simulations

Equations:

Results: Decrease of the curvature radius was accompanied by a strong intensification of the secondary transverse flows. They also showed that the secondary flows strength was directly related to the radial pressure gradient intensity.

Conclusions: The prediction by the TCL SMC was generally reliable for the flow fields in the U-bend ducts with both curvature ratios. Its overall performance was better than the one by the Shima model.

Author: Xu, J.I., Ma, H.Y., and Huang, Y.N.

Year: 2008

Title: Nonlinear Turbulence Models for Predicting Strong Curvature Effects

Journal: Applied Mathematics and Mechanics - English Edition - Shanghai, Vol. 29, No. 1, pp. 31-42.

Problem: Analyzed the curvature effects on the structure of turbulence and conducted numerical simulations of a turbulent U-duct flow with a number of typical non-linear eddy viscosity turbulence models in order to assess their overall performance. ($Re = 6 \times 10^4, R_c/D_h = 1$)

Model: NLEVM, EASM and RSM

Equations:

Results:

Conclusions: The numerical results showed that a cubic Nonlinear Eddy Viscosity Turbulence Model (NLEVM) that performs considerably well in other benchmark turbulent flows was able to capture the major features of the highly curved turbulent U-duct flow, including the damping of turbulence near the convex wall, the enhancement of turbulence near the concave wall, and the subsequent turbulent flow separation. The predictions of the cubic models were quite close to that of the Reynolds Stress Model (RSM), in relatively good agreement with the experimental data of Monson and Seegmiller.

Author: Djebedjian, B., Mohamed, M.S., and Elsayed, A.

Year: 2008

Title: Numerical studies of curvature effect on turbulent flows in 180° curvature ducts
Journal: Proceedings of IEC 2008, 6th International Engineering Conference, Mansoura/Sharm El-Sheikh, Egypt, 20-23 March, Vol. 2, pp.347-370

Problem: Investigated numerically the two-and three-dimensional incompressible turbulent flow through two types of square sectioned U-bend duct flows with mild and strong curvatures (mild: $Re = 5.67 \times 10^4, R_{c1}/D = 3.357$; strong: $Re = 5.67 \times 10^5, R_{c2}/D = 0.65$). Calculations were carried out using the flow analysis program FLUENT.

Model: Standard $k - \epsilon$ model, Renormalization-group (RNG) $k - \epsilon$ model, Realizable $k - \epsilon$ model, $k - \omega$ model and RSM

Equations:

$$\text{Continuity: } \frac{\partial \rho}{\partial t} + \frac{\partial}{\partial x_j}(\rho u_j) = 0$$

$$\text{Momentum: } \rho \left(\frac{\partial u_i}{\partial t} + u_j \frac{\partial u_i}{\partial x_j} \right) = -\frac{\partial P}{\partial x_i} + \frac{\partial}{\partial x_i} \left[\mu \left(\frac{\partial u_i}{\partial x_j} + \frac{\partial u_j}{\partial x_i} - \frac{2}{3} \delta_{ij} \frac{\partial u_k}{\partial x_k} \right) \right] + \frac{\partial}{\partial x_i} (-\overline{\rho u_j u_i})$$

Where u_i is the mean velocity vector

δ_{ij} is the Kronecker delta

$\overline{u_j u_i}$ is the unknown Reynolds stress tensor

Conclusions: All models managed to mimic the general flow patterns and to predict a later separation position than the experiment. The reattachment lengths predicted by all models were overpredicted. More advanced turbulence model such as the Reynolds stress model and RNG $k - \epsilon$ model had more reliable numerical results especially at separation zone. All models give more reliable results in the three-dimensional analysis in comparison with twodimensional.

Author: M. Raisee, H. Aleml and H. Iacovides

Year: 2006

Title: Prediction of developing turbulent flow in 90°-curved ducts using linear and non-linear low-Re $k - \epsilon$ model

Journal: Int. J. Numer. Meth. Fluids 2006; 51:1379–1405

Problem: Numerical prediction of the velocity and pressure fields in flow through two 90°-curved ducts, one of a square cross-section and one of a rectangular cross-section (Square: $Re = 4 \times 10^4, R_c/D_h = 2.3$; Square: $Re = 224000, R_c/D_h = 3$).

Model: Linear and non-linear low-Re $k - \epsilon$ model

Equations: Steady incompressible flow

$$\text{Continuity: } \frac{\partial U_j}{\partial x_j} = 0$$

$$\text{Momentum: } \frac{\partial (U_j U_i)}{\partial x_j} = -\frac{1}{\rho} \frac{\partial P}{\partial x_i} + \frac{\partial}{\partial x_i} (v \frac{\partial U_i}{\partial x_j} - \overline{u_j u_i})$$

Where P is the pressure, upper and lower case U's denote mean and fluctuating velocities and $\overline{u_j u_i}$ is unknown Reynolds stress.

Nonlinear eddy viscosity model (NLEVM)

$$a_{ij} = \frac{\overline{u_j u_i}}{k} - \frac{2}{3} \delta_{ij} = -\frac{v_t}{k} S_{ij} + c_1 \frac{v_t}{\epsilon} (S_{ik} S_{kj} - \frac{1}{3} S_{kl} S_{kl} \delta_{ij}) + c_2 \frac{v_t}{\epsilon} (\Omega_{ik} S_{kj} + \Omega_{kj} S_{ki}) + c_3 \frac{v_t}{\epsilon} (\Omega_{ik} \Omega_{kj} - \frac{1}{3} \Omega_{kl} \Omega_{kl} \delta_{ij})$$

$$+c_4 \frac{v_t k}{\epsilon} (S_{ik}\Omega_{lj} + S_{kj}\Omega_{li}) + c_5 \frac{v_t k}{\epsilon^2} (\Omega_{il}\Omega_{lm}S_{mj} + S_{il}\Omega_{lm}\Omega_{mj} - \frac{2}{3}S_{lm}\Omega_{mn}\Omega_{nl}\delta_{ij}) + c_6 \frac{v_t k}{\epsilon^2} S_{ij}S_{kl}S_{kl} + c_7 \frac{v_t k}{\epsilon^2} S_{ij}S_{kl}S_{kl}$$

Where S_{ij} and Ω_{ij} are strain and vorticity rate tensors, respectively,

$$S_{ij} = \frac{\partial U_i}{\partial x_j} + \frac{\partial U_j}{\partial x_i}, \Omega_{ij} = \frac{\partial U_i}{\partial x_j} - \frac{\partial U_j}{\partial x_i}$$

c_1	c_2	c_3	c_4	c_5	c_6	c_7
-0.1	0.1	0.26	$-10c_\mu^2$	0	$-5c_\mu^2$	$5c_\mu^2$

$$\text{Where } c_\mu = \min[0.09, \frac{12}{1 + 3.5\eta + f_{RS}}]$$

$$\text{with } \eta = \max(\tilde{S}, \tilde{\Omega}), \tilde{S} = \frac{k}{\epsilon} \sqrt{0.5S_{ij}S_{ij}}, \tilde{\Omega} = \frac{k}{\epsilon} \sqrt{0.5\Omega_{ij}\Omega_{ij}}$$

$$\text{and } f_{RS} = 0.235[\max(0, \eta - 3.333)]^2 \exp(-\frac{\tilde{R}_t}{400})$$

Turbulent viscosity

$$v_t = c_\mu f_\mu \frac{k^2}{\epsilon}$$

$$\text{The viscous damping of } v_t, f_\mu = 1 - \exp\{-\left(\frac{\tilde{R}_t}{90}\right)^{1/2} - \left(\frac{\tilde{R}_t}{400}\right)^2\}$$

The transportation equation of the turbulent kinetic energy k and homogeneous dissipation rate ϵ are similar to those of linear model:

Turbulent kinetic energy transport equation

$$\frac{\partial(u_j k)}{\partial x_j} = \frac{\partial}{\partial x_j} \left[\left(v + \frac{v_t}{\sigma_k} \right) \frac{\partial k}{\partial x_j} \right] + P_k - \epsilon - 2\nu \left(\frac{\partial \sqrt{k}}{\partial x_j} \right)^2$$

Turbulent dissipation rate transport equation

$$\frac{\partial(u_j \tilde{\epsilon})}{\partial x_j} = \frac{\partial}{\partial x_j} \left[\left(v + \frac{v_t}{\sigma_k} \right) \frac{\partial \tilde{\epsilon}}{\partial x_j} \right] + f_1 C_{1\epsilon} \frac{\tilde{\epsilon}}{k} P_k - f_2 C_{2\epsilon} \frac{\tilde{\epsilon}^2}{k} + E + S_\epsilon$$

$$f_1 \text{ and } f_2 \text{ are given by } f_1 = 1, f_2 = 1 - 0.3 \exp(-\tilde{R}_t^2)$$

$$\text{Where } \tilde{R}_t = \frac{k^2}{\nu \tilde{\epsilon}} \text{ is the local turbulent Reynolds number}$$

The near wall source term E is expressed as

$$E = \begin{cases} 0.0022 \frac{\tilde{S} v_t k^2}{\tilde{\epsilon}} \left(\frac{\partial^2 U_i}{\partial x_i \partial x_j} \right)^2 & \text{for } \tilde{R}_t \leq 250 \\ 0 & \text{for } \tilde{R}_t \geq 250 \end{cases}$$

$$S_\epsilon = NYP = \max[C_\omega F(F+1) \frac{\tilde{\epsilon}^2}{k}, 0]$$

$$\text{Where } F = \left[\left(\frac{\partial l}{\partial x_j} \frac{\partial l}{\partial x_j} \right)^{1/2} - \frac{\partial l_e}{\partial y} \right] / C_1$$

$$\text{with } l = \frac{k^{3/2}}{\tilde{\epsilon}}, \frac{\partial l_e}{\partial y} = C_1 [1 - \exp(-B_\epsilon R_t) + B_\epsilon C_1 R_t \exp(-B_\epsilon R_t)]$$

$$\text{Here } C_1 = 2.55, B_\epsilon = 0.1069,$$

$$C_\omega = \frac{0.83 \min(1, \tilde{R}_t/5)}{0.8 + 0.7(\eta'/3.33)^{1/2} \exp(-\tilde{R}_t/125)}$$

$$\text{Where } \eta' = \max\left[\frac{k}{\tilde{\epsilon}}, \sqrt{\frac{\nu}{\epsilon}}\right] \eta$$

The homogeneous dissipation rate relates with the real dissipation rate through:

$$\tilde{\epsilon} = \epsilon - 2\nu \left(\frac{\partial \sqrt{k}}{\partial x_j} \right)^2$$

Linear low-Re $k - \epsilon$ model

$$\overline{u_i u_j} = -v_t \left(\frac{\partial u_i}{\partial x_j} + \frac{\partial u_j}{\partial x_i} \right) + \frac{2}{3} k \delta_{ij}$$

The turbulent viscosity v_t , is obtained from $v_t = c_\mu f_\mu \frac{k^2}{\epsilon}$

Transportation equation of the turbulent kinetic energy

$$\frac{\partial(u_j k)}{\partial x_j} = \frac{\partial}{\partial x_j} \left[\left(v + \frac{v_t}{\sigma_k} \right) \frac{\partial k}{\partial x_j} \right] + P_k - \tilde{\epsilon} - 2v \left(\frac{\partial \sqrt{k}}{\partial x_j} \right)^2$$

Transportation equation for the homogeneous dissipation rate $\tilde{\epsilon}$

$$\frac{\partial(u_j \tilde{\epsilon})}{\partial x_j} = \frac{\partial}{\partial x_j} \left[\left(v + \frac{v_t}{\sigma_k} \right) \frac{\partial \tilde{\epsilon}}{\partial x_j} \right] + f_1 C_{1\epsilon} \frac{\tilde{\epsilon}}{k} P_k - f_2 C_{2\epsilon} \frac{\tilde{\epsilon}^2}{k} + E + S_\epsilon$$

Where $E = 2v v_t \left(\frac{\partial^2 u_i}{\partial x_i \partial x_j} \right)^2$, $S_\epsilon = NYP = \max[C_\omega F(F+1) \frac{\tilde{\epsilon}^2}{k}, 0]$

Where $F = \left[\left(\frac{\partial l}{\partial x_j} \frac{\partial l}{\partial x_j} \right)^{1/2} - \frac{\partial l_e}{\partial y} \right] / C_1$

with $l = \frac{k^{3/2}}{\tilde{\epsilon}}$, $\frac{\partial l_e}{\partial y} = C_1 [1 - \exp(-B_\epsilon R_t) + B_\epsilon C_1 R_t \exp(-B_\epsilon R_t)]$

Here $C_1 = 2.55$, $B_\epsilon = 0.1069$, $C_\omega = 0.83$

The homogeneous dissipation rate relates with the real dissipation rate through:

$$\tilde{\epsilon} = \epsilon - 2v \left(\frac{\partial \sqrt{k}}{\partial x_j} \right)^2$$

The damping functions f_μ, f_1 and f_2 are given by

$$f_\mu = \exp[-3.4/(1 + 0.02\tilde{R}_t)^2], f_1 = 1, f_2 = 1 - 0.3 \exp(\tilde{R}_t^2)$$

Where $\tilde{R}_t = \frac{k^2}{v\tilde{\epsilon}}$ is the local turbulent Reynolds number

C_μ	σ_k	σ_ϵ	σ_T	$C_{1\epsilon}$	$C_{2\epsilon}$
0.09	1.0	1.3	0.9~1.0	1.43	1.92

Results: It was shown that for the bend of square cross-section the curvature induces a strong secondary motion, while for rectangular cross-section the secondary flow is confined to the corner regions. The curvature also influences the flow development along the straight upstream section of the duct by inducing a weak cross-duct motion near the entrance of the curved section. Curvature causes the pressure gradient to change sign along the convex and concave walls of the curved section, which results in local redistribution of the stream-wise velocity profile along the curved section. The effects of curvature are also present downstream of the curved section, though slowly diminishing with the development of the main stream. In the case of bend of square cross-section an extra pair of vortices appears along the convex surface near the bend exit which results in strong span-wise gradient of the stream-wise velocity in the duct core. These features are not present in the bend of rectangular cross-section.

Conclusions: Both turbulent models can produce reasonable predictions for square cross-section bend, while the non-linear $k - \epsilon$ model returns superior predictions of the turbulence field and also of the pressure and friction coefficients in rectangular cross-section bend. However, the weakness of the non-linear $k - \epsilon$ is in the prediction of the flow recovery after the bend exit. To address this weakness, would probably require the use of full second-moment closures that account for transport effects on the turbulent stresses.

Author: William D. York and D.Keith Walters, James H. Leylek

Year: 2009

Title: A simple and robust linear eddy-viscosity formulation for curved and rotating flows

Journal: International Journal of Numerical Methods for Heat & Fluid Flow, Vol. 19 Iss: 6, pp.745 - 776

Problem: A new eddy-viscosity formulation to exhibit a correct response to streamline curvature and flow rotation.

($Re = 10^6, R_c/D_h = 2$)

Model: Linear $k - \varepsilon$ model + near wall treatment

Equations: The formulation is a linear $k - \varepsilon$ model with a two-layer near-wall treatment in FLUENT solver. The model solves equations for turbulent kinetic energy (k) and dissipation rate (ε) in the far-field, while solving only the k equation near the wall and prescribing a length scale based on wall distance. The dissipation rate is calculated via an empirical correlation based on local wall distance. The interface between the near wall region and the far field is evaluated based on the smaller of the two length scales determined by either the wall distance or the dissipation rate. The Reynolds-stress anisotropic tensor is based on modified form of the differential Reynolds-stress model of Speziale(1991) and the assumption of local structural equilibrium (weak equilibrium). Specifically, the eddy viscosity coefficient C_μ is formulated to reproduce the proper response to streamline curvature and/or reference frame rotation, yielding a curvature-corrected linear eddy viscosity model. In contrast to the non-linear model forms for which the anisotropic tensor includes higher-order constructions of S_{ij} and/or Ω_{ij} .

Turbulent kinetic energy transport equation

$$\frac{\partial(\bar{\rho}k)}{\partial t} + \frac{\partial}{\partial x_j}(\bar{\rho}U_j k) = \frac{\partial}{\partial x_j}[(\mu + \frac{\mu_T}{Pr_k}) \frac{\partial k}{\partial x_j}] + [2\mu_T(S_{ij} - \frac{1}{3}\delta_{ij}\frac{\partial U_l}{\partial x_l}) - \frac{2}{3}\bar{\rho}k\delta_{ij}] \frac{\partial U_i}{\partial x_j} - \bar{\rho}\varepsilon$$

Turbulent dissipation rate transport equation

$$\frac{\partial(\bar{\rho}\varepsilon)}{\partial t} + \frac{\partial}{\partial x_j}(\bar{\rho}U_j \varepsilon) = \frac{\partial}{\partial x_j}[(\mu + \frac{\mu_T}{Pr_\varepsilon}) \frac{\partial \varepsilon}{\partial x_j}] + C_{\varepsilon 1} \frac{\varepsilon}{k} [2\mu_T(S_{ij} - \frac{1}{3}\delta_{ij}\frac{\partial U_l}{\partial x_l}) - \frac{2}{3}\bar{\rho}k\delta_{ij}] \frac{\partial U_i}{\partial x_j} - C_{\varepsilon 2} \bar{\rho} \frac{\varepsilon^2}{k}$$

Turbulent viscosity

$$\mu_T = C_\mu \bar{\rho} \frac{k^2}{\varepsilon}$$

Turbulent viscosity coefficient

$$C_\mu = \frac{K_1 + K_2 C_\mu (\frac{Sk}{\varepsilon})^2 + K_3 C_\mu (\frac{Sk}{\varepsilon}) + K_4 C_\mu^2 (\frac{Sk}{\varepsilon})^3}{K_5 + K_6 C_\mu (\frac{Sk}{\varepsilon})^2 + K_7 C_\mu^2 (\frac{Sk}{\varepsilon})^4 + K_8 (\frac{Wk}{\varepsilon})^2}$$

Where

$$S = \sqrt{2S_{ij}S_{ij}}, W = \sqrt{2W_{ij}W_{ij}}$$

Modified flow rotation term

$$W = \left| S \cdot \left(1 - \frac{C_4 - 4}{C_4 - 2}\right) + \Omega \cdot \frac{C_4 - 4}{C_4 - 2} \right| = \left| \frac{9}{4}\Omega - \frac{5}{4}S \right|$$

Where the relative fluid rotation rate magnitude computed in an inertial frame is:

$$\Omega = \sqrt{2\Omega_{ij}\Omega_{ij}}$$

Turbulent stress (Boussinesq's Assumption)

$$-\overline{\rho u_i u_j} = 2\mu_T S_{ij} - \frac{2}{3}\delta_{ij}(\mu_T \frac{\partial U_l}{\partial x_l} + \bar{\rho}k)$$

Model turbulent length scale

$$L_T = \min\left(\frac{C_{LY} k^{3/2}}{\varepsilon}\right)$$

Near-wall turbulent dissipation rate (when $\frac{C_{LY}}{\varepsilon}$ is minimum)

$$\varepsilon = \frac{k^{3/2}}{l_\varepsilon}$$

$$\text{Where } l_\varepsilon = C_{LY} \left[1 - \exp\left(-\frac{\text{Re}_y}{A_\varepsilon}\right)\right]$$

Near-wall turbulent viscosity (when $\frac{C_{LY}}{\varepsilon}$ is minimum)

$$\mu_T = C_\mu \bar{\rho} \sqrt{k} C_{LY} \left[1 - \exp\left(-\frac{\text{Re}_y}{A_\varepsilon}\right)\right],$$

$$\text{Where } \text{Re}_y = \frac{\sqrt{k} y}{\nu}$$

Model constants

$$\text{Pr}_k = 1.0, \text{Pr}_\varepsilon = 1.19, C_{\varepsilon 1} = 1.44, C_{\varepsilon 2} = 1.92, K_1 = 0.66, K_2 = 3.9, K_3 = 1.0, K_4 = 5.3, K_5 = 2.9, \\ K_6 = 17.0, K_7 = 10.0, K_8 = 3.84, C_4 = 0.4, C_L = 2.495, A_\varepsilon = 4.99, A_\mu = 25.0$$

Results: The new model is tested on several two- and three-dimensional problems, including rotating channel flow, U-bend flow and internally cooled turbine airfoil conjugate heat transfer. Predictions are compared to those with popular eddy-viscosity models. For the 2-D flow in a U-bend, the model exhibits the correct response to the curvature, including the velocity profile and turbulent kinetic energy at $\theta = 90^\circ$, $\theta = 180^\circ$ in the U-bend, as well as skin friction coefficient for inner and outer walls respectively.

Conclusions: The new model shows better results than SKE model and RKE model. The approach adopted here for linear eddy-viscosity models may be extended in a straightforward manner to non-linear eddy-viscosity or explicit algebraic stress models.

Important concepts:

(1) Weak-equilibrium assumption

Reynolds stress anisotropy tensor $b_{ij} = \frac{\overline{\rho u_i' u_j'}}{\bar{\rho} k} - \frac{2}{3} \delta_{ij}$ to be constant along a streamline. This assumption is untrue in flows with streamline curvature, and the effect is amplified in cases where such curvature is significant.

(2) Boussinesq approximation

$$-\overline{\rho u_i' u_j'} = 2\mu_T S_{ij} - \frac{2}{3} \delta_{ij} (\mu_T \frac{\partial U_l}{\partial x_l} + \bar{\rho} k)$$

(3) Turbulence intensity

$$TI = \frac{u'}{U}$$

Where u' is the root-mean-square of the turbulence velocity fluctuations and U is the mean velocity (Reynolds averaged).

If the turbulent energy k is known, then u' can be computed as:

$$u' = \sqrt{\frac{1}{3} (u_x'^2 + u_y'^2 + u_z'^2)} = \sqrt{\frac{2}{3} k}$$

U can be computed from the three mean velocity components U_x , U_y and U_z :

$$U = \sqrt{U_x^2 + U_y^2 + U_z^2}$$

High-turbulence case: High-speed flow inside complex geometries like heat-exchangers and flow inside rotating machinery (turbines and compressors). Typically the turbulence intensity is between 5% and 20%

Medium-turbulence case: Flow in not-so-complex devices like large pipes, ventilation flows etc. or low speed flows (low Reynolds number). Typically the turbulence intensity is between 1% and 5%

Low-turbulence case: Flow originating from a fluid that stands still, like external flow across cars, submarines and aircrafts. Very high-quality wind-tunnels can also reach really low turbulence levels. Typically the turbulence intensity is very low, well below 1%.

(4) Averaging

General N-S equations

$$\frac{\partial \rho}{\partial t} + \frac{\partial(\rho u_j)}{\partial x_j} = 0$$
$$\rho \left(\frac{\partial u_i}{\partial t} + u_j \frac{\partial u_i}{\partial x_j} \right) = -\frac{\partial P}{\partial x_i} + \frac{\partial \tau_{ij}^{(v)}}{\partial x_i}$$

Where $\tau_{ij}^{(v)}$ is viscous stress tensor.

$$\tau_{ij}^{(v)} = 2\mu(S_{ij} - \frac{1}{3}S_{kk}\delta_{ij})$$

$$S_{ij} = \frac{1}{2}\left(\frac{\partial u_i}{\partial x_j} + \frac{\partial u_j}{\partial x_i}\right)$$

General incompressible N-S equations

$$\frac{\partial u_i}{\partial x_i} = 0$$

$$\rho\left(\frac{\partial u_i}{\partial t} + u_j \frac{\partial u_i}{\partial x_j}\right) = -\frac{\partial P}{\partial x_i} + \mu \frac{\partial^2 u_i}{\partial x_j^2}$$

4-1 Favre-averaging (density weighted time averaging)

Favre-averaging is sometimes used in compressible flow to separate turbulent fluctuations from the mean-flow.

$$\Phi = \tilde{\Phi} + \Phi''$$

Where

$$\text{the mean part } \tilde{\Phi} = \frac{\int_T \rho(t)\Phi(t)dt}{\int_T \rho(t)dt} = \frac{\overline{\rho\Phi}}{\bar{\rho}}$$

the auxiliary relations

$$\overline{\rho\Phi''} = 0 \text{ (but } \overline{\Phi''} \neq 0), \overline{\rho\tilde{\Phi}} = \bar{\rho}\tilde{\Phi} = \overline{\rho\Phi}$$

General Favre-averaged continuity equation

$$\frac{\partial(\rho\phi)}{\partial t} + \frac{\partial(\rho\phi\tilde{u}_i)}{\partial x_i} = \frac{\partial(\bar{\rho}\tilde{\phi})}{\partial t} + \frac{\partial(\bar{\rho}\tilde{\phi}\tilde{u}_i)}{\partial x_i} + \frac{\partial(\overline{\rho\phi''u_i})}{\partial x_i} = 0$$

Continuity equation ($\phi = 1, \phi'' = 0$):

$$\frac{\partial\bar{\rho}}{\partial t} + \frac{\partial(\bar{\rho}\tilde{u}_i)}{\partial x_i} = 0$$

Momentum equation ($\phi = u_j, \phi'' = u_j''$)

$$\frac{\partial(\bar{\rho}\tilde{u}_j)}{\partial t} + \frac{\partial(\bar{\rho}\tilde{u}_j\tilde{u}_i + \delta_{ij}\bar{P} + \overline{\rho u_j'' u_i''} - \bar{\tau}_{ij})}{\partial x_i} = 0$$

Energy equation

$$\frac{\partial(\bar{\rho}\tilde{e}_0)}{\partial t} + \frac{\partial}{\partial x_i}(\bar{\rho}\tilde{e}_0\tilde{u}_i + \tilde{u}_i\bar{P} + \overline{P u_i''} + \overline{\rho e_0'' u_i''} + \bar{q}_i - \bar{u}_j\bar{\tau}_{ij}) = 0$$

Where the density averaged total energy \tilde{e}_0 is given, $\tilde{e}_0 = \tilde{e} + \frac{\overline{u_k'' u_k''}}{2} + k$

Where the turbulent energy $k = \frac{\overline{u_k'' u_k''}}{2}$

$$\bar{\tau}_{ij} = \tilde{\tau}_{ij} + \overline{\tau_{ij}''}$$

$$\overline{P u_i''} + \overline{\rho e_0'' u_i''} = C_P \overline{\rho u_i'' T} + u_j \overline{\rho u_j'' u_i''} + \frac{\overline{\rho u_j'' u_j'' u_i''}}{2}$$

$$\bar{q}_i = -C_P \frac{\mu}{\text{Pr}} \frac{\partial \bar{T}}{\partial x_i} = -C_P \frac{\mu}{\text{Pr}} \frac{\partial \tilde{T}}{\partial x_i} - C_P \frac{\mu}{\text{Pr}} \frac{\partial \overline{T''}}{\partial x_i}$$

$$\overline{u_j \tau_{ij}} = \tilde{u}_j \tilde{\tau}_{ij} + \overline{u_j'' \tau_{ij}''} + \tilde{u}_j \overline{\tau_{ij}''}$$

After simplification,

$$\frac{\partial \bar{\rho}}{\partial t} + \frac{\partial(\bar{\rho} \tilde{u}_i)}{\partial x_i} = 0$$

$$\frac{\partial(\bar{\rho} \tilde{u}_j)}{\partial t} + \frac{\partial(\bar{\rho} \tilde{u}_j \tilde{u}_i + \delta_{ij} \bar{P} + \tau_{ij}^{tot})}{\partial x_i} = 0$$

$$\frac{\partial(\bar{\rho} \tilde{e}_0)}{\partial t} + \frac{\partial}{\partial x_i} (\bar{\rho} \tilde{e}_0 \tilde{u}_i + \tilde{u}_i \bar{P} + \tilde{q}_i^{tot} - \tilde{u}_j \tau_{ij}^{tot}) = 0$$

Where

$$\tau_{ij}^{tot} = \tau_{ij}^{lam} + \tau_{ij}^{turb}$$

$$\tau_{ij}^{lam} = \tau_{ij} = \mu \left(\frac{\partial \tilde{u}_i}{\partial x_j} + \frac{\partial \tilde{u}_j}{\partial x_i} - \frac{2}{3} \frac{\partial \tilde{u}_k}{\partial x_k} \delta_{ij} \right)$$

$$\tau_{ij}^{turb} = -\overline{\rho u_j u_i} = \mu_t \left(\frac{\partial \tilde{u}_i}{\partial x_j} + \frac{\partial \tilde{u}_j}{\partial x_i} - \frac{2}{3} \frac{\partial \tilde{u}_k}{\partial x_k} \delta_{ij} \right) - \frac{2}{3} \bar{\rho} k \delta_{ij}$$

$$\tilde{q}_i^{tot} = \tilde{q}_i^{lam} + \tilde{q}_i^{turb}$$

$$\tilde{q}_i^{lam} = \tilde{q}_i \approx -C_P \frac{\mu}{Pr} \frac{\partial \tilde{T}}{\partial x_i} = -\frac{\gamma}{\gamma - 1} \frac{\mu}{Pr} \frac{\partial}{\partial x_i} \left[\frac{\bar{P}}{\bar{\rho}} \right]$$

$$\tilde{q}_i^{turb} = C_P \overline{\rho u_j u_i} = -C_P \frac{\mu_t}{Pr_t} \frac{\partial \tilde{T}}{\partial x_i} = -\frac{\gamma}{\gamma - 1} \frac{\mu_t}{Pr_t} \frac{\partial}{\partial x_i} \left[\frac{\bar{P}}{\bar{\rho}} \right]$$

$$\bar{P} = (\gamma - 1) \bar{\rho} \left(\tilde{e}_0 - \frac{\tilde{u}_k \tilde{u}_k}{2} - k \right)$$

4-2 Reynolds averaging

There are three most common perceptions of this term: time averaging, space averaging or ensemble averaging.

A. Time averaging

Time averaging is appropriate when considering a stationary turbulence. That is when the flow does not vary on the average in time. In such cases time average is defined by:

$$F(\mathbf{r}) = \lim_{T \rightarrow \infty} \left(\frac{1}{T} \int_t^{t+T} f(\mathbf{r}, t) dt \right)$$

B. Space averaging

Space average is appropriate for homogenous turbulence. That is a turbulent flow that on the average does not vary in any direction. Space average is defined by:

$$F(t) = \lim_{V \rightarrow \infty} \left(\frac{1}{V} \int \int \int f(\mathbf{r}, t) dV \right)$$

C. Ensemble average

Ensemble average is the most general aspect of Reynolds average. It should be understood as an average of N identical experiments. Ensemble average is both time- and space-dependent. It is defined by:

$$F(\mathbf{r}, t) = \lim_{N \rightarrow \infty} \frac{1}{N} \sum_{n=1}^N f_n(\mathbf{r}, t)$$

Reynolds-Averaged N-S equations

The main idea of Reynolds averaging is to decompose the flow to averaged and fluctuating component (Reynolds decomposition):

$$\begin{aligned} u_i &= \tilde{u}_i + u_i' \\ P &= \tilde{P} + P' \\ \tau_{ij}^{(v)} &= \tilde{\tau}_{ij}^{(v)} + \tau_{ij}'^{(v)} \end{aligned}$$

Averaged governing equations for incompressible flow:

$$\begin{aligned} \frac{\partial \tilde{u}_i}{\partial x_i} &= 0 \\ \frac{\partial u_i'}{\partial x_i} &= 0 \\ \rho \left(\frac{\partial \tilde{u}_i}{\partial t} + \tilde{u}_j \frac{\partial \tilde{u}_i}{\partial x_j} \right) &= - \frac{\partial \tilde{P}}{\partial x_i} + \frac{\partial \tilde{\tau}_{ij}^{(v)}}{\partial x_i} - \frac{\partial}{\partial x_j} (\overline{u_i' u_j'}) \end{aligned}$$

Where $\overline{u_i' u_j'}$ is a re-worked contribution of the fluctuating velocities to the change of the averaged ones, having the same structure and dimension as the viscous stress tensor.

References

- [1] Rowe, M., 1970, "Measurements and Computations of Flow in Pipe Bends," *Journal of Fluid Mechanics*, Vol. 43, Part 4, pp. 771-783.
- [2] S.M. Chang, J.A.C. Humphrey, A. Modavi, "Turbulent Flow in a Strongly Curved U-bend and Downstream Tangent of Square Cross-Sections," *PhysicoChemical Hydrodynamics*, Vol. 4 (1983), No. 3, pp. 243-269.
- [3] Azzola, J., Humphrey, J.A.C., Iacovides, H., and Launder, B.E., 1986, "Developing Turbulent Flow in a U-Bend of Circular Cross-Section: Measurement and Computation," *ASME Journal of Fluids Engineering*, Vol. 108, pp. 214-221.
- [4] Sandborn, V.A., and Shin, J.C., 1989, "Water Flow Measurements in a 180 Degree Turn-Around Duct," Report Prepared under Contract No. NAS8-36354.
- [5] Anwer, M., So, R.M.C., and Lai, Y.G., 1989, "Perturbation by and Recovery from Bend Curvature of a Fully Developed Turbulent Pipe Flow", *Journal of Physics of Fluids A*, Vol. 1, No. 8, pp. 1387-1397.
- [6] Monson, D.J., and Seegmiller, H.L., 1992, "An Experimental Investigation of Subsonic Flow in a Two-Dimensional U-Duct," *NASA Technical Memorandum* 103931.
- [7] Cheah, S.C., Iacovides, H., Jackson, D.C., Ji, H., and Launder, B.E., 1996, "LDA Investigation of the Flow Development through Rotating U-Ducts," *ASME Journal of Turbomachinery*, Vol. 118, pp. 590-596.
- [8] Sudo, K., Sumida, M., and Hibara, H., 2000, "Experimental Investigation on Turbulent Flow through a Circular-Sectioned 180° Bend," *Experiments in Fluids*, Vol. 28, pp. 51-57.
- [9] Lee, G.H., Choi, Y.D., and Han, S.H., 2007, "Measurement of Developing Turbulent Flow in a U-Bend of Circular Cross-Section," *Journal of Mechanical Science and Technology*, Vol. 21, No. 2, pp. 348-359.
- [10] Choi, Y-D., Iacovides, H., and Launder, B.E., 1989, "Numerical Computation of Turbulent Flow in a Square Cross-Sectioned 180° Bend," *ASME Journal of Fluids Engineering*, Vol. 111, pp. 59-68.
- [11] Iacovides, H., Launder, B.E., Loizou, P.A., and Zhao, H.H., 1990, "Turbulent Boundary-Layer Development around a Square-Sectioned UBend: Measurements and Computation," *ASME Journal of Fluids Engineering*, Vol. 112, pp. 409-415.
- [12] Rumsey, C.L., Gatski, T.B., and Morrison, J.H., 2000, "Turbulence Model Prediction of Strongly Curved Flow in a U-Duct," *AIAA Journal*, Vol. 38, No. 8, pp. 1394-1402.
- [13] Suga, K., 2003, "Predicting Turbulence and Heat Transfer in 3-D Curved Ducts by Near-Wall Second Moment Closures," *International Journal of Heat and Mass Transfer*, Vol. 46, pp. 161-173.
- [14] Sugiyama, H., and Hitomi, D., 2005, "Numerical Analysis of Developing Turbulent Flow in a 180° Bend Tube by an Algebraic Reynolds Stress Model," *International Journal for Numerical Methods in Fluids*, Vol. 47, pp. 1431-1449.
- [15] Münch, C., and Métais, O., 2007, "Large Eddy Simulations in Curved Square Ducts: Variation of the Curvature Radius," *Journal of Turbulence*, Vol. 8, No. 28, pp. 1-18.
- [16] Xu, J.I., Ma, H.Y., and Huang, Y.N., 2008, "Nonlinear Turbulence Models for Predicting Strong Curvature Effects," *Applied Mathematics and Mechanics - English Edition - Shanghai*, Vol. 29, No. 1, pp. 31-42.
- [17] Djebedjian, B., Mohamed, M.S., and Elsayed, A., 2008, "NUMERICAL STUDIES OF CURVATURE EFFECT ON TURBULENT FLOWS IN 180° CURVED DUCTS" *Proceedings of IEC 2008, 6th International Engineering Conference, Mansoura/Sharm El-Sheikh, Egypt, 20-23 March*, Vol. 2, pp.347-370.
- [18] S.V.Patankar, D.B.Spalding, Prediction of turbulent flow in curved pipes, *J. Fluid Mech.*,1975,Vol. 67, 583-595,

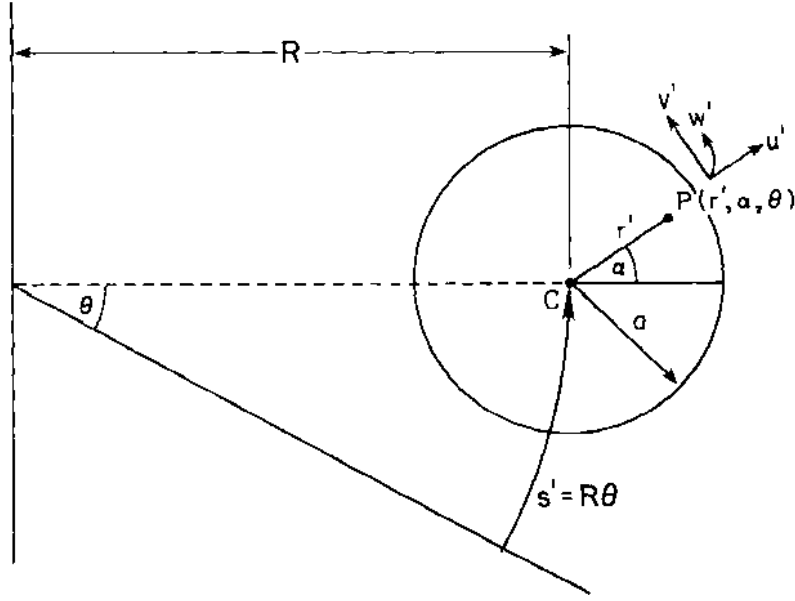
- [19] William D. York and D.Keith Walters, James H. Leylek, A simple and robust linear eddy-viscosity formulation for curved and rotating flows, *International Journal of Numerical Methods for Heat & Fluid Flow*, Vol. 19 Iss: 6, pp.745 - 776
- [20] Sudo, K., Sumida, M., and Hibara, H., "Experimental investigation on turbulent flow through a circular-sectioned 90° bend," *Experimental Fluids* 1998; 25:42–49.
- [21] Enayet MM, Gibson MM, Taylor AMKP, Yianneskis M. Laser-doppler measurements of laminar and turbulent flow in a pipe bend. *International Journal of Heat and Fluid Flow* 1982; 3:213–219.
- [22] Kreskovsky JP, Briley WR, McDonald H. Prediction of laminar and turbulent primary and secondary flows in strongly curved ducts. NASA Report, No. CR.3388, 1981.
- [23] Taylor AMKP, Whitelaw JH, Yianneskis M. Curved ducts with strong secondary motion: velocity measurements of developing laminar and turbulent ow. *Journal of Fluids Engineering (ASME)* 1982; 104:350–359.
- [24] Iacovides H, Launder BE, Loizou PA. Numerical computation of turbulent ow through a square-sectioned 90° bend. *International Journal of Heat and Fluid Flow* 1987; 8(4):320–325.
- [25] M. Raisee, H. Alemi1 and H. Iacovides, Prediction of developing turbulent flow in 90°-curved ducts using linear and non-linear low-Re $k - \epsilon$ models, *Int. J. Numer. Meth. Fluids* 2006; 51:1379–1405
- [26] Xiaohua Wang, Siva Thangam, Development and application of an anisotropic two-equation model for flows with swil and curvature, *Journal of applied mechanics*, Vol. 73, pp.397-, May, 2006

Governing equations for curved pipe flow

1 Laminar flow

1.1 Small curvature pipe (Small Dean number: $0 < De < 96$)^[1,2]

Steady incompressible laminar flow in toroidal coordinate (r, ψ, θ) , U, V and W are independent of θ :



Toroidal coordinate

$$\frac{\partial U}{\partial r} + \frac{U}{r} + \frac{U \sin \psi}{R + r \sin \psi} + \frac{1}{r} \frac{\partial V}{\partial \psi} + \frac{V \cos \psi}{R + r \sin \psi} = 0$$

$$U \frac{\partial U}{\partial r} + \frac{V}{r} \frac{\partial U}{\partial \psi} - \frac{V^2}{r} - \frac{W^2 \sin \psi}{R + r \sin \psi} = -\frac{\partial}{\partial r} \left(\frac{P}{\rho} \right) - v \left[\left(\frac{1}{r} \frac{\partial}{\partial \psi} + \frac{\cos \psi}{R + r \sin \psi} \right) \left(\frac{\partial V}{\partial r} + \frac{V}{r} - \frac{1}{r} \frac{\partial U}{\partial \psi} \right) \right]$$

$$U \frac{\partial V}{\partial r} + \frac{V}{r} \frac{\partial V}{\partial \psi} + \frac{UV}{r} - \frac{W^2 \cos \psi}{R + r \sin \psi} = -\frac{1}{r} \frac{\partial}{\partial \psi} \left(\frac{P}{\rho} \right) + v \left[\left(\frac{\partial}{\partial r} + \frac{\sin \psi}{R + r \sin \psi} \right) \left(\frac{\partial V}{\partial r} + \frac{V}{r} - \frac{1}{r} \frac{\partial U}{\partial \psi} \right) \right]$$

$$U \frac{\partial W}{\partial r} + \frac{V}{r} \frac{\partial W}{\partial \psi} + \frac{UW \sin \psi}{R + r \sin \psi} + \frac{VW \cos \psi}{R + r \sin \psi} = -\frac{1}{R + r \sin \psi} \frac{\partial}{\partial \theta} \left(\frac{P}{\rho} \right) + v \left[\left(\frac{1}{r} + \frac{\partial}{\partial r} \right) \left(\frac{\partial W}{\partial r} + \frac{W \sin \psi}{R + r \sin \psi} \right) + \frac{1}{r} \frac{\partial}{\partial \psi} \left(\frac{1}{r} \frac{\partial W}{\partial \psi} + \frac{W \cos \psi}{R + r \sin \psi} \right) \right]$$

When curvature is small: that is a/R is small, terms of order a^2/R^2 are ignored. And we assume

$$U = u, V = v, W = A(a^2 - r^2) + w, P/\rho = Cz + \frac{P}{\rho}$$

Where A and C are constants, and z is the distance (measured long the central line) of any section of the pipe from a fixed section.

The governing equations become $\left(\frac{1}{R} \frac{\partial}{\partial \theta} = \frac{\partial}{\partial z} \right)$

$$\frac{\partial u}{\partial r} + \frac{u}{r} + \frac{1}{r} \frac{\partial v}{\partial \psi} = 0$$

$$-\frac{A^2(a^2 - r^2)^2 \sin \psi}{R} = -\frac{\partial}{\partial r} \left(\frac{P}{\rho} \right) - \frac{v}{r} \frac{\partial}{\partial \psi} \left(\frac{\partial v}{\partial r} + \frac{v}{r} - \frac{1}{r} \frac{\partial u}{\partial \psi} \right)$$

$$-\frac{A^2(a^2 - r^2)^2 \cos \psi}{R} = -\frac{1}{r} \frac{\partial}{\partial \psi} \left(\frac{P}{\rho} \right) + v \frac{\partial}{\partial r} \left(\frac{\partial v}{\partial r} + \frac{v}{r} - \frac{1}{r} \frac{\partial u}{\partial \psi} \right)$$

$$-2Aru = -\left(1 - \frac{r \sin \psi}{R} \right) \frac{\partial}{\partial z} \left(Cz + \frac{P}{\rho} \right) + v \left(\frac{\partial^2}{\partial r^2} + \frac{1}{r} \frac{\partial}{\partial r} + \frac{1}{r^2} \frac{\partial^2}{\partial \psi^2} \right) [A(a^2 - r^2) + w]$$

$$+ v \left(\frac{1}{r} + \frac{\partial}{\partial r} \right) \frac{A(a^2 - r^2) \sin \psi}{R} + \frac{v}{r} \frac{\partial}{\partial \psi} \left[\frac{A(a^2 - r^2) \cos \psi}{R} \right]$$

$C = -4vA$ gives the relation between pressure gradient and rate of flow in a circular straight pipe.

Asymptotic solutions for velocities and pressure are function of r and ψ :

$$u = u' \sin \psi, v = v' \cos \psi, w = w' \sin \psi, P/\rho = P' \sin \psi,$$

Where u', v', w', P' are function of r only, with boundary conditions: $u' = 0, v' = 0, w' = 0, P' = 0$ at $r = 0$.

Therefore,

$$u = A^2 \sin \psi (a^2 - r^2)(4a^2 - r^2)/288Rv$$

$$v = A^2 \cos \psi (a^2 - r^2)(4a^2 - 23a^2r^2 + 7r^4)/288Rv$$

$$w' = -\frac{3Ar}{4R} (a^2 - r^2) + \frac{A^3r}{1152Rv^2} [4a^6(a^2 - r^2) - 3a^4(a^4 - r^4) + a^2(a^6 - r^6) - (a^8 - r^8)/10]$$

$$P'/r = A^2(a^2 - r^2)^2/R + v \frac{d}{dr} \left(\frac{dv'}{dr} + \frac{v'}{r} - \frac{u'}{r} \right)$$

or in non-dimensional form, through defining $n = Aa^3/v, r' = r/a$

$$U/W_0 = na \sin \psi (1 - r'^2)^2 (4 - r'^2)/288R$$

$$V/W_0 = na \cos \psi (1 - r'^2)(4 - 23r'^2 + 4r'^4)/288R$$

$$W/W_0 = (1 - r'^2) \left[1 - \frac{3r \sin \psi}{4R} + \frac{n^2 r \sin \psi}{11520R} (19 - 21r'^2 + 9r'^4 - r'^6) \right]$$

The differential equation to any stream-line is

$$\frac{dr}{U} = \frac{rd\psi}{V} = \frac{Rd\theta}{A(a^2 - r^2)} \Rightarrow \frac{dr}{(1 - r'^2)(4 - r'^2) \sin \psi} = \frac{rd\psi}{(4 - 23r'^2 + 4r'^4) \cos \psi}$$

By integration,

$$\sec \psi = kr' (1 - r'^2)(1 - r'^2/4)$$

Where k is an arbitrary constant.

1.2 Small curvature pipe (Median Dean number: $96 < De < 600$)^[3]

Dimensionless variables are introduced as: $r = ar^*, w = v(R/2a^3)^{1/2}w^*, \phi = v\phi^*$

Governing equations

$$\nabla^{*2} w^* + \frac{1}{r^*} \left(\frac{\partial \phi^*}{\partial r^*} \frac{\partial w^*}{\partial \psi^*} - \frac{\partial w^*}{\partial r^*} \frac{\partial \phi^*}{\partial \psi^*} \right) = -D$$

$$\nabla^{*4} \phi^* + \frac{1}{r^*} \left(\frac{\partial \phi^*}{\partial r^*} \frac{\partial}{\partial \psi^*} - \frac{\partial \Omega^*}{\partial r^*} \frac{\partial}{\partial \psi^*} \right) \nabla^{*2} \phi^* = w^* \left(\sin \psi^* \frac{\partial w^*}{\partial r^*} + \frac{\cos \psi^*}{r^*} \frac{\partial w^*}{\partial \psi^*} \right)$$

$$\text{Where } D = \frac{Ga^2}{\mu} \sqrt{\frac{2a^3}{v^2L}}, \nabla^{*2} = \frac{\partial^{*2}}{\partial r^{*2}} + \frac{1}{r^*} \frac{\partial}{\partial r^*} + \frac{1}{r^{*2}} \frac{\partial^2}{\partial \psi^{*2}}$$

With $G = -\frac{1}{R} \frac{\partial P}{\partial \theta}$ (axial pressure gradient is constant)

Introduce $w = \sum_{n=0}^{\infty} w_n \cos n\psi, \phi = \sum_{n=0}^{\infty} \phi_n \sin n\psi, \zeta = \sum_{n=0}^{\infty} \zeta_n \sin n\psi$ (where w_n, ϕ_n and ζ_n are functions of r only)

By equating coefficients of $\cos n\psi$, the following equations are obtained (the following dimensionless equations are without *)

For $n = 0$,

$$\frac{d^2 w_0}{dr^2} + \frac{1}{r} \frac{dw_0}{dr} = f_0(r)$$

$$\text{Where } f_0(r) = \frac{1}{2r} \left[\sum_{m=1}^{\infty} m\phi_m \frac{dw_m}{dr} + \sum_{m=1}^{\infty} mw_m \frac{d\phi_m}{dr} \right] - D$$

For $n \geq 1$

$$\frac{d^2w_n}{dr^2} + \frac{1}{r} \frac{dw_n}{dr} - \frac{n^2}{r^2} w_n = f_n(r)$$

$$\frac{d_n^2\phi}{dr^2} + \frac{1}{r} \frac{d\phi_n}{dr} - \frac{n^2}{r^2} \phi_n = \zeta_n$$

$$\frac{d^2\zeta_n}{dr^2} + \frac{1}{r} \frac{d\zeta_n}{dr} - \frac{n^2}{r^2} \zeta_n = F_n(r)$$

$$\text{Where } f_n(r) = \frac{1}{2r} \sum_{m=-\infty}^{\infty} m\phi_m \frac{ds_{n-m}}{dr} - \frac{1}{r} \sum_{m=-\infty}^{\infty} ms_m \frac{d\phi_{n-m}}{dr}$$

$$F_n = -\frac{1}{r} \sum_{m=-\infty}^{\infty} m\zeta_m \frac{d\phi_{n-m}}{dr} + \frac{1}{r} \sum_{m=-\infty}^{\infty} m\phi_m \frac{d\zeta_{n-m}}{dr} - \frac{1}{4} \sum_{m=-\infty}^{\infty} \frac{ds_m}{dr} (s_{n-(m+1)} - s_{n-(m-1)}) \\ + \frac{1}{4r} \sum_{m=-\infty}^{\infty} ms_m (s_{n-(m+1)} + s_{n-(m-1)})$$

We have following relations for above two equations

$$s_m = w_m$$

$$\phi_{-m} = -\phi_m \quad (m > 0)$$

$$\zeta_{-m} = -\zeta_m \quad (m > 0)$$

$$s_m = w_{-m} \quad (m < 0)$$

$$s_0 = 2w_0$$

Solutions

$$w_0 = \int_r^1 (\xi \ln \xi) f_0(\xi) d\xi + \ln r \int_0^r \xi f_0(\xi) d\xi$$

$$w_n = \frac{r^n}{2n} \int_0^1 \xi^{n+1} f_n(\xi) d\xi + \frac{r^n}{2n} \int_1^r \xi^{-n+1} f_n(\xi) d\xi - \frac{r^{-n}}{2n} \int_0^r \xi^{n+1} f_n(\xi) d\xi$$

$$\phi_n = \frac{r^n}{2n} \int_1^r \xi^{-n+1} \zeta_n(\xi) d\xi - \frac{r^{-n}}{2n} \int_0^r \xi^{n+1} \zeta_n(\xi) d\xi \quad (\text{using the fact that } \int_0^1 \xi^{n+1} \zeta_n(\xi) d\xi = 0)$$

$$\zeta_n = \frac{(n+1)r^n}{2n} \int_0^1 \xi^{n+1} F_n(\xi) d\xi - \frac{r^{-n}}{2n} \int_0^1 \xi^{n+3} F_n(\xi) d\xi + \frac{r^n}{2n} \int_1^r \xi^{-n+1} F_n(\xi) d\xi - \frac{r^{-n}}{2} \int_0^r \xi^{n+1} F_n(\xi) d\xi$$

1.3 Small curvature pipe (large Dean number: $600 < De < 5000$)^[4]

Introduce the dimensionless variables,

$$r = ar^*, u = vu^*/a, v = vv^*/a, w = v(R/2a^3)^{1/2} w^*, \phi = v\phi^*, u^* = \frac{1}{r^*} \frac{\partial \phi^*}{\partial \psi^*}, v^* = -\frac{\partial \phi^*}{\partial r^*}$$

Thus the dimensionless governing equations for steady incompressible laminar flow are (based on Dean's equation):

$$\nabla^{*2} \phi^* = -\Omega^*$$

$$\nabla^{*2} w^* + \frac{1}{r^*} \left(\frac{\partial \phi^*}{\partial r^*} \frac{\partial w^*}{\partial \psi^*} - \frac{\partial w^*}{\partial r^*} \frac{\partial \phi^*}{\partial \psi^*} \right) = -D$$

$$\nabla^{*2} \Omega^* + \frac{1}{r^*} \left(\frac{\partial \phi^*}{\partial r^*} \frac{\partial \Omega^*}{\partial \psi^*} - \frac{\partial \Omega^*}{\partial r^*} \frac{\partial \phi^*}{\partial \psi^*} \right) = w^* \left(\sin \psi^* \frac{\partial w^*}{\partial r^*} + \frac{\cos \psi^*}{r^*} \frac{\partial w^*}{\partial \psi^*} \right)$$

$$\text{Where } \nabla^{*2} = \frac{\partial^{*2}}{\partial r^{*2}} + \frac{1}{r^*} \frac{\partial}{\partial r^*} + \frac{1}{r^{*2}} \frac{\partial^2}{\partial \psi^{*2}} \text{ and } D = Ga^3(2a/R)^{1/2}/(\mu v)$$

$$\text{with } G = -\frac{1}{R} \frac{\partial P}{\partial \theta} \quad (\text{axial pressure gradient is constant})$$

Boundary conditions:

$$(1) w^* = \phi^* = \frac{\partial \phi^*}{\partial r^*} = 0 \text{ at } r^* = 1$$

(2) Symmetric about $\psi^* = 0, \pi$ from which it follows that, for $0 \leq \psi^* \leq \pi$,
 $\phi^*(r^*, \psi^*) = -\phi^*(r^*, \psi^*), w^*(r^*, \psi^*) = -w^*(r^*, \psi^*), \Omega^*(r^*, \psi^*) = -\Omega^*(r^*, \psi^*)$

$$(3) \phi^* = \Omega^* = 0, \frac{\partial w^*}{\partial \psi^*} = 0 \text{ when } \psi^* = 0, \pi$$

2 Curvature-corrected turbulence models

2.1 Linear eddy-viscosity models

Launder (1977), Howard (1980), Leschziner and Rodi (1981)^[5], Gooray (1985), Park and Chung (1989) attempted to incorporate rotation and curvature corrections into LEVM. However, they were based on ad hoc modifications and did not typically satisfy mathematical invariance principles.

2.1.1 Linear $k - \epsilon$ turbulence model + wall function ^[6]

Steady incompressible turbulent flow in toroidal coordinate (r, θ, ψ)

The governing differential equations in the central region of the flow (fully turbulent flows)

$$\begin{aligned} \frac{\partial U_r}{\partial r} + \frac{U_r}{r} + \frac{U_r \sin \psi}{R + r \sin \psi} + \frac{1}{r} \frac{\partial U_\psi}{\partial \psi} + \frac{U_\psi \cos \psi}{R + r \sin \psi} &= 0 \\ \rho(U_r \frac{\partial U_r}{\partial r} + \frac{U_\theta}{r} \frac{\partial U_r}{\partial \theta} - \frac{U_\theta^2}{r} + \frac{1}{R} \frac{\partial U_r}{\partial \psi} - \frac{U_\psi^2 \cos \theta}{R}) &= -\frac{\partial P}{\partial r} + \frac{\partial \tau_{rr}}{\partial r} + \frac{1}{r} \frac{\partial \tau_{r\theta}}{\partial \theta} - \frac{\tau_{\theta\theta}}{r} + \frac{\tau_{rr}}{r} - \frac{\tau_{\psi\psi}}{R} \cos \theta \\ &\quad + \frac{\tau_{rr}}{R} \cos \theta - \frac{\tau_{r\theta}}{R} \sin \theta \\ \rho(U_r \frac{\partial U_\theta}{\partial r} + \frac{U_\theta}{r} \frac{\partial U_\theta}{\partial \theta} + \frac{U_r U_\theta}{r} + \frac{U_\psi}{R} \frac{\partial U_\theta}{\partial \psi} + \frac{U_\psi^2 \sin \theta}{R}) &= -\frac{1}{r} \frac{\partial P}{\partial \theta} + \frac{\partial \tau_{r\theta}}{\partial r} + \frac{1}{r} \frac{\partial \tau_{\theta\theta}}{\partial \theta} + \frac{2\tau_{r\theta}}{r} + \frac{r}{R^2} \tau_{\theta\psi} \sin \theta \\ &\quad + \frac{\tau_{r\theta}}{R} \cos \theta - \frac{\tau_{\theta\theta}}{R} \sin \theta \\ \rho[U_r \frac{\partial U_\psi}{\partial r} + \frac{U_\theta}{r} \frac{\partial U_\psi}{\partial \theta} + \frac{U_\psi}{R} \frac{\partial U_\psi}{\partial \psi} + \frac{U_\psi}{R} (\frac{U_r \cos \theta - U_\theta \sin \theta}{R})] &= -\frac{1}{R} \frac{\partial \bar{P}}{\partial \psi} + \frac{\partial \tau_{r\psi}}{\partial r} + \frac{\tau_{r\psi}}{R} \cos \theta + \frac{1}{r} \frac{\partial \tau_{\psi\theta}}{\partial \theta} \\ &\quad - \frac{\tau_{\theta\psi}}{R} \sin \theta + \frac{\tau_{r\psi}}{r} \\ \rho(U_r \frac{\partial k}{\partial r} + \frac{U_\theta}{r} \frac{\partial k}{\partial \theta} + \frac{U_\psi}{R} \frac{\partial k}{\partial \psi}) &= \frac{1}{r} \frac{\partial}{\partial r} (\frac{\mu_t}{\sigma_k} r \frac{\partial k}{\partial r}) + \frac{\mu_t}{R \sigma_k} (\frac{\partial k}{\partial r} \cos \theta - \frac{\partial k}{r \partial \theta} \sin \theta) + \frac{\partial}{r^2 \partial \theta} (\frac{\mu_t}{\sigma_k} r \frac{\partial k}{\partial \theta}) + G - \rho \bar{\epsilon} \\ \rho(U_r \frac{\partial \epsilon}{\partial r} + \frac{U_\theta}{r} \frac{\partial \epsilon}{\partial \theta} + \frac{U_\psi}{R} \frac{\partial \epsilon}{\partial \psi}) &= \frac{1}{r} \frac{\partial}{\partial r} (\frac{\mu_t}{\sigma_\epsilon} r \frac{\partial \epsilon}{\partial r}) + \frac{\mu_t}{R \sigma_\epsilon} (\frac{\partial \epsilon}{\partial r} \cos \theta - \frac{\partial \epsilon}{r \partial \theta} \sin \theta) + \frac{\partial}{r^2 \partial \theta} (\frac{\mu_t}{\sigma_\epsilon} r \frac{\partial \epsilon}{\partial \theta}) + C_1 \frac{\epsilon}{k} G - \end{aligned}$$

Shear stress

$$\tau_{ij} = (\mu_l + \mu_t) D_{ij}$$

Where

μ_l is the molecular viscosity of the fluid (assumed constant throughout the pipe cross-section).

$$\mu_t = C_\mu \rho k^2 / \epsilon$$

$\{D_{ij}\}$ is the deformation tensor,

Expanding D_{ij} in the (r, ψ, θ) coordinate

$$\tau_{rr} = 2\mu \frac{\partial U_r}{\partial r},$$

$$\tau_{r\theta} = \mu \left(\frac{\partial U_r}{r \partial \theta} - \frac{U_\theta}{r} + \frac{\partial U_\theta}{\partial r} \right) = \tau_{\theta r},$$

$$\tau_{r\psi} = \mu \left(\frac{\partial U_r}{r \partial \psi} - \frac{U_\psi \cos \theta}{R} + \frac{\partial U_\psi}{\partial r} \right) = \tau_{\psi r},$$

$$\tau_{\theta\psi} = \mu \left(\frac{\partial U_\psi}{r \partial \theta} + \sin \theta \frac{U_\psi}{R} + \frac{\partial U_\theta}{R \partial \psi} \right) = \tau_{\psi \theta},$$

$$\tau_{\psi\psi} = 2\mu \left(\frac{\partial U_\psi}{R \partial \psi} + \frac{1}{R} (U_r \cos \theta - U_\theta \sin \theta) \right),$$

$$\tau_{\theta\theta} = 2\mu \left(\frac{\partial U_\theta}{r \partial \theta} + \frac{U_r}{r} \right),$$

$$G = \mu_r \left\{ 2 \left[\left(\frac{\partial U_r}{\partial r} \right)^2 + \left(\frac{\partial U_\theta}{r \partial \theta} \right)^2 + \left(\frac{U_r}{r} \right)^2 + \frac{2}{r^2} U_r \frac{\partial U_\theta}{\partial \theta} - \frac{U_\theta}{r} \left(\frac{\partial U_r}{r \partial \theta} + \frac{\partial U_\theta}{\partial r} \right) \right] + \left(\frac{\partial U_\theta^2}{\partial r} + \frac{\partial U_r}{r \partial \theta} \right) + \left(\frac{\partial U_\psi^2}{\partial r} \right) + \left(\frac{\partial U_\psi}{r \partial \theta} \right)^2 + \frac{U_\theta^2}{r^2} + \frac{U_\psi^2}{R^2} + \frac{2}{R} U_\psi \left(\frac{\partial U_\psi}{r \partial \theta} \sin \theta - \frac{\partial U_\psi}{\partial r} \right) \right\}$$

With constants: $C_\mu = 0.09, C_1 = 1.47, C_2 = 1.92, \sigma_k = 1.0, \sigma_\epsilon = 1.3$

Wall regions (low Reynolds number of turbulence $\rho k^{1/2} l / \mu_l$, where $l = k^{3/2} / \epsilon$)

Point P is located sufficiently far from the wall for the local turbulent Reynolds number $(\rho k^{1/2} l / \mu_l)_P$ to be much greater than unity. It is then assumed that a logarithmic velocity profile prevails in the region between the wall and the node P, the expression for the velocity being

Near-wall shear stress

$$\tau_P = \frac{\rho \kappa C_\mu^{1/4} k_P^{1/2} U_P}{\ln(E y_P C_\mu^{1/4} k_P^{1/2} / \mu_l)}$$

Where the subscript P indicates values at grid node P,

y_P is the distance of P from the wall,

κ and E are the log-law constants.

Near-wall shear stress kinetic dissipation rate (the length scale varies linearly with the distance from the wall)

$$\epsilon_P = C_\mu^{3/4} k_P^{3/2} / \kappa y_P$$

Where k_P represents the turbulent kinetic energy near the wall and is calculated from the regular balance equation, the diffusion of energy being set equal to zero. The dissipation term in the kinetic-energy equation is assigned an average value over the control volume for the node near the wall,

$$\rho \bar{\epsilon} = \rho \int_0^{y_N} \epsilon dy = C_\mu^{3/4} k_P^{3/2} \int_0^{y_N} \frac{1}{\kappa y} dy$$

2.1.2 Two-layer linear $k - \epsilon$ model^[19]

A linear $k - \epsilon$ model with a two-layer near wall treatment. k and ϵ equations are solved in far field. The two-layer type of near-wall treatment was included in the new turbulence model to allow the integration of the flow to the wall. The model employs the one equation model of Wolfstein (1969) in the near wall-layer zone. The transportation equation for k is solved within the wall-layer, while ϵ is calculated via an empirical correlation based local wall distance.

Turbulent kinetic energy transport equation

$$\frac{\partial(\bar{\rho}k)}{\partial t} + \frac{\partial}{\partial x_j} (\bar{\rho} U_j k) = \frac{\partial}{\partial x_j} \left[\left(\mu + \frac{\mu_T}{Pr_k} \right) \frac{\partial k}{\partial x_j} \right] + [2\mu_T (S_{ij} - \frac{1}{3} \delta_{ij} \frac{\partial U_l}{\partial x_l}) - \frac{2}{3} \bar{\rho} k \delta_{ij}] \frac{\partial U_i}{\partial x_j} - \bar{\rho} \epsilon$$

Turbulent dissipation rate transport equation

$$\frac{\partial(\bar{\rho}\epsilon)}{\partial t} + \frac{\partial}{\partial x_j} (\bar{\rho} U_j \epsilon) = \frac{\partial}{\partial x_j} \left[\left(\mu + \frac{\mu_T}{Pr_\epsilon} \right) \frac{\partial \epsilon}{\partial x_j} \right] + C_{\epsilon 1} \frac{\epsilon}{k} [2\mu_T (S_{ij} - \frac{1}{3} \delta_{ij} \frac{\partial U_l}{\partial x_l}) - \frac{2}{3} \bar{\rho} k \delta_{ij}] \frac{\partial U_i}{\partial x_j} - C_{\epsilon 2} \bar{\rho} \frac{\epsilon^2}{k}$$

Turbulent viscosity

$$\mu_T = C_\mu \bar{\rho} \frac{k^2}{\varepsilon}$$

Turbulent viscosity coefficient

$$C_\mu = \frac{K_1 + K_2 C_\mu \left(\frac{Sk}{\varepsilon}\right)^2 + K_3 C_\mu \left(\frac{Sk}{\varepsilon}\right) + K_4 C_\mu^2 \left(\frac{Sk}{\varepsilon}\right)^3}{K_5 + K_6 C_\mu \left(\frac{Sk}{\varepsilon}\right)^2 + K_7 C_\mu^2 \left(\frac{Sk}{\varepsilon}\right)^4 + K_8 \left(\frac{Wk}{\varepsilon}\right)^2}$$

Where

$$S = \sqrt{2S_{ij}S_{ij}}, W = \sqrt{2W_{ij}W_{ij}}$$

Modified flow rotation term

$$W = \left| S \cdot \left(1 - \frac{C_4 - 4}{C_4 - 2}\right) + \Omega \cdot \frac{C_4 - 4}{C_4 - 2} \right| = \left| \frac{9}{4}\Omega - \frac{5}{4}S \right|$$

Where the relative fluid rotation rate magnitude computed in an inertial frame is:

$$\Omega = \sqrt{2\Omega_{ij}\Omega_{ij}}$$

Turbulent stress (Boussinesq's assumption)

$$-\overline{\rho u_i u_j} = 2\mu_T S_{ij} - \frac{2}{3} \delta_{ij} \left(\mu_T \frac{\partial U_l}{\partial x_l} + \bar{\rho} k \right)$$

Model turbulent length scale

$$L_T = \min\left(\frac{C_{LY} k^{3/2}}{\varepsilon}\right)$$

Near-wall turbulent dissipation rate (when $\frac{C_{LY}}{\varepsilon}$ is minimum)

$$\varepsilon = \frac{k^{3/2}}{l_\varepsilon}$$

$$\text{Where } l_\varepsilon = C_{LY} \left[1 - \exp\left(-\frac{\text{Re}_y}{A_\varepsilon}\right)\right]$$

Near-wall turbulent viscosity (when $\frac{C_{LY}}{\varepsilon}$ is minimum)

$$\mu_T = C_\mu \bar{\rho} \sqrt{k} C_{LY} \left[1 - \exp\left(-\frac{\text{Re}_y}{A_\varepsilon}\right)\right],$$

$$\text{Where } \text{Re}_y = \frac{\sqrt{k} y}{\nu}$$

Model constants

$$\text{Pr}_k = 1.0, \text{Pr}_\varepsilon = 1.19, C_{\varepsilon 1} = 1.44, C_{\varepsilon 2} = 1.92, K_1 = 0.66, K_2 = 3.9, K_3 = 1.0, K_4 = 5.3, K_5 = 2.9, \\ K_6 = 17.0, K_7 = 10.0, K_8 = 3.84, C_4 = 0.4, C_L = 2.495, A_\varepsilon = 4.99, A_\mu = 25.0$$

2.1.3 SA model with rotation and/or curvature effects (SARC)^[8]

SA turbulence model is a one-equation model that was presented by Spalart and Allmaras in 1992. Curvature-corrected SA model is based on a Galilean invariant measure of turbulence for sensitizing eddy viscosity turbulence models to the effects of streamline curvature. The equations for the SARC turbulence model are the same as those for the standard SA model, except that the production term is multiplied by a rotation function f_{r1} .

In SA model/SARC model, a single partial differential transport equation is solved at each time step.

Turbulent viscosity transportation equation

$$\frac{\partial(\rho \tilde{\nu})}{\partial t} + \frac{\partial}{\partial x_j} (\rho U_j \tilde{\nu}) = G_{\tilde{\nu}} + \frac{1}{\sigma_{\tilde{\nu}}} \left[\frac{\partial}{\partial x_i} \left\{ (\mu + \rho \tilde{\nu}) \frac{\partial}{\partial x_i} \right\} + C_{b2} \rho \left(\frac{\partial \tilde{\nu}}{\partial x_j} \right)^2 \right] - Y_{\tilde{\nu}} + S_{\tilde{\nu}}$$

Where

$G_{\tilde{\nu}}$ is the production of turbulent viscosity,
 $Y_{\tilde{\nu}}$ is the destruction of turbulent viscosity,
 $S_{\tilde{\nu}}$ is a source term, ν is the molecular kinematic viscosity,
 σ_ν and C_{b2} are calibrated constants.

Turbulent viscosity

$$\mu_t = \rho \tilde{\nu} f_{\nu 1}.$$

Where $f_{\nu 1}$ is a viscous damping function defined as

$$f_{\nu 1} = \frac{(\frac{\tilde{\nu}}{\nu})^3}{(\frac{\tilde{\nu}}{\nu})^3 + C_{\nu 1}^3}$$

Production of turbulent viscosity

$$G_{\tilde{\nu}} = C_{b1} \rho \tilde{\nu} [S + \frac{\tilde{\nu}}{\kappa^2 d^2} (1 - \frac{\tilde{\nu}/\nu}{1 + f_{\nu 1} \tilde{\nu}/\nu})] f_{r1}$$

Where

d is the distance from the wall,

S is the scalar measure of the deformation tensor,

κ is von Karman constant ($\kappa \approx 0.41$).

$$f_{r1} = (1 + C_{r1}) \frac{2r^*}{1 + r^*} [1 - C_{r3} \tan^{-1}(C_{r2} \tilde{r})] - C_{r1},$$

$$\text{With } r^* = \frac{S}{\Omega}, \tilde{r} = \frac{2\Omega_{ik} S_{jk}}{D^4} (\frac{DS_{ij}}{Dt}),$$

$$\text{Where } S^2 = 2S_{ij}S_{ij}, \Omega^2 = 2\Omega_{ij}\Omega_{ij}, D^2 = \frac{1}{2}(\Omega^2 + S^2), C_{r1} = 1, C_{r2} = 12, C_{r3} = 1$$

Turbulent destruction

$$Y_{\tilde{\nu}} = C_{w1} \rho f_w (\frac{\tilde{\nu}}{d})^2$$

$$\text{Where } f_w = g [\frac{1 + C_{w3}^6}{g^6 + C_{w3}^6}]^{1/6}, g = r + C_{w2}(r^6 - r), r = \frac{\tilde{\nu}}{(S + \frac{\tilde{\nu}}{\kappa^2 d^2} f_{\nu 2}) \kappa^2 d^2},$$

C_{w1} , C_{w2} and C_{w3} are calibrated constants.

2.2 Non-linear eddy-viscosity models (NLEVM)

Some models have been explicitly sensitized to rotation and curvature, resulting in further improvement to their predictive capability. Girimaji (1997), Rumsey and Gatski (2001), Fu and Qian (2002), Wallin and Johansson (2002), Hellsten (2002), Grunderstam (2005), Wang and Thangam (2006). The curvature corrections in these recent models have been based primarily on mathematically consistent application of invariance and frame indifference principles, in contrast to the ad hoc modifications found in earlier attempts.

2.2.1 Corrected nonlinear $\nu^2 - f$ model^[8]

Durbin developed the $\nu^2 - f$ model to be used in flows in which near-wall turbulence is of significant importance, specifically flows with separation, recirculation or heat transfer. The model solves four transport equations, those for k , ϵ , ν^2 (velocity scale) and f (elliptic relaxation factor).

Turbulent kinetic energy transportation equation

$$\frac{\partial(\rho k)}{\partial t} + \frac{\partial}{\partial x_j}(\rho U_j k) = P_k - \rho \varepsilon + \frac{\partial}{\partial x_j} \left[\left(\mu + \frac{\mu_t}{\text{Pr}_k} \right) \frac{\partial k}{\partial x_j} \right]$$

Turbulent energy diffusion rate transportation equation

$$\frac{\partial(\rho \varepsilon)}{\partial t} + \frac{\partial}{\partial x_j}(\rho U_j \varepsilon) = \frac{\partial}{\partial x_j} \left[\left(\mu + \frac{\mu_t}{\text{Pr}_\varepsilon} \right) \frac{\partial \varepsilon}{\partial x_j} \right] + \frac{C_{\varepsilon 1}^* P_k - \rho C_{\varepsilon 2} \varepsilon}{T}$$

Turbulent velocity scale transportation equation

$$\frac{\partial(\rho \overline{v^2})}{\partial t} + \frac{\partial(\rho \overline{v^2} U_j)}{\partial x_j} = \rho k f - 6 \rho \overline{v^2} + \frac{\partial}{\partial x_j} \left[\left(\mu + \frac{\mu_t}{\text{Pr}_k} \right) \frac{\partial \overline{v^2}}{\partial x_j} \right]$$

Turbulent elliptic relaxation factor transportation equation

$$L \frac{\partial f^2}{\partial x_j} - f = \frac{1}{T} (C_1 - 1) \left(\frac{\overline{v^2}}{k} - \frac{2}{3} \right) - C_2 \frac{P_k}{\rho k}$$

Where $C_1 = 1.6, C_2 = 0.3$

the production of turbulence kinetic energy P_k due to mean flow velocity gradients is

$$P_k = 2\mu_t S^2$$

Reynold stress model

$$-\overline{\rho u_i u_j} / \overline{\rho} = \frac{2}{3} \delta_{ijk} - 2C_{\mu 1}^* \overline{v^2} \tau_1 S_{ij} - V \tau^2 [C_{\mu 2}^* (S_{ik} W_{kj}^* - S_{jk} W_{ki}^*) - C_{\mu 3}^* (S_{ik} S_{kj} - \frac{1}{3} |S^2| \delta_{ij})]$$

Turbulence viscosity coefficient

$$C_\mu^* = C_\mu \frac{1 + \alpha_2 |\eta_3| + \alpha_3 |\eta_3|}{1 + \alpha_4 |\eta_3|} \left[\sqrt{\frac{1 + \alpha_5 \eta_1}{1 + \alpha_5 \eta_2}} + \alpha_1 \sqrt{\eta_2} \sqrt{|\eta_3| - \eta_3} \right]^{-1}$$

Where

$$\alpha_1 = 0.055 \sqrt{f_1}, \alpha_2 = \frac{1}{2} f_1, \alpha_3 = \frac{1}{4} f_1, \alpha_4 = \frac{1}{5} f_1, \alpha_5 = \frac{1}{40},$$

$$f_1 = \sqrt{\left(\frac{\overline{v^2}}{k} \right) / \left(\frac{\overline{v^2}}{k} \right)_\infty}, \text{ with } \left(\frac{\overline{v^2}}{k} \right)_\infty = 0.376$$

Turbulence time scale

The turbulence time scale can not be less than the Kolmogoroff scale $\sqrt{\frac{\mu}{\rho \varepsilon}}$.

$$T = \max \left[\frac{k}{\varepsilon}, C_T \sqrt{\frac{\mu}{\rho \varepsilon}} \right]$$

Where $C_T = 6$

Turbulence length scale

The turbulence length scale L can not be less than Kolmogoroff scale $(\overline{v^3}/\varepsilon)^{1/4}$.

$$L = C_L \max \left[\frac{k^{3/2}}{\varepsilon}, C_\eta \left(\frac{\mu^3}{\rho^3 \varepsilon} \right)^{1/4} \right]$$

Where $C_L = 0.23, C_\eta = 60$

Turbulence viscosity

$$\mu_t = \rho C_\mu \overline{v^2} T$$

Calibrated constants

$$C_{\mu 1}^* = C_\mu F,$$

$$C_{\mu 2}^* = \frac{6}{5} \frac{\sqrt{1 - (C_{\mu 1}^* \frac{\overline{v^2}}{k})^2 \eta_1}}{\beta_1 + \sqrt{\eta_1 \eta_2}},$$

$$C_{\mu 3}^* = \frac{6}{5} \frac{1}{\gamma_1 + \eta_1}$$

$$C_\mu = 0.2, \sigma_k = 1$$

$$V = \max\left(\frac{2}{3} - \frac{\bar{v}^2}{k}, 0\right), \beta_1 = \frac{1}{0.1 + \sqrt{\eta_1 \eta_2}}, \gamma_1 = \frac{1}{0.1 + \eta},$$

$$\eta_1 = \frac{k^2}{\varepsilon^2} \left| \frac{1}{2} \left(\frac{\partial U_i}{\partial x_j} + \frac{\partial U_j}{\partial x_i} \right) \right|^2,$$

$$\eta_2 = \frac{k^2}{\varepsilon^2} \left| \frac{1}{2} \left(\frac{\partial U_i}{\partial x_j} - \frac{\partial U_j}{\partial x_i} \right) + C_\varepsilon \Omega_{ij} + \bar{\Omega}_{ij} \right|,$$

$$\eta_3 = \eta_2 - \eta_1,$$

$$\text{where } \bar{\Omega}_{ij} = -e_{ijk} \bar{\omega}_k, \bar{\omega}_i = \frac{\Pi_1^2 \delta_{ij} + 12\Pi_2 S_{ij} + 6\Pi_1 S_{ik} S_{kj}}{2\Pi_1^3 - 12\Pi_2^2} S_{pl} S'_{pl} e_{pqj}, \Pi_1 = \text{trace}(S^2), \Pi_2 = \text{trace}(S^3),$$

()' is material derivative,

The objective vorticity tensor $\bar{\Omega}_{ij}$ is

$$\begin{bmatrix} \bar{\Omega}_{11} & \bar{\Omega}_{12} & \bar{\Omega}_{13} \\ \bar{\Omega}_{21} & \bar{\Omega}_{22} & \bar{\Omega}_{23} \\ \bar{\Omega}_{31} & \bar{\Omega}_{32} & \bar{\Omega}_{33} \end{bmatrix} = \begin{bmatrix} 0 & -\omega_3 & \omega_2 \\ \omega_3 & 0 & -\omega_1 \\ -\omega_2 & \omega_1 & 0 \end{bmatrix}$$

$$\begin{bmatrix} \omega_1 \\ \omega_2 \\ \omega_3 \end{bmatrix} = \frac{1}{2\Pi_1^3 - 12\Pi_2^2} \left(\Pi_1^2 \begin{bmatrix} 1 & 0 & 0 \\ 0 & 1 & 0 \\ 0 & 0 & 1 \end{bmatrix} + 12\Pi_2 \begin{bmatrix} S_{11} & S_{12} & S_{13} \\ S_{21} & S_{22} & S_{23} \\ S_{31} & S_{32} & S_{33} \end{bmatrix} + 6\Pi_1 a \begin{bmatrix} S_{11} & S_{12} & S_{13} \\ S_{21} & S_{22} & S_{23} \\ S_{31} & S_{32} & S_{33} \end{bmatrix}^2 \right)$$

$$\times \begin{bmatrix} S_{23} S'_{23} - S_{32} S'_{32} \\ S_{31} S'_{31} - S_{13} S'_{13} \\ S_{12} S'_{12} - S_{21} S'_{21} \end{bmatrix}$$

References

- [1] W.R. Dean, Note on the motion of fluid in a curved pipe, *Phil. Mag.*,4, 208(1927)
- [2]W.R. Dean, the streamline motion of fluid in a curved pipe, *Phil. Mag.*5,673(1928)
- [3] D.J.McConalogue, R.S. Srivastava, Motion of a fluid in a curved tube, *Proc.Roy.Soc.A.* 307, 37-53(1968)
- [4]S.C.R. Dennis, Calculation of the steady flow through a curved tube using a new finite-difference method, *J. Fluid Mech.*, Vol.99, part 3, 449-467
- [5]Launder, B. E., Reece, G. J., and Rodi, W. Progress in the development of a Reynolds stress turbulence closure.*J. FluidMech.*, 1975, 68, 537–566.
- [6]S.V.Patankar, D.B.Spalding, Prediction of turbulent flow in curved pipes, Vol. 67, 583-595, *J. Fluid Mech.*,1975
- [7]William D. York and D.Keith Walters, James H. Lylek, A simple and robust linear eddy-viscosity formulation for curved and rotating flows, *International Journal of Numerical Methods for Heat & Fluid Flow*, Vol. 19 Iss: 6, pp.745 - 776
- [8] Travis Marshall Storm, Assessing the $v^2 - f$ turbulence models for circulation control applications, Master thesis, April, 2010.